UNIVERSITÀ DI PARMA

UNIVERSITA' DEGLI STUDI DI PARMA

DOTTORATO DI RICERCA IN

"SCIENZE CHIMICHE"

CICLO XXXI

Expanding the chemistry of stable trinuclear all-metal aromatics

Coordinatore:

Chiar.mo Prof. Roberto Corradini

Tutore:

Chiar.mo Prof. Giovanni Maestri

Dottorando: Anna Monfredini

Anni 2015/2018

Table of contents

Chapter 1

SYNTHESIS OF ZWITTERIONIC TRIPALLADIUM CLUSTERS

1.1 Introduction

1.1.1 Aromaticity and All-Metal Aromaticity

Aromaticity has been fascinating chemists since 1865, when August Kekulé proposed the six-membered ring structure with delocalized double bonds for the benzene.[1] The concept was firstly developed to describe few classes of molecules, namely monocyclic planar conjugate hydrocarbons and corresponding ions with (4n+2) π electrons, polycyclic conjugate hydrocarbons made up of fused benzene rings and polycyclic conjugate carbocyclic hydrocarbons with four-, five-, seven- and eight-membered rings.[2] Nowadays it finds a broader applicability, since it has been used to refer to several heterocyclic compounds and three-dimensional molecules, such as ferrocene and related sandwich systems,[2b-3] pyramidal hydrocarbons,[4] boron hydrides, carbon- and hetero-boranes[5] and fullerenes.[6] In 1979 Thorn and Hoffmann extended the concept to compounds containing a transition metal atom, proposing an hypothetical six-membered ring derived from benzene in which a C-H group was replaced by an isolobal transition-metal fragment *(Fig. 1)*.

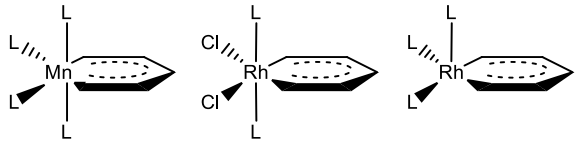

Fig. 1: Examples of metallacycles discussed by Thorn and Hoffmann

---

[1] A. Kekulé, *Bull. Soc. Chim. Fr. (Paris)*, **1865**, *3*, 98.
[2] a) P. v. R. Schleyer, *Chem. Rev*., **2001**, *5*, 101; b) A. R. Katritzky, *Chem. Rev*., **2004**, *5*, 104; c) M. Randik, *Chem. Rev*., **2003**, *103*, 3449.
[3] a) A. Togni, R. L. Haltermann, *Metallocenes*, Wiley_VCH: New York, **1998**; b) F. A. Cotton, G. Wilkinson, C. A. Murillo, M. Bochmann, *Advanced Inorganic Chemistry*, 6th Ed.,Wiley: New York, **1999**.
[4] V. I. Minkin, M. N. Glukhovtsev, B. Y. Simkin, *Aromaticity and Antiaromaticity. Electronic and structural aspects.*, Wiley: New York, **1994**.
[5] R. B. King, *Chem. Rev*., **2001**, *101*, 1119.
[6] a) H. W. Kroto, *Pure Appl. Chem.*, **1990**, *62*, 407; b) M. Buhl, A. Hirsch, *Chem. Rev*., **2001**, *101*, 1153.

In analogy to the benzene ring, it should exhibit delocalized bonding and a consequent aromatic character.[7] The term *metalloaromaticity* was in parallel introduced by Bursten and Frenske to describe the covalent C_4H_4-Fe bond of the iron-cyclobutadiene complex, which resulted in a delocalization of six electrons in the π-orbitals of the metal ring.[8] Few years later Elliot et al. isolated an osmabenzene, the first example of stable metallobenzene,[9] while Bleeke an co-workers obtained a family of iridabenzenes.[10] A further improvement was made by Rothwell et al., with a series of dimetallobenzenes incorporating two metal atoms into the six-membered ring.[11] The first organometallic compound with an aromatic ring completely made up of metal atoms was not long in coming, since in 1995 Robinson et al. obtained a trinuclear complex of gallium, which will be described later in this chapter.[12] Solid compounds containing aromatic metalloid and metal clusters were characterized as well. The most interesting examples concern aromatic square clusters such as Se_4^{2+}, Te_4^{2+},[13] Sb_4^{2-} and Bi_4^{2-},[14] which are isoelectronic to the aromatic hydrocarbon $C_4H_4^{2-}$, together with planar pentagonal aromatic clusters such as As_5^-,[15] Sn_5^{6-} and Pb_5^{6-},[16] which are isoelectronic to $C_5H_5^-$. In

[7] D. L. Thorn, R. Hoffmann, *Nouv. J. Chim.*, **1979**, *3*, 39.
[8] B. E. Bursten, R. F. Fenske, *Inorg. Chem.*, **1979**, *18*, 1760.
[9] G. P. Elliot, W. R. Roper, J. M. Waters, *J. Chem. Soc., Chem. Commun.*, **1982**, 811.
[10] a) J. R. Bleeke, Y. F. Xie, W. J. Peng, M. Chiang, *J. Am. Chem. Soc*., **1989**, *111*, 4118; b) J. R. Bleeke, R. Behm, Y. F. Xie, T. W. Jr. Clayton, K. D. J. Robinson, *J. Am. Chem. Soc*., **1994**, *116*, 4093; c) J. R. Bleeke, R. Behm, Y. F. Xie, M. Chiang, K. D. J. Robinson, A. M. Betty, *Organometallics*, **1997**, *16*, 606.
[11] a) R. D. Profilet, P. E. Fanwick, I. P. Rothwell, *Angew. Chem. Int. Ed.*, **1992**, *31*, 1261; b) P. N. Riley, R. D. Profilet, M. M. Salberg, P. E. Fanwick, I. P. Rothwell, *Polyhedron*, **1998**, *17*, 773.
[12] X. W. Li, T. Penninghton, G. H. Robinson, *J. Am. Chem. Soc*., **1995**, *117*, 7578.
[13] a) R. J. Gillespie, J. Passmore, *Acc. Chem. Res.*, **1971**, *4*, 413; b) I. D. Brown, D. B. Crump, R. J. Gillespie, *Chem. Commun*., **1968**, 963; c) R. J. Gillespie, J. P. Pez, *Inorg. Chem.*, **1969**, *8*, 1229.
[14] a) S. C. Critchlow, J. D. Corbett, *Inorg. Chem.*, **1984**, *23*, 770; b) A. Cisar, J. D. Corbett, *Inorg. Chem.*, **1977**, *16*, 2482; c) D. G. Adolphson, J. D. Corbett, D. J. Marryman, *J. Am. Chem. Soc*., **1976**, *98*, 7234.
[15] a) O. J. Scherer, *Angew. Chem. Int. Ed.*, **1990**, *29*, 1104; b) A. L. Rheingold, M. J. Foley, P. J. Sullivan, *J. Am. Chem. Soc*., **1982**, *104*, 4727.

2001 the concept of aromaticity was also extended to gas-phase metal clusters, when Boldyrev et al. made a series of bimetallic clusters, $LiAl^{4-}$, $NaAl^{4-}$ and $CuAl^{4-}$, whose most stable isomers contained the square planar Al_4^{2-} dianion that proved to be aromatic.[17]

Aromaticity and antiaromaticity acquire a very specific connotation if referred to metal-containing compounds instead of to organic systems. Cyclic electron delocalization in organic compounds leads to bond length equalization, abnormal chemical shifts as the result of the molecular ring current and magnetic anisotropies, together with chemical and physical properties that witness an energetic stabilization. In addition, aromatic compounds display exalted diamagnetic susceptibility, while antiaromatic compounds exalted paramagnetic susceptibility. Many of the criteria proposed for π-aromatic and π-antiaromatic molecules are also applicable to σ- and δ-aromatic/antiaromatic species, even if many specific deviations are expected in transition-metal systems. Nevertheless, the overall delocalized chemical bonding and the molecular properties that characterize transition-metal compounds described in following paragraphs could be rationalized using these concepts. The involvement of the d electron shell of transition metals in these systems make them different from the traditional organic compounds. Their peculiar bonding mode could lead to multiple aromaticity, antiaromaticity and conflicting aromaticity, namely the simultaneous presence of π-antiaromaticity and σ-aromaticity or σ-antiaromaticity and π-aromaticity. If chemical bonding derives from the combination of s-atomic orbitals, only σ-aromaticity or σ-antiaromaticity could in principle be generated, while if p- or d-atomic orbitals are involved more sceneries are possible, since π- and δ-aromaticity could also occur.

---

[16] I. Todorov, S. C. Sevov, *Inorg. Chem.*, **2004**, *43*, 6490.
[17] X. Li, A. E. Kuznetsov, H. F. Zhang, A. I. Boldyrev, L. S. Wang, *Science*, **2001**, *291*, 859.

Huang et al. combined photoelectron spectroscopy and theoretical calculations to obtain the first cases of d-orbital aromaticity in 4d and 5d transition metal-oxide clusters $Mo_3O_9^-$ and $W_3O_9^-$.[18] M_3O_9, $M_3O_9^-$ and $M_3O_9^{2-}$ exhibit a D_{3h} structure in which each metal atom is bonded to two bridged and two terminal oxygen atoms, but M-M distances in $M_3O_9^-$ are significantly shortened if compared to the neutral species. The σ-HOMO in $M_3O_9^-$ and $M_3O_9^{2-}$ has a completely bonding nature, in addition a sizable resonance energy of -7.6 kcal mol^{-1} was estimated for $W_3O_9^-$. Nucleus Indipendent Chemical Shift (NICS) calculations further supported the presence of σ-aromaticity. NICS is a theoretical tool that allows to evaluate the presence of an aromatic ring in a cyclic molecule by calculating the absolute magnetic shield of a series of relevant points of the space around the cycle of interest. If the molecule is aromatic, negative values should be obtained along the perpendicular axis. Negative values were obtained at the center of both $Mo_3O_9^{2-}$ and $W_3O_9^{2-}$ (-21.5 and -20.5 ppm respectively). In 2007 Zhai et al. identified π- and δ- double aromaticity in $Ta_3O_3^-$, originated from the combination of d-atomic orbitals.[19] The present cluster possess a global minimum with a D_{3h} planar triangular structure. Analysis of molecular orbitals reveals that ten of the 34 valence electrons of $Ta_3O_3^-$ are responsible for the metal-metal bonding, while the other 24 belong to oxygen lone pairs or are involved in the formation of Ta-O bonds. δ-aromatic character is due to the $HOMO^{-1}$, which derives from the combination of the d_{z^2} orbital on each Ta atom. The present molecular orbital has major overlaps above and below the molecular plane, showing a typical arrangement of π-type orbitals. However, its symmetry with respect to the molecular plane and its two nodal surfaces perpendicular to the C_3 axis are clearly in agreement with a δ-aromatic character.

[18] X. Huang, H. J. Zhai, B. Kiran, L. S. Wang, *Angew. Chem. Int. Ed.*, **2005**, *44*, 7251.
[19] H. J. Zhai, B. B. Averkiev, D. Yu. Zubarev, L. S. Wang, *Angew. Chem. Int. Ed.*, **2007**, *46*, 4277.

1.1.2 Stable triangular all-metal aromatic clusters

Stable and readily available aromatic clusters with an aromatic ring completely composed by metal atoms are quite rare. The few remarkable examples that recently entered the scene are described below.

1.1.2.1 π-aromatic cyclogallenes

In 1995 Robinson and his research group introduced the first *cyclogallene*, $Na_2[(Mes_2C_6H_3)Ga]_3$ (**1**),[12] a trinuclear metallic ring system which showed aromatic properties. They were investigating the behaviour of aryl-based ligands for heavier group 13 elements, while they found 2,6-dimesitylphenyl to be an excellent ligand to obtain gallium and indium chloride derivatives, namely $(Mes_2C_6H_3)_2GaCl_2$[20] and $[(Mes_2C_6H_3)_2InCl_2]_2$.[21] $Na_2[(Mes_2C_6H_3)Ga]_3$ was isolated from the alkali metal reduction of $(Mes_2C_6H_3)_2GaCl_2$ in ether. The trinuclear compound exhibits a planar Ga_3 core that presents one Ga-Ga bond distance, 2.441 Å, and Ga-Ga-Ga angles of 60.0°, which make the triangle equilateral. The metal core is completed by two sodium atoms centered above and below the plane of the gallium triangle, forming a Na_2-Ga_3 trigonal bipyramid with a Na-Ga distance of 3.220 Å *(Fig. 2)*.

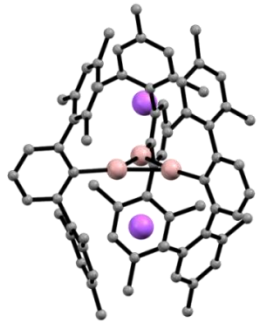

*Fig. 2: X-Ray structure of $Na_2[(Mes_2C_6H_3)Ga]_3$ (**1**)*

[20] X. W. Li, T. Penninghton, G. H. Robinson, *Organometallics*, **1995**, *14*, 2109.
[21] G. H. Robinson, X. W. Li, T. Penninghton, *J. Organomet. Chem.*, **1995**, *501*, 399.

This very short value for Ga-Ga bonds compared to that of known tetranuclear[22] gallium compounds encouraged the group to gain more insights into the origin of this peculiar structure. They indeed proposed a 2π-electrons system in which the two Na atoms donate one electron each to the unoccupied p orbitals of gallium atoms, thus providing the two π-electrons delocalized in the metal core. Ga_3^{2-} was isoelectronic with the triphenylcyclopropenium cation, which is an aromatic compound. A further confirmation was provided by NICS calculation. According to the hypothesis of a π-aromaticity, a theoretical $(GaH)_3^{2-}$ gave a value of -17.6, in sharp contrast with that displayed by the anti-aromatic[23] $(GaH)_3$ species (+90.6). In addition, chemical shifts for alkali metals centered along the center axis above and below the plane of the triangle are clearly upfield shifted, in agreement with the presence of a considerable ring current that should lead to a reduced magnetic field strength in the cyclogallene moiety. $Na_2[(Mes_2C_6H_3)Ga]_3$ proved to be the first example of metalloaromaticity.

1.1.2.2 σ-aromatic trigold cations

Between 2012 and 2014 several examples of trigold clusters increased the number of available metalloaromatic complexes.

Considering the analogies often drawn between $[LAu]^+$ and $[H]^+$,[24] Sadighi and co-workers exploited the concept of isolobality in the synthesis of a gold analogue of $[H_3]^+$, the simplest three-center, two-electron bond. They used an *N*-heterocyclic carbene ligand to stabilize the trigold cation $[(LAu)_3]^+$, synthesized through the reduction between a cationic trigold (I) carbonate and

[22] a) W. Uhl, W. Hiller, M. Layh, W. Schwarz, *Angew. Chem. Int. Ed Engl*., **1992**, *31*, 1364; b) W. Hiller, K. W. Klinkhammer, W. Uhl, J. Wagner, *Angew. Chem. Int. Ed Engl*., **1991**, *30*, 179.

[23] P. v. R. Schleyer, C. Maerker, A. Dransfeld, H. Jiao, N. v. E. Hommes, *J. Am. Chem. Soc*., **1996**, *118*, 6317.

[24] H. G. Raubenheimer, H. Schmidbaur, *Organometallics*, **2012**, *31*, 2507.

carbon monoxide.[25] The synthesis of the present compound revealed quite tricky, since the first strategy of reducing the corresponding μ_3-oxo complex $[(LAu)_3O]^+$ led to a mixture of products. They overcame this issue generating a cationic siloxide-bridge digold complex from [LAuOTf] and $[LAuOSiMe_3]$, $[(LAu)_2OSiMe_3]^+OTf^-$, which easily reacted with $[LAuOSiMe_3]$ to give the trigold (I) carbonate $[(LAu)_3CO_3]^+OTf^-$ in the presence of CO_2 *(Scheme 1)*.

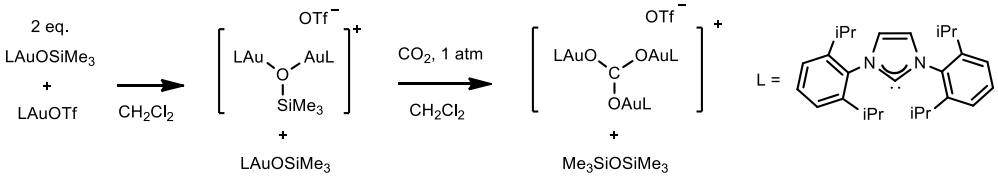

Scheme 1: Synthesis of the trigold (I) carbonate $[(LAu)_3CO_3]^+OTf^-$

$[(LAu)_3]^+$ exhibits a D_3 symmetry, with the imidazolydene rings canted by 63.1(4) and 77.7(4) Å. The three Au atoms are not positioned in a perfectly equilateral geometry, since bond angles swing between 59.603(9)° and 60.331(8)°, and Au-Au distances from 2.6438(5) to 2.6633(5) Å. Gold-bonded carbons are essentially coplanar with the Au_3 ring. Regarding electronic properties, frontier orbitals remind those of $[H_3]^+$. The HOMO is indeed a single degenerate a_1 combination of s-type orbitals of gold. In addition, the HOMO-LUMO gap is large, with a calculated value of 5.42 eV, thus explaining the inertia of $[(LAu)_3]^+$.

The other examples of trinuclear mixed-valence gold(I)/gold(0) clusters arose from Bertrand's research group in 2014 *(Fig. 3)*.[26] They managed to obtain cluster **2** in two steps, firstly by treating $(CAAC_{c\text{-}Hex})AuCl$ with Ag_2O in the presence of $NaBF_4$ to form the μ_3-oxo complex, then by reducing it with carbon monoxide. Despite the reaction afforded the desired product in good yield

[25] T. J. Robilotto, J. Bacsa, T. J. Gray, J. P. Sadighi, *Angew. Chem. Int. Ed*., **2012**, *51*, 12077.
[26] L. Jin, D. S. Weinberger, M. Melaimi, C. E. Moore, A. L. Rheingold, G. Bertrand, *Angew. Chem. Int. Ed*., **2014**, *53*, 9059.

(75%), the mononuclear Au precursor could be obtained only in 41% yield, making this strategy not viable. A second attempt based on ligand exchange proved decisive and paved the way for the preparation of carbene-supported multi-nuclear gold clusters. Clusters **3** and **4** could indeed be obtained by ligand exchange on the corresponding μ_3-oxo phosphine complex, followed by reduction with carbon monoxide.

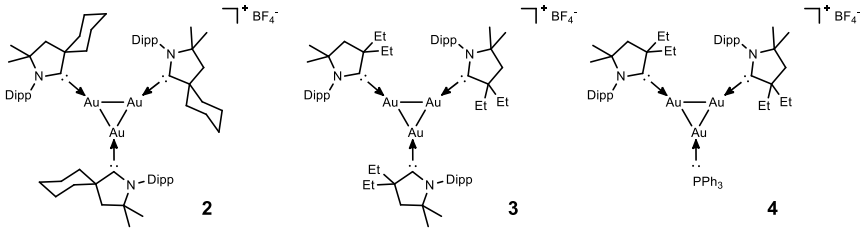

Fig. 3: Bertrand's trigold clusters

1.1.2.3 σ-aromatic trizinc clusters

In 2015 Fischer and co-workers obtained two examples of σ-aromatic triangular clusters, $[Zn_3Cp^*_3]^+$(**5**) and $[Zn_2CuCp^*_3]$ (**6**), which could be considered embryonic models for zinc and brass respectively.[27] They were obtained upon the addition of the electophilic and isolobal species $[ZnCp^*]^+$ and $[CuCp^*]$ to Carmona's compound $[Cp^*Zn\text{-}ZnCp^*]$, without observing the splitting of zinc-zinc bond. Reaction conditions were quite complex, since low temperature and very careful and controlled crystallization procedures were required, together with the use of a glove box through these operations. Despite both compounds could be obtained in crystalline form, they proved very labile and rapidly decomposed at room temperature, both in solution and in the solid state. Core structures of $[Zn_3]^+$ and $[Zn_2Cu]$ have an almost perfectly equilateral arrangement of the metal atoms. Bond angles in $[Zn_3]^+$

[27] K. Freitag, C. Gemel, P. Jerabeck, I. M. Oppel, R. W. Seidel, G. Frenking, H. Banh, K. Dilchert, R. A. Fischer, *Angew. Chem. Int. Ed*., **2015**, *54*, 4370.

vary between 61.06(2)° and 59.22(1)°, while Zn-Zn distances are nearly identical with an average of 2.430(1) Å. In $[Zn_2Cu]$ bond angles are 60.34(3)°, 59.33(2)° and 60.34(3)° Å. In contrast with $[Zn_3]^+$, the heterometallic cluster has two equal Zn-Cu bonds of 2.381(1) Å and a slightly shortened Zn-Zn bond of 2.357(1) Å *(Fig. 4)*.

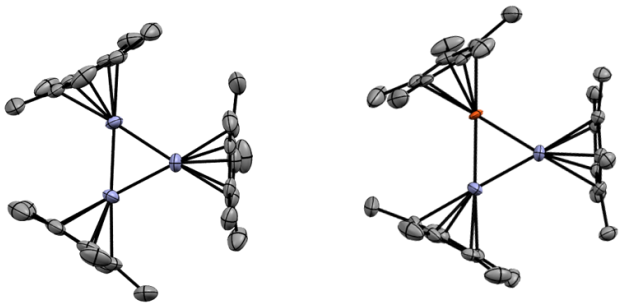

*Fig. 4: X-Ray structures of $[Zn_3]^+$(**5**) and $[Zn_2Cu]$ (**6**) clusters*

1.1.3 Pd_3^+ clusters and analogues

1.1.3.1 First generation synthesis of Pd_3^+ clusters

The first Pd_3^+ cluster was synthesized by chance when our research group was investigating the oxidative addition ability of the C-S bond of isothioureas on low valent palladium complexes. It was obtained upon the reaction between the isothiourea in *Scheme 2* with 1 equivalent of $Pd(dba)_2$ and 1 equivalent of tris(4-fluorophenyl) phosphine in degassed dichloromethane.[28]

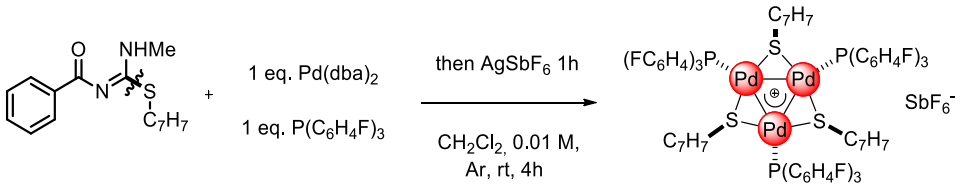

Scheme 2: First generation synthesis of Pd_3^+ clusters

[28] S. Blanchard, L. Fensterbank, G. Gontard, E. Lacôte, G. Maestri, M. Malacria, *Angew. Chem. Int. Ed.*, **2014**, *53*, 1987.

The deep red powder isolated showed the peculiar isotopic pattern of a tripalladium cluster by ESI⁺/TOF. However, the mass peak corresponded to the cation $[(SC_7H_7P(C_6H_4F)_3Pd)_3]^+$, which exhibited the pattern of the thiol moiety but not that of the rest of the isothiourea. This finding clearly suggested that the C-S bond was activated during the reaction. The addition of 1 equivalent of $AgSbF_6$ upon the full conversion of the thiourea allowed to isolate the cluster in *Scheme 2*, which crystallized in the form of monoclinic red crystals. Surprisingly, these crystals proved to be stable to oxygen and moisture at room temperature and could be handled in air without any precaution. They indeed became the first example of stable and isolable δ-aromatic clusters.

Clusters with different steric and electronic features could be obtained varying the organic fragments on the ligands. This methodology provided Pd_3^+ complexes in good yields, but the scope was limited to aryl substituents *(Table 1)*.

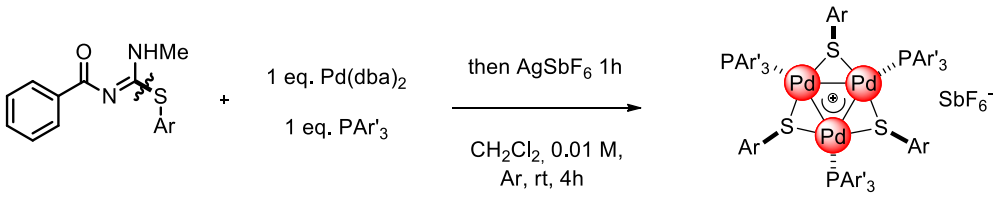

Entry	Complex	Ar	Ar'	Yield (%)
1	7	4-Me-C_6H_4	4-F-C_6H_4	93
2	8	4-Me-C_6H_4	4-Me-C_6H_4	84
3	9	4-NH_2-C_6H_4	4-F-C_6H_4	75
4	10	Ph	Ph	88
5	11	4-OMe-C_6H_4	Ph	81
6	12	4-Cl-C_6H_4	4-Me-C_6H_4	91

Table 1: Pd_3^+ clusters obtained through the first generation synthetic method

As the matter of fact, intractable mixtures and very low yields were obtained with alkyl phosphines or alkyl isothioureas.

The high selectivity towards the desired clusters and the good yields were of course attractive, but the synthesis of the isothiourea revealed to be much less convenient. Our research group recently improved the procedure to obtain isothioureas, establishing a new protocol consisting in two reaction steps from isothiocyanates derivatives *(Scheme 3)*.[29]

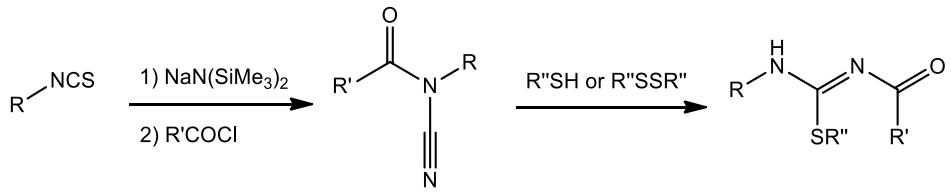

Scheme 3: Two-step synthesis of isothioureas from isothiocyanates

This method allowed to obtain isothioureas with different substituents in yields from 19 to 93%. Thinking about our reaction however, time and atom economy were limited, since just the thiolate moiety was kept in the cluster structure. An improvement in the synthetic methodology was at this point required.

1.1.3.2 Second generation synthesis of Pd_3^+ clusters

A great improvement was achieved in 2015, when the research group developed a simple synthetic method to obtain Pd_3^+ clusters *(Scheme 4)*.[30] Disulfides seemed to be much more convenient as starting materials, since it was well known that Pd(0) can catalyse the addition of disulfides and

[29] a) G. Maestri, M. H. Larraufie, C. Ollivier, M. Malacria, L. Fensterbank, E. Lacôte, *Org. Lett.*, **2012**, *14*, 5538; b) M. H. Larraufie, G. Maestri, M. Malacria, C. Ollivier, L. Fensterbank, E. Lacôte, *Synthesis*, **2012**, *44*, 1279.

[30] Y. Wang, P.-A. Deyris, T. Cañeque, F. Blanchard, Y. Li, F. Bigi, R. Maggi, S. Blanchard, G. Maestri, M. Malacria, *Chem. –Eur. J.*, **2015**, *21*, 12271.

diselenides on terminal alkynes.[31] This strategy allowed to overcome the issues concerning the isothioureas. Pd_3^+ clusters were obtained in chloroform upon the reaction between $Pd(dba)_2$ with one equivalent of phosphine and 0.5 equivalents of disulfide.

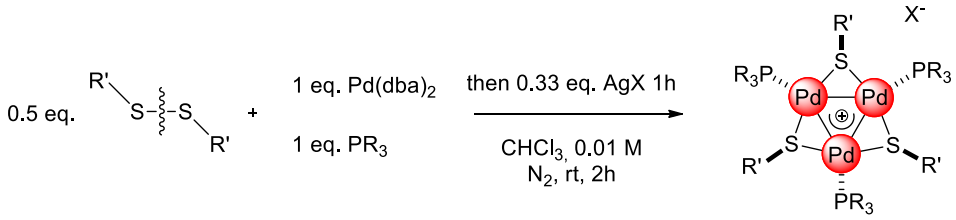

Scheme 4: Second generation synthesis of Pd_3^+ clusters

After 2 hours of stirring and the addition of 0.33 equivalents of a silver salt, the desired complex could be obtained without the formation of any relevant byproduct. In contrast with the first generation synthesis, the reaction in dichloromethane did not work. To purify the cluster, the crude mixture was simply filtered on a short pad of celite to remove silver salts and any possible traces of black metals, then volatiles were removed under vacuum. The solid was washed with a mixture of chloroform/hexane in a ratio 1/30 v/v to afford the precipitation of the product and to remove dba from the mixture. The resulting solid easily recrystallized by vapour diffusion using $CHCl_3$/hexane or THF/hexane. The present method revealed much more effective than the previous one. First of all, it required the employment of commercial reagents, avoiding the time consuming synthesis of isothioureas. In addition, it also tolerated alkyl groups on thiolates and phosphines, allowing to extend the scope of the reaction.

[31] I. Beletskaya, C. Moberg, *Chem. Rev.*, **1999**, *99*, 3435.

Entry	Complex	R'	R	X	Yield (%)	Yield 1st gen. synth. (%)
1	7	4-Me-C_6H_4	4-F-C_6H_4	SbF_6	89	93
2	10	Ph	Ph	SbF_6	99	88
3	12	4-Cl-C_6H_4	4-Me-C_6H_4	SbF_6	97	91
4	13	4-Cl-C_6H_4	4-F-C_6H_4	SbF_6	90	
5	14	4-Cl-C_6H_4	4-Me-C_6H_4	CF_3COO	89	
6	15	4-Cl-C_6H_4	4-MeO-C_6H_4	SbF_6	80	
7	16	Me	4-F-C_6H_4	SbF_6	85	
8	17	Me	4-Me-C_6H_4	SbF_6	94	
9	18	4-Me-C_6H_4	Et	SbF_6	98	
10	19	4-Cl-C_6H_4	Et	SbF_6	97	
11	20	Me	Ph	BF_4	91	

Table 2: Pd_3^+ clusters obtained through the second generation synthetic method

The non coordinating counterion can also be tuned in order to introduce tetrafluoroborate or triflate instead of hexafluoroantimonate.

Table 2 highlights the improvement both in terms of the feasibility of the reaction and the number of structures available.

1.1.3.3 Analogues of Pd_3^+ clusters

The second generation synthetic methodology enabled to vary both the transition metal and the bridging ligand. Regarding the metal core, palladium could be successfully replaced by the isoelectronic platinum. The standard protocol was repeated using $Pt(dba)_3$ as precursor of Pt(0) and lead to obtain two examples of triplatinum clusters.

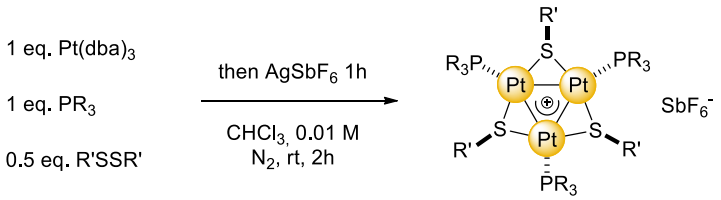

Entry	Complex	R'	R	Yield (%)
1	21	4-Cl-C_6H_4	4-F-C_6H_4	60
2	22	Me	4-Me-C_6H_4	40

Table 3: Pt_3^+ clusters obtained through the second generation synthetic method

The scope of the reaction with platinum is quite limited and yields are much lower compared to those of palladium clusters *(Table 3)*. Issues probably concern the higher difficulty of $Pt(dba)_3$ to lose three ligands instead of two as in the case of $Pd(dba)_2$ and the requirement of an additional chromatographic purification to afford the pure cluster. As the matter of fact, standard washings with chloroform/hexane can efficiently remove dba, but were inefficient towards the removal of the other byproducts formed during the reaction.

In addition, sulphur in the bridging position could be replaced by selenium, since Pd(0) can easily undergo oxidative addition on diselenides too. Examples of clusters with selenium in the bridging position could be obtained both with palladium and platinum *(Table 4)*.

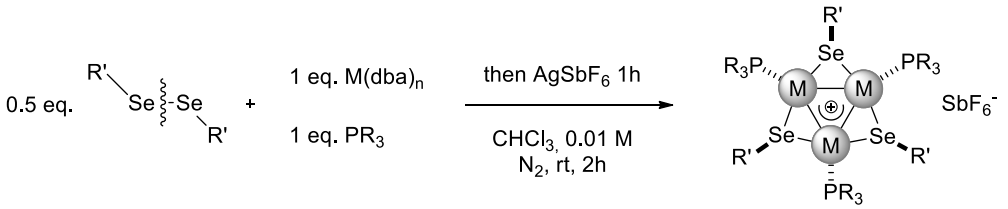

Entry	Complex	M	R'	R	Yield (%)
1	23	Pd	Ph	4-F-C_6H_4	50
2	24	Pt	Ph	4-F-C_6H_4	41

Table 4: M_3^+ clusters with bridging selenolates obtained through the second generation synthetic method

Clusters with 4-fluorophenyl phosphine and methyl selenolate of palladium and platinum could be accessed in 50 and 41% yields. Even in this case a chromatographic purification was required, since the selectivity towards the formation of the desired complex was slightly lower.

To summarize, analogues of Pd_3^+ clusters with platinum or selenium are more difficult to obtain. Nevertheless, the proposed methodology proved to be practical and tolerant to different fuctional groups.

1.1.3.4 Steric and electronic properties

Crystallization of Pd_3^+ or Pt_3^+ clusters by vapour diffusion using THF/hexane or $CHCl_3$/hexane provided crystals suitable for X-Ray analysis *(example in Fig. 5)*. Such complexes have a metal core of three palladium or platinum atoms, each one bearing a phosphinic ligand. Thiolates or selenolates occupy instead the bridging position between metal atoms.

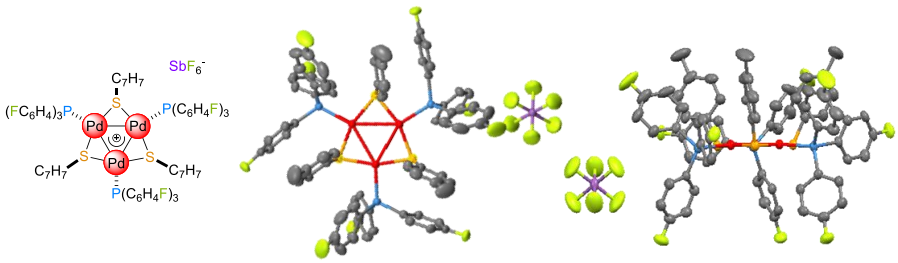

Fig. 5: X-Ray structure of Pd_3^+ cluster ***7***

Pd_3^+ is a triangular cluster with a C_3 symmetry. The three metal-metal distances in **7** are exactly equal at 2.8872(1) Å, which is below the sum of their Van der Waals radii (3.26 Å). This distance is comparable to that reported for 44 cve tripalladium clusters[32] and to that of some palladium (II) dimers showing d_8-d_8 bonding interactions.[33] The three angles of the palladium triangle are 60.00(2)°, demonstrating that the triangle is perfectly equilateral. The Pd-S-Pd and S-Pd-S angles are 78.40(3)° and 161.38(4)° respectively, while Pd-S and Pd-P distances are 2.284(2) and 2.306(2) Å. The first sphere of coordination exhibits a D_{3h} symmetry and all the heteroatoms which complete the first sphere of coordination of palladium atoms are coplanar to the metal core. The phosphines point slightly out of the plane, as indicated by the corresponding dihedral angle of 8.2(1)°, while the aryl groups of the thiolate moieties are nearly perpendicular to the plane containing metals (112.3(1)°). All the phosphines point in the same direction, while all the substituents on the bridging ligands point in the opposite direction, giving a trans 1,2 relationship relative to the Pd_3^+ cycle.

The high symmetry of Pd_3^+ clusters is also highlighted by multinuclear NMR analysis. ^{31}P NMR shows one broad resonance, even at -80°C when dynamic processes should be inhibited. Organic fragments on thiolate ligands exhibit the same behaviour, since a single pattern of signals can be observed in the ^1H NMR spectrum. In addition, chemical shifts of aromatic protons of aryl-thiolates are unusually upfield shifted compared to those observed for

[32] A. D. Burrows, D. M. P. Mingos, *Coord. Chem. Rev*., **1996**, *154*, 19.

[33] a) T. Murahashi, H. Kurosawa, *Coord. Chem. Rev*., **2002**, *231*, 207; b) L. M. Mirica, J. R. Khusnutdinova, *Coord. Chem. Rev*., **2013**, *257*, 299; c) C. Eerdun, S. Hisanaga, J.-i. Setsune, *Angew. Chem.*, **2013**, 1*25*, 963; *Angew. Chem. Int. Ed.*, **2013**, 52, 929; d) T. Murahashi, K. Takase, M.-a. Oka, S. Ogoshi, *J. Am. Chem. Soc.*, **2011**, 1*33*, 14908; e) G. Maestri, E. Motti, N. Della Cà, M. Malacria, E. Derat, M. Catellani, *J. Am. Chem. Soc.*, **2011**, 1*33*, 8574.

palladium thiolate complexes.[34] The symmetry at the solid state is indeed retained even in solution.

This trinuclear cluster has 44 core valence electrons, which is a quite rare feature among the previously reported trinuclear palladium clusters. The metal core is formally composed by two palladium (I) and a palladium (II). However, it should be more appropriate to attribute a formal oxidation state of +4/3 to each palladium atom, since the triangle is perfectly equilateral and displays an overall C_3 symmetry. Further insights into the origin of this high symmetry were acquired through a theoretical approach. DFT calculations were performed on complex **10**. The crystalline structure was used as starting geometry with different DFT functionals (BP86, B3LYP, M06) and the optimizations were then performed without any symmetry constraint. No matter which linear or cyclic combination of fragments was used as initial geometry, the optimization led invariably to the same quasi-symmetric triangular structure, suggesting that it has a global-minimum character. All the calculated atomic charges of the same elements were indeed nearly identical and the largest differences in bond lengths were in the ppm range in all cases. The geometry calculated at the M06/def2-svp level of theory provided the best correlation with the solid state structure.

The most interesting orbitals are shown in *Figure 6*. Energies are given relative to the HOMO and atomic orbital contribution is indicated in brackets. Phenyl groups are omitted for clarity.

[34] a) M. Bierenstiel, E. D. Cross, *Coord. Chem. Rev*., **2011**, *255*, 574; b) V. K. Jain, L. Jain, *Coord. Chem. Rev*., **2005**, *249*, 3075; c) S. Brooker, *Coord. Chem. Rev*., **2001**, *222*, 33.

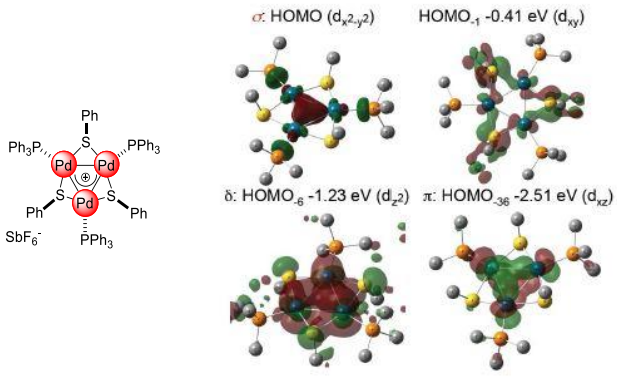

*Fig. 6: Relevant molecular orbitals of complex **10***

The HOMO is a delocalized three-centers, two-electrons bond. This is a σ-type bonding orbital, which derives from the combination of d_{x2-y2} atomic orbitals (top left). Other valence d orbitals are mainly engaged in back donation to the sulphur atoms. $HOMO^{-1}$ (top right) originates for example from d_{xy} palladium orbitals. The antibonding repulsion in the C_3-symmetric framework is minimized by their combination with sulphur p orbitals in a hexagonal array. The $HOMO^{-6}$ (bottom left) results instead from the overlap of the d_{z2} orbital of each palladium atom, settling far below the HOMO at -1.23 eV. It is a δ-type orbital characterized by two nodal surfaces perpendicular to the C_3 axis of the molecule and by a plane of symmetry, which corresponds to the plane of the triangle. Finally the $HOMO^{-36}$ is a π molecular orbital that results from the partial overlap of d_{xy} atomic orbitals and lies -2.51 eV below the HOMO.

The cyclic delocalization can indeed explain the structural observations, equal metal-metal distances and one angle for the triangle, making the three palladium atoms equivalent.

Natural bond orbital analysis on the same complex was then performed to confirm the original atomic orbital contribution to the delocalized bond responsible for aromaticity. The cluster presents a delocalized bonding HOMO deriving from a combination of atomic orbitals with a d-type character

between 49 and 94% depending on the basis set, together with a smaller p-type hybridization between 4 and 27%. These data confirm that Pd_3^+ has a d-orbital aromaticity.

Adaptive natural density partitioning (AdNDP) is another theoretical approach for obtaining patterns of chemical bonding, which could be useful to establish the presence of aromaticity.[35] The analysis on a model cluster in which aromatic rings were replaced by hydrogen atoms, $[PdSHPH_3]_3^+$, revealed the presence of a multicenter, delocalized, three-center, two electron bonds between the palladium atoms with a σ-like symmetry.

Taken together, these features make our clusters the noble-metal analogues of the π-aromatic, D_{3h}-symmetric cyclopropenyl cation $[C_3H_3]^+$. For comparison, the same analysis were performed on two model 42 and 44 cve tripalladium clusters, $[Pd(CO)PPh_3]_3$ and $[Pd_3(CO)_2dppm_3]^{2+}$ commonly considered non-aromatic. As expected, they did not show any delocalized orbitals among the three palladium atoms.

Finally nucleus-indipendent chemical shift (NICS) measurements[36] confirmed the presence of an aromatic ring. Chemical shifts calculated for the complex in *Figure 7* along the axis perpendicular to the plane of the triangle are always negative up to 5 Å above the palladium triangle *(Fig. 7, bottom)*, confirming the presence of an aromatic ring.

[35] D. Y. Zubarev, A. I. Boldyrev, *Phys. Chem. Chem. Phys*., **2008**, *10*, 5207.
[36] Z. Chen, C. S. Wannere, C. Corminboeuf, R. Putcha, P. V. Schleyer, *Chem. Rev*., **2005**, *105*, 9888.

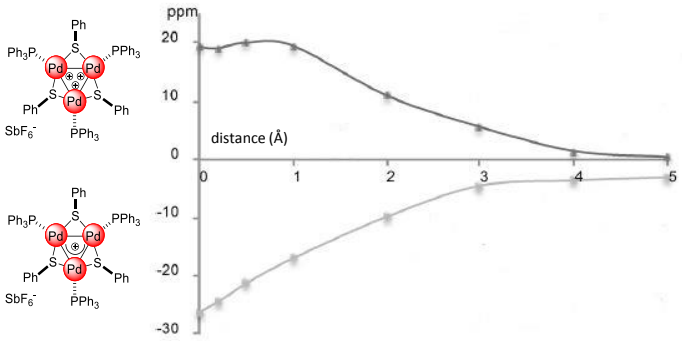

*Fig. 7: $NICS_{zz}$ analysis on complex **10** and its tricationic analogue*

The same analysis was then performed on a theoretical analogue of complex **10** in which the two electrons responsible for metal aromaticity were removed. As expected, values obtained were always positive, in agreement with the absence of aromaticity *(Fig. 7, top)*.

The presence of an aromatic ring in the cluster can also explain the unusual upfield shifted chemical shifts of aryl substituents on the bridging ligands, since they likely point in the shielding cone.

The presence of a ring current could be assessed measuring the magnetic susceptibility by SQUID experiments. In the case of aromatic delocalization, high magnetic susceptibility values should be obtained. For example, a paramagnetic molecule with spin ½, such as TEMPO (2,2,6,6-tetramethylpiperidin-1-oxyl), shows a susceptibility value (χT) of 0.5 emuKmol^{-1} at room temperature, while non-aromatic diamagnetic derivatives show no significant susceptibility. Analysis on complex **10** gave a χT of 0.41 emuKmol^{-1} at 300K, while the non-aromatic $[Pd(CO)PPh_3]_3$ gave a value of one order of magnitude lower, 0.031 emuKmol^{-1} at 300K. In addition, while magnetic susceptibility usually decreases proportionally with the temperature, the susceptibility of Pd_3^{+} cluster proved to be independent from temperature

in the 20-300K range, in agreement with other examples of diamagnetic molecules featuring a ring current.[37]

[37] a) J. Aihara, *J. Am. Chem. Soc*., **2006**, *128*, 2873; b) C. Lupu, C. Downie, A. M. Guloy, T. A. Albright, J. G. Mao, *J. Am. Chem. Soc*., **2004**, *126*, 4386; c) F. De Proft, P. V. Schleyer, J. H. van Lenthe, F. Stahl, P. Geerlings, *Chem. Eur. J*., **2002**, *8*, 3402; d) J. A. N. F. Gomes, R. B. Maillion, *Chem. Rev*., **2001**, *101*, 1349.

1.2 Results and discussion

1.2.1 Studies on the mechanism of formation of Pd_3^+ complexes

To gain insights into factors governing the formation of delocalized metal-metal bonds, we tried to monitor the synthesis of the Pd_3^+ complex by NMR. We mixed 0.2 mmol of $Pd(dba)_2$, 0.2 mmol of PPh_3 and 0.1 mmol of diphenyldisulfide in 20 mL of $CDCl_3$, then we took 0.5 mL samples at regular intervals to record ^1H and ^{31}P NMR spectra. Surprisingly the broad and diagnostic ^{31}P resonance of the Pd_3^+ cation at 15.5 ppm was already visible after just a few minutes and the free phosphine at -5 ppm was no longer present *(Fig. 8)*.

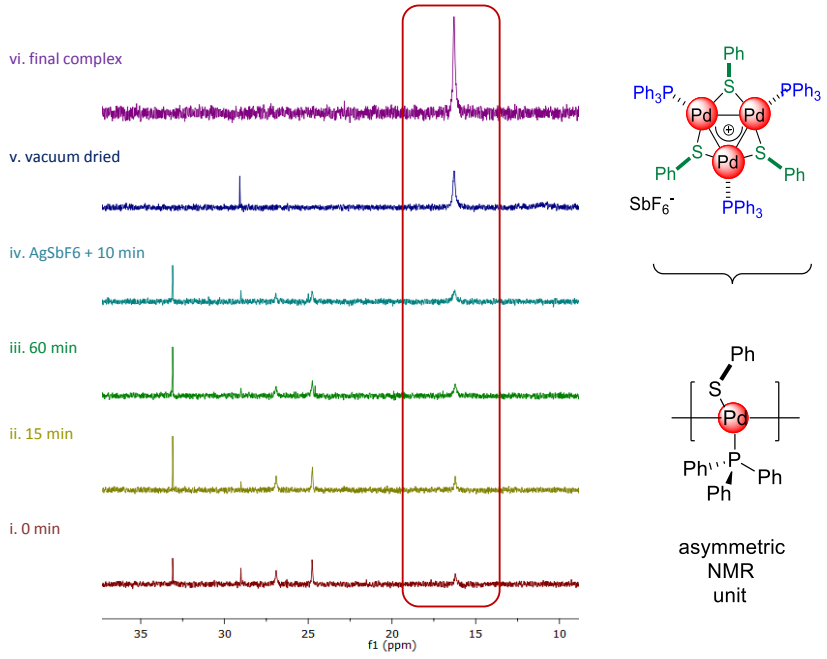

*Fig. 8: ^{31}P NMR spectra of crude samples from the synthesis of complex **10** highlighting its diagnostic resonance*

Two other broad ^{31}P resonances were observed at 24 and 27 ppm, but we were so far unable to unambiguously assign these signals. Their intensity slowly decreases through time with a corresponding increase of the resonance at 15.5 ppm. 60 minutes upon the beginning of the reaction the yield of Pd_3^+ corresponded to 40% (green line) and the subsequent addition of 0.33 eq. of $AgSbF_6$ resulted in a further increase of the desired resonance. Upon filtration over celite and concentration in vacuo the Pd_3SbF_6 complex became the almost exclusive species in the crude mixture (blue line, 86% isolated yield).

Taken together, these findings let to suppose that the addition of the silver salt was not necessary to promote the formation of the metal aromatic Pd_3^+ cluster. The chlorinated solvent instead could play the key role in the formation of the metal core.

The overall process involves the formal oxidation of Pd(0) to Pd(4/3). Considering the stoichiometry of the reaction, the disulfide can oxidise the noble metal to Pd(I). Radical palladium species[38] might be sufficiently strong reductants to promote SET (single electron transfer) on a chloroform molecule (-1.09 V vs. SCE):[39] this would form the corresponding radical anion, which eventually collapses into a radical and a chloride ion. The formal oxidation of a cationic Pd(II) fragment on a neutral Pd(I) dimer would then deliver the Pd_3^+ cation isolable as chloride salt, in analogy to the step-wise assembly of Au_3^+ complexes from an Au(I) cation and an Au(0) dimer reported by Bertrand.[26]

Pd_3^+ cation barely forms in CH_2Cl_2, while its formation is almost instantaneous in CCl_4, despite the low solubility of $Pd(dba)_2$ in the solvent. These results

[38] a) G. Maestri, M. Malacria, E. Derat, *Chem. Commun*., **2013**, *49*, 10424; b) T. Troadec, S. Y. Tan, C. J. Wedge, J. P. Rourke, P. R. Unwin, A. B. Chaplin, *Angew. Chem. Int. Ed*., **2016**, *55*, 3754; c) G. Manolikades, P. Knochel, *Angew. Chem. Int. Ed*., **2009**, *48*, 205; d) Q. Liu, X. Dong, H. Liu, *ACS Catal.*, **2015**, *5*, 6111.

[39] a) A. Studer, D. Curran, *Nat. Chem*., **2014**, *6*, 765; b) J. Bertrand, I. Gallardo, M. Moreno, J. M. Saveant, *J. Am. Chem. Soc*, **1992**, *114*, 9576; c) X. Q. Hu, X. Qi, J. R. Chen, Q. Q. Zhao, Q. Wei, Y. Lan, W. J. Xiao, *Nat. Commun*., **2016**, *7*, 11188.

match with the trend of C-Cl BDE and reduction potentials among chlorinated solvents.[39]

The addition of AgX salts thus just favours the anion metathesis, promoted by the precipitation of AgCl in chloroform. This suggests that Pd_3^+ complexes can be synthesized in any solvent if a suitable mild stoichiometric oxidant is added.

Intrigued by these results we decided to go deeper into these phenomena performing some additional experiments.

Addition of twofold excess of phosphine to the standard method for the synthesis of Pd_3^+ complexes inhibited their formation. From this reaction we were able to isolate and characterize a mono and a dimeric Pd(II) complexes *(Fig. 9)* that we found useful to better understand the mechanism of formation of metal aromatic clusters.[40]

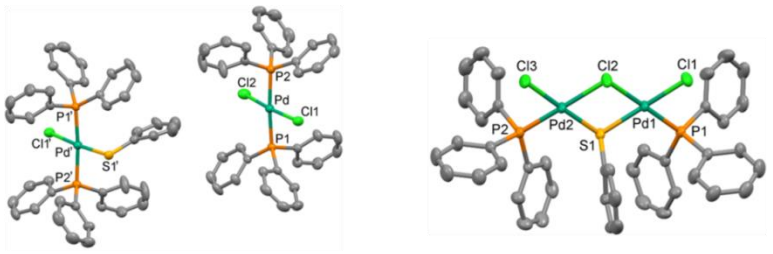

*Fig. 9: X-Ray structures of complexes **25** (left) and **26** (right)*

In $[Pd(PPh_3)_2(PhS)Cl][Pd(PPh_3)_2Cl_2]$ (**25**) the asymmetric unit comprises two cocrystallized square planar Pd(II) complexes, namely $[Pd(PPh_3)_2(PhS)Cl]$ and $[Pd(PPh_3)_2Cl_2]$. The phosphorous atoms are in trans position in both systems. In $[Pd(PPh_3)_2(PhS)Cl]$ a thiolate group is in trans to the chloride anion, while $[Pd(PPh_3)_2Cl_2]$ is more symmetric since two chloride anions complete the first metal coordination sphere.

[40] A. Monfredini, V. Santacroce, L. Marchiò, R. Maggi, F. Bigi, M. Malacria, G. Maestri, *ACS Sustainable Chem. Eng*., **2017**, *5*, 8205.

Dimer $[Pd_2(PPh_3)_2(PhS)Cl_3]$ (**26**) presents a symmetric dinuclear structure in which the Pd atom possess a square planar geometry with a terminal chloride anion, a bridging thiolate and a bridging chloride anion. The Pd-Cl_{bridge} bond distance are approximately 0.1 Å, slightly longer than the Pd-$Cl_{terminal}$ ones. The molecular structure is similar to dinuclear complexes with bridging thiolates and chloride anions.[41] While literature examples present a clam shell arrangement, in our case the dimer remains perfectly flat.

Most importantly, both complexes represent the proof that the chlorinated solvent is actually a reagent, supporting our preliminary hypothesis that the oxidation of Pd(0) is most likely to occur via single electron transfer involving both a chlorinated solvent with a suitable C-H BDE and the disulfide.

[41] a) E. M. Padilla, J. A. Golen, P. N. Richmann, C. M. Jensen, *Polyhedron*, **1991**, *10*, 1343; b) J. H. Yamamoto, G. P. A. Yap, C. M. Jensen, *J. Am. Chem. Soc*, **1991**, *113*, 5060; c) V. K. Jain, R. P. Patel, K. V. Muralidharan, R. Bohra, *Polyhedron*, **1989**, *8*, 2151.

1.2.2 Zwitterionic clusters

Reasoning on the fact that the Pd_3^+ species could be formed in chloroform even without the addition of any other metal salts, we decided to exploit this finding to attempt the synthesis of a zwitterionic cluster.

We performed the reaction with 0.33 equivalents of a sodium sulfonate phosphine without adding the silver salt and we subsequently filtered off the coproduct NaCl. We managed to obtain the desired zwitterionic cluster with a sulfonated phosphine that could act as counterion for the Pd_3^+ cluster *(Scheme 5)*.

We then prepared a library of such complexes with different steric and electronic features varying the organic fragments *(Table 5)*.[42]

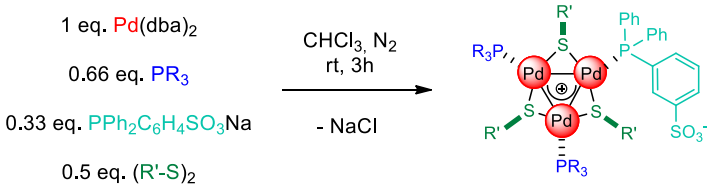

Entry	Complex	R	R'	Yield (%)
1	27	4-F-C_6H_4	4-Me-C_6H_4	71
2	28	4-F-C_6H_4	Me	55
3	29	4-Me-C_6H_4	Ph	59
4	30	4-Me-C_6H_4	Me	72
5	31	Ph	C_6H_5	52

*Scheme 5: Synthesis of zwitterionic clusters **27-31***

Table 5: Zwitterionic clusters bearing two neutral phosphines and a sulfonate phosphine

[42] A, Monfredini, V. Santacroce, P.-A. Deyris, R. Maggi, F. Bigi. G. Maestri, M. Malacria, *Dalton Trans.*, **2016**, *45*, 15786.

Complexes **27-31** could be purified through a series of solvent washings by using a mixture of chloroform/hexane = 1/60 v/v.

We performed the same reaction using 1 equivalent of the sodium sulfonate phosphine and we obtained the corresponding zwitterionic clusters with an anionic phosphine and two phosphines with Na^+ still on the sulfonate group *(Scheme 6, Table 6)*.

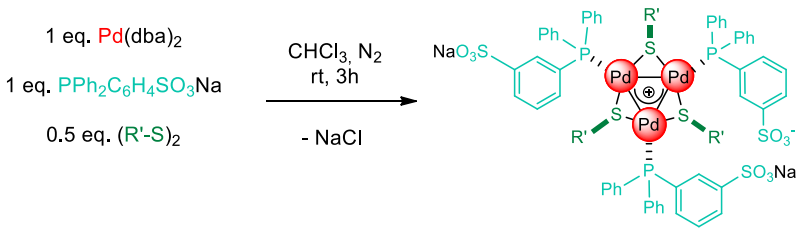

Entry	Complex	R'	Yield (%)
1	32	Me	72
2	33	C_6H_5	79

*Scheme 6: Synthesis of zwitterionic clusters **32** and **33***

Table 6: Zwitterionic clusters bearing three sulfonate phosphines

The increased number of ionic couples makes complexes **32** and **33** significantly less soluble in chloroform compared to complexes **27-31**. They could thus be easily purified by precipitation in chloroform after the Schlenk filtration.

Reasoning on the fact that the low solubility of **32** and **33** in apolar and medium-polar solvents could hamper further applications, we tried to increase the solubility replacing the sodium cations with two tetrabutylammonium moieties. These could be easily introduced by ligand exchange on complex **32** *(Scheme 7)*.[40]

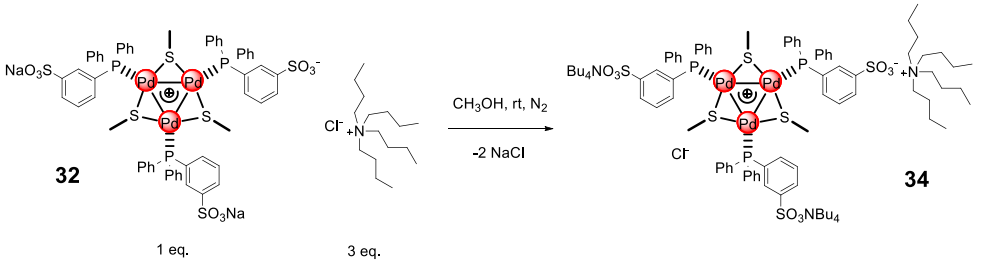

*Scheme 7: Synthesis of zwitterionic cluster **34***

Complex **34** was obtained in methanol in quantitative yield.

Clusters **27-34** were characterized by HRMS or MS analysis and multinuclear NMR experiments.

In contrast to C_3-symmetric Pd_3X complexes, which showed $[Pd_3]^+$ cations in ESI^+ experiments, we invariably observed protonated molecular adducts for complexes **27-31**, confirming their zwitterionic nature.

Regarding NMR, two patterns of resonances in 2 : 1 ratio were observed for the bridging thiolate fragments in the ^1H-NMR spectra. ^{31}P signals showed the same behaviour since a broad triplet and two overlapping broad doublets corresponding to the sulfonated and neutral phosphines respectively were observed in a 1 : 2 ratio for each of them *(Fig. 10)*.

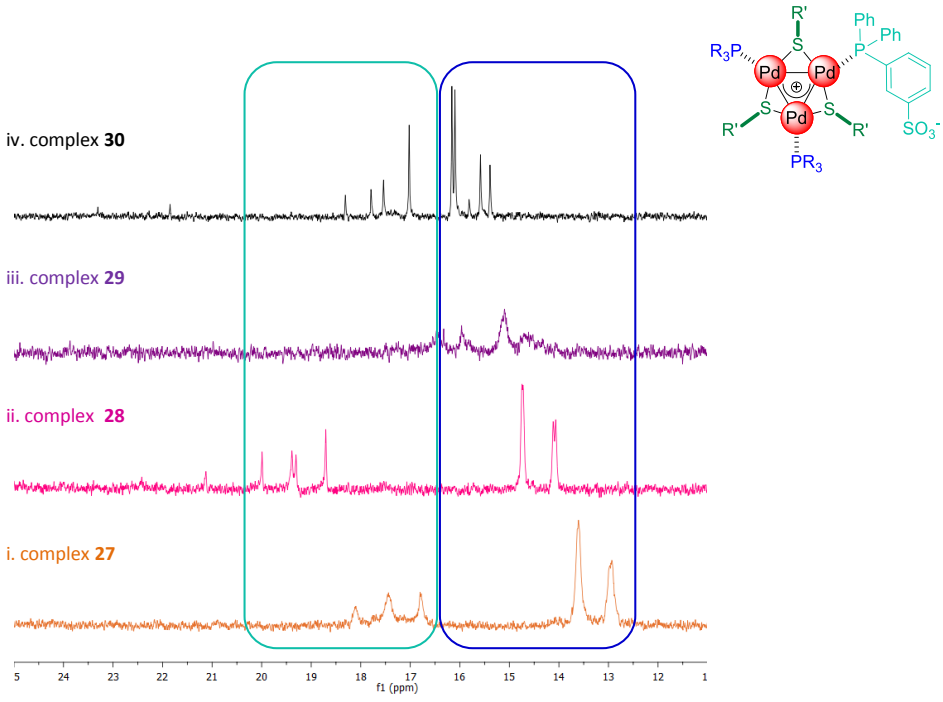

*Fig.10: ^{31}P NMR spectra of clusters **27-30** highlighting the diagnostic pattern of resonances*

The high mobility of the sulfonate groups made any attempt of crystallization unsuccessful. With the purpose of gaining more information about their structure we performed a DFT analysis using Gaussian09 *(Fig. 11)*.

The X-ray structure of complex **17** was taken as starting point. It presents three identical Pd-P distances (2.2612(11) Å). Full optimization without any constraint of its Pd_3^+ cation was carried out at the M06/lacvp(d), M06/Def2-svp and M11/lacvp(d) level, since these models proved accurate to describe the delocalized metal-metal bonding of these complexes.[28] In all cases the optimized structures remained very similar to that observed at the solid state. The best correlation was obtained with the M11 functional, but in all the three calculated structures the cation **17** presents three degenerate Pd-P distances. With the three levels described above the distances are 2.3480, 2.3381 and 2.2979 Å respectively.

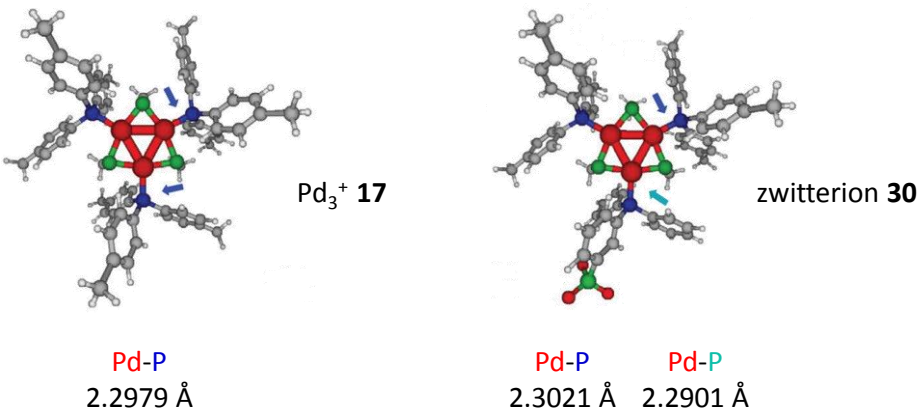

*Fig. 11: Comparison of optimized structures of cationic complex **17** and zwitterionic complex **30** (optimization obtained at the M11/lacvp(d) level)*

We then modelled zwitterionic complex **30** at the same level. The Pd-P distance of the sulfonated phosphine becomes slightly shorter in all the three cases, 2.3423, 2.3311 and 2.2901 Å at the M06/lacvp(d), M06/Def2-svp and M11/lacvp(d) level respectively. This finding is consistent with a relatively stronger Pd-P($Ph_2C_6H_4SO_3^-$) bond. On the contrary, the Pd-P bond on the other side of the metal core moved inversely and the distance results slightly longer than those observed with cation **17**. Values in the three cases are 2.3518, 2.3399 and 2.3021 Å respectively. This is consistent with a relatively weaker Pd-P(C_7H_7)$_3$ bond and could lead to interesting implications in catalysis.

1.3 Conclusions

Studies on the mechanism of formation of Pd_3^+ complexes let us to state that the oxidation of Pd(0) occurs via single electron transfer involving both a chlorinated solvent with a suitable C-H BDE and the disulfide. In addition, this approach let us to extend the number of structures available since we synthesized a family of zwitterionic tripalladium clusters. They feature a Pd-P($Ph_2C_6H_4SO_3^-$) bond stronger than the other two Pd-P bonds involving the

neutral phosphine, in agreement with the presence of a *trans*-like effect of the anionic ligand that would make the phosphines on the opposite edge of the cluster more labile. Catalytic properties arising from this effect will be discussed in *Chapter 2*.

1.4 Experimental section

1.4.1 General remarks

$Pd(dba)_2$, disulfides and phosphines were purchased from commercial sources and used as received. 3-(Diphenylphosphino)benzenesulfonic acid sodium salt was kept under vacuum for at least 30 minutes prior to use. Solvents were degassed by bubbling N_2 for at least 40 minutes prior to use. Reactions and filtrations were carried out under N_2 using standard Schlenk technique.

^1H NMR spectra were recorded in $CDCl_3$ or methanol-d_4 at 298 K on Bruker 400 AVANCE and Bruker 300 AVANCE spectrometers fitted with a BBFO probe-head at 400 and 300 MHz respectively, using the solvent as internal standard (7.26 ppm for $CDCl_3$ and 3.34 ppm for methanol-d_4).

^{31}P NMR spectra were recorded in $CDCl_3$ or methanol-d_4 at 298 K on a Bruker 400 AVANCE spectrometer fitted with a BBFO probe-head at 162 MHz, using 85% H_3PO_4 as external standard (0 ppm).

^{19}F NMR spectra were recorded in $CDCl_3$ at 298 K on a Bruker 400 AVANCE spectrometer fitted with a BBFO probe-head at 376 MHz, using hexafluorobenzene as external standard (-164.9 ppm).

The terms m, s, d, t, q represent multiplet, singlet, doublet, triplet, quadruplet respectively, and the term br means a broad signal.

Exact masses of complexes **27**-**30** and **34** were recorded on a LTQ ORBITRAP XL Thermo Mass Spectrometer (electrospray source). Mass analysis on complex **31**, **32** and **33** were performed on an Infusion Water Acquity Ultra Performance LC HO6UPS-823M instrument (electrospray source, quadrupole analyser).

1.4.2 Synthesis of zwitterionic tripalladium complexes 27-31

$Pd(dba)_2$ (1 eq., 0.2 mmol, 115 mg) was added to a 50 ml schlenk and the vessel underwent at least three vacuum/N_2 cycles. 20 ml of freshly degassed

$CHCl_3$ were immediately syringed under N_2 to obtain a deep red solution. 3-(Diphenylphosphino)benzenesulfonic acid sodium salt (0.33 eq., 0.066 mmol, 24 mg), the desired phosphine (0.66 eq., 0.132 mmol) and disulfide (0.5 eq., 0.1 mmol) were then added under N_2. The resulting mixture was kept under magnetic stirring at room temperature for 3 hours and then filtered through a celite pad under N_2 to remove NaCl and traces of black metals. The solvent was removed under vacuum and the resulting solid was purified by $CHCl_3$/hexane washings (1/60 v/v, 3x30 ml). Pure clusters were obtained as orange/red solids. Zwitterionic clusters **27-31** were characterized by HRMS or MS analysis and ^{1}H, ^{31}P, ^{19}F NMR spectroscopy.

1.4.3 Synthesis of zwitterionic tripalladium complexes 32-33

$Pd(dba)_2$ (1 eq., 0.2 mmol, 115 mg) was added to a 50 ml schlenk and the vessel underwent at least three vacuum/N_2 cycles. 20 ml of freshly degassed $CHCl_3$ were immediately syringed under N_2 to obtain a deep red solution. 3-(Diphenylphosphino)benzenesulfonic acid sodium salt (1 eq., 0.2 mmol, 73 mg) and the desired disulfide (0.5 eq., 0.1 mmol) were then added under N_2. The resulting mixture was kept under magnetic stirring at room temperature for 3 hours and then filtered through a celite pad under N_2 to remove NaCl and traces of black metals. The product was allowed to precipitate in chloroform for at least 3 hours. The red solution was filtered off to afford an orange solid. Zwitterionic clusters **32** and **33** were characterized by MS analysis and ^{1}H, ^{31}P NMR spectroscopy.

1.4.4 Synthesis of zwitterionic tripalladium complex 34

Cluster **32** (40.0 mg, 0.026 mmol, 1 eq.,) and tetrabutylammonium chloride (21.8 mg, 0.078 mmol, 3 eq.) were introduced in a Schlenk-type flask and the vessel underwent at least three vacuum/N_2 cycles. 10 ml of freshly degassed methanol were then syringed under N_2 and the resulting orange solution was

stirred at room temperature for 2 hours. Methanol was removed under vacuum and 10 ml of degassed chloroform were added to the solid residue. The resulting suspension was then filtered through a celite pad under $N_2$to remove NaCl. Volatiles were removed under vacuum to obtain a red solid (quantitative yield).

1.4.5 Spectroscopic data of complexes 25-26

- **Complex 25**

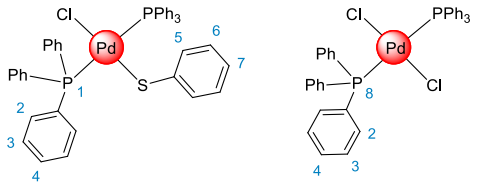

Isolated as violet crystals obtained upon crystallization by vapour diffusion using $CHCl_3$/hexane.

Spectroscopic data of each complex that cocrystallized in **25** are in accordance with those described in the literature.[43] They proved however unstable under MS conditions.

^{1}H NMR (400 MHz, $CDCl_3$) δ (ppm): 7.68 (m, 24H, H_2), 7.40 (m, 36H, $H_{3\text{-}4}$), 6.86 (d, *J* = 7.68 Hz, 2H, H_5), 6.64 (t, *J* = 7.40 Hz, 1H, H_7),6.54 (t, *J* = 7.61 Hz, 2H, H_6).

^{31}P NMR (162 MHz, $CDCl_3$) δ (ppm): 23.26 (s, P_8), 25.00 (s, P_1).

[43] a) T. Boschi, B. Crociani, L. Toniolo, U. Bellucco, *Inorg. Chem.,* **1970**, *9*, 532; b) A. Naghipour, A. Ghorbani-Chogharmarani, H. Babaee, M. Hashemi, B. Notash, *J. Organomet. Chem*. **2017**, *841*, 31.

- **Complex 26**

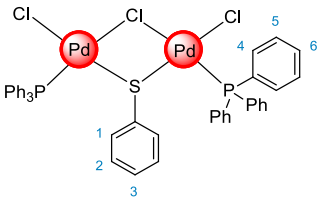

Isolated as yellow crystals obtained upon crystallization by vapour diffusion using $CHCl_3$/hexane.

Complex **26** decomposes in solvents suitable for MS analysis (MeCN, MeOH).

^{1}H NMR (400 MHz, $CDCl_3$) δ (ppm): 7.71 (m, 12H, H_4), 7.40 (m, 23H, $H_{1\text{-}3}$,$H_{5\text{-}6}$).

^{31}P NMR (162 MHz, $CDCl_3$) δ (ppm): 23.25.

1.4.6 Spectroscopic data of clusters 27-34

- **Complex 27**

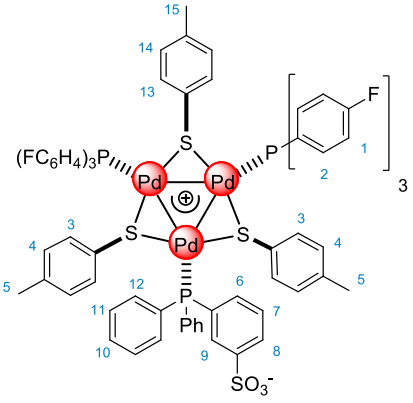

Isolated as a red powder. Yield = 71%

HRMS calculated for $C_{75}H_{60}F_6O_3P_3Pd_3S_4$ $[M+H]^+$: 1662.9680, found: 1662.9676.

^{1}H NMR (400 MHz, $CDCl_3$) δ (ppm): 8.67 (d, J = 14.37 Hz, 1H, H_9), 8.16 (d, J = 7.58 Hz, 1H, H_8), 7.11 (m, 12H, H_1), 7.00 (m, 10H, $H_{10\text{-}12}$), 6.88 (t, J = 8.56 Hz,

12H, H_2), 6.74 (m, 2H, H_6, H_7), 6.52 (d, *J* = 7.87 Hz, 2H, H_{14}), 6.44 (d, *J* = 8.02 Hz, 4H, H_4), 6.16 (d, *J* = 8.03 Hz, 2H, H_{13}), 6.12 (d, *J* = 7.99 Hz, 4H, H_3), 2.17 (s, 3H, H_{15}), 2.14 (s, 6H, H_5).

^{31}P NMR (162 MHz, $CDCl_3$) δ (ppm): 17.45 (t, *J* = 106.92 Hz, $P(C_{18}H_{14}SO_3^-)$), 13.27 (2 overlapping d, *J* = 108.51 Hz, $2P(C_6H_4F)_3$).

^{19}F NMR (376 MHz, $CDCl_3$) δ (ppm): -108.39.

- **Complex 28**

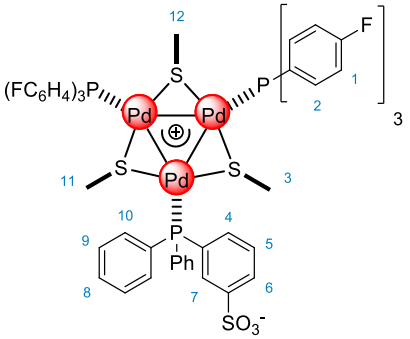

Isolated as an orange powder. Yield = 55%

HRMS calculated for $C_{57}H_{48}F_6O_3P_3Pd_3S_4$ $[M+H]^+$: 1432.8734, found: 1432.8742.

^{1}H NMR (400 MHz, $CDCl_3$) δ (ppm): 8.18 (d, *J* = 7.33 Hz, 1H, H_6), 8.15 (d, *J* = 14.72 Hz, 1H, H_7), 7.49 (m, 24H, H_1, H_4, H_5, $H_{8\text{-}10}$), 7.17 (t, *J* = 8.56 Hz, 12H, H_2), 1.18 (s, 3H, H_3), 1.15 (s, 3H, H_{11}), 1.07 (s, 3H, H_{12}).

^{31}P NMR (162 MHz, $CDCl_3$) δ (ppm): 19.35 (dd, *J* = 97.2, 110.79 Hz, $P(C_{18}H_{14}SO_3^-)$), 14.41 (2 overlapping d, *J* = 100.44, 106 Hz, $2P(C_6H_4F)_3$).

^{19}F NMR (376 MHz, $CDCl_3$) δ (ppm): -106.72.

- **Complex 29**

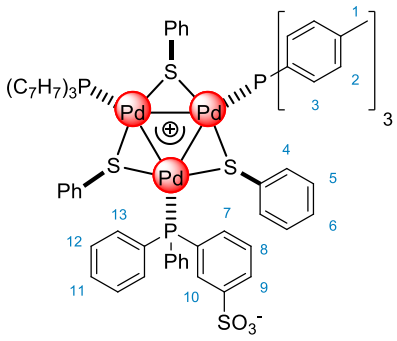

Isolated as a red powder. Yield = 59%

HRMS calculated for $C_{78}H_{72}O_3P_3Pd_3S_4$ $[M+H]^+$: 1597.0716, found: 1597.0702.

^{1}H NMR (400 MHz, $CDCl_3$) δ (ppm): 8.10 (m, 1H, H_{10}), 7.18 (m, 47H, $H_{2\text{-}9}$, $H_{11\text{-}13}$), 6.60 (m, 3H, H_5, H_6), 6.24 (m, 2H, H_4), 2.32 (m, 18H, H_1).

^{31}P NMR (162 MHz, $CDCl_3$) δ (ppm): 16.47 (t, J = 82.62 Hz, $P(C_{18}H_{14}SO_3^-)$), 14.85 (2 overlapping d, J = 79.38 Hz, $2P(C_7H_7)_3$).

- **Complex 30**

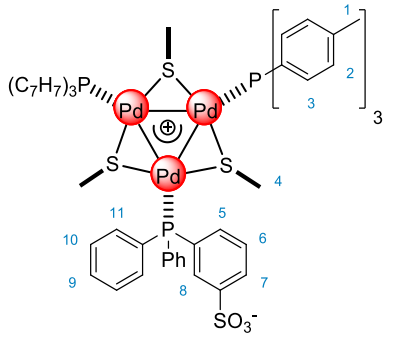

Isolated as an orange powder. Yield = 76%

HRMS calculated for $C_{63}H_{66}O_3P_3Pd_3S_4$ $[M+H]^+$: 1409.0240, found: 1409.0236.

^{1}H NMR (400 MHz, $CDCl_3$) δ (ppm): 8.13 (d, J = 7.94 Hz, 1H, H_7), 8.07 (d, J = 12.80 Hz, 1H, H_8), 7.61 (m, 4H, H_{11}), 7.37 (m, 18H, H_3, H_9, H_{10}), 7.18 (d, J = 7.70

Hz, 12H, H_2), 7.07 (d, *J* = 7.25 Hz, 1H, H_5), 6.92 (d, *J* = 8.07 Hz, 1H, H_6), 2.37 (s, 18H, H_1), 1.05 (m, 9H, H_4).

^{31}P NMR (162 MHz, $CDCl_3$) *δ* (ppm): 17.67 (dd, *J* = 124.9, 83.7 Hz, $P(C_{18}H_{14}SO_3^-)$), 15.81 (2 overlapping d, *J* = 124.7, 84.2 Hz, $2P(C_7H_7)_3$).

- **Complex 31**

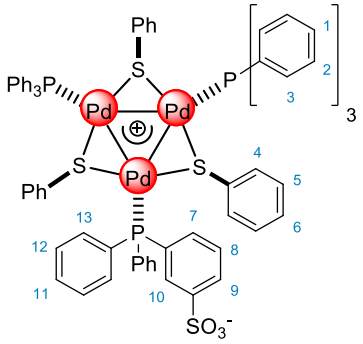

Isolated as a red powder. Yield = 52%

MS calculated for $C_{72}H_{59}O_3P_3Pd_3S_4$ $[M+H]^+$: 1513.98, found: 1513.37.

^{1}H NMR (400 MHz, $CDCl_3$) *δ* (ppm): 8.41 (d, *J* = 11.2 Hz, 1H, H_{10}), 8.08 (d, *J* = 7.4 Hz, 1H, H_9), 7.09 (m, 40H, $H_{1\text{-}3}$, $H_{11\text{-}13}$), 7.00 (m, 10H, $H_{10\text{-}12}$), 6.85 (m, 3H, H_6), 6.72 (m, 2H, $H_{6\text{-}7}$), 6.62 (7, *J* = 7. 7 Hz, 6H, H_5), 6.27 (d, *J* = 7.5 Hz, 6H, H_4).

^{31}P NMR (162 MHz, $CDCl_3$) *δ* (ppm): 16.52 (bs, $P(C_{18}H_{14}SO_3^-)$), 16.16 (bs, $2P(C_6H_5)$).

- **Complex 32**

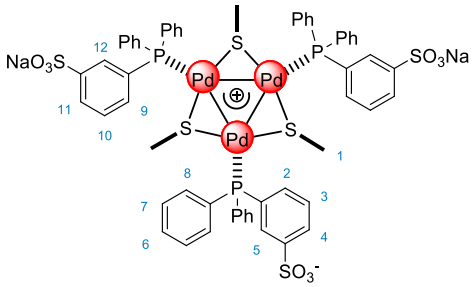

Isolated as an orange powder. Yield = 72%

MS calculated for $C_{57}H_{51}Na_3O_9P_3Pd_3S_6$ $[M+Na]^+$: 1552.79, found: 1552.83.

^{1}H NMR (300 MHz, methanol-*d*$_4$) δ (ppm): 8.11 (2 overlapping d, *J* = 10.21, 6 Hz, 5H, H_5, H_{11}, H_{12}), 7.98 (d, *J* = 7.12 Hz, 3H, H_2, H_9), 7.84 (m, 4H, $H_{3\text{-}4}$, H_{10}), 7.63 (m, 30H, $H_{6\text{-}8}$), 1.07 (bs, 9H, H_1).

^{31}P NMR (162 MHz, methanol-*d*$_4$) δ (ppm): 17.39 (s, 3P).

- **Complex 33**

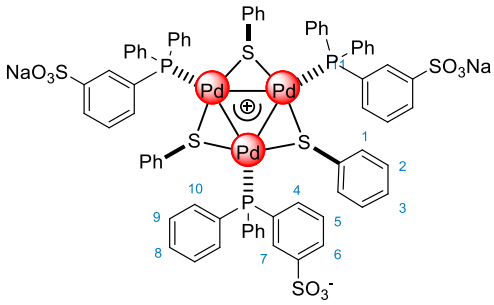

Isolated as an orange powder. Yield = 79%

MS calculated for $C_{72}H_{57}Na_3O_9P_3Pd_3S_6$ $[M+Na]^+$: 1738.81, found: 1738.91.

^{1}H NMR (300 MHz, methanol-*d*$_4$) δ (ppm): 8.13 (m, 3H, H_7), 8.10 (m, 3H, H_6), 7.85 (m, 6H, $H_{4\text{-}5}$), 7.21 (m, 30H, $H_{8\text{-}10}$), 6.39 (d, *J* = 7.33 Hz, 6H, H_1).

^{31}P NMR (162 MHz, methanol-d_4) δ (ppm): 23.19 (s, 3P).

- **Complex 34**

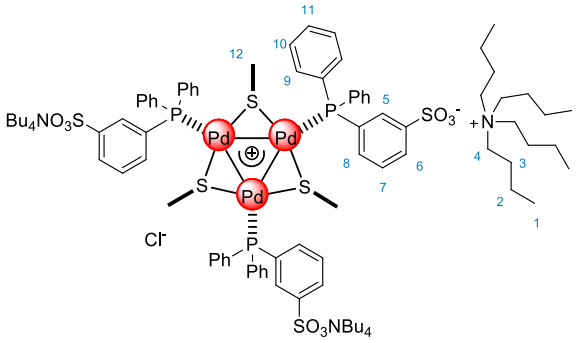

Isolated as a red powder. Yield = 99%

HRMS (ESI-*neg*ative) calculated for $C_{57}H_{51}O_9P_3Pd_3S_6$ $[M]^{2-}$: 741.9107, found: 741.9102.

^{1}H NMR (400 MHz, $CDCl_3$) δ (ppm): 8.01 (m, 6H, $H_{5\text{-}6}$), 7.50 (m, 12H, H_9), 7.39 (m, 24H, $H_{7\text{-}8}$,$H_{10\text{-}11}$), 3.22 (m, 24H, H_4), 1.58 (dt, J_1= 8.02, J_2= 15.78 Hz, 24H, H_3), 1.34 (m, 24H, H_2), 0.99 (s, 9H, H_{12}), 0.91 (t, J = 7.33 Hz, 36H, H_1).

^{31}P NMR (162 MHz, $CDCl_3$) δ (ppm): 18.04.

1.4.7 Summary of X-Ray diffraction analysis on complexes 25-26

Single crystal data were collected with Bruker Smart APEXII and Breeze area detector diffractometers, Mo Kα: λ = 0.71073 Å. The unit cell parameters were obtained using 60 ω-frames of 0.5° width and scanned from three different zone of reciprocal lattice. The intensity data were integrated from several series of exposures frames (0.3° width) covering the sphere of reciprocal space (SMART (control) and SAINT (integration) software for CCD systems; Bruker AXS: Madison, WI, 1994). Absorption correction were applied using the program SADABS (Area-Detector Absorption Correction; Siemens Industrial Automation, Inc.: Madison, WI, 1996). The structure was solved by the dual space algorithm implemented in the SHELXT code (G. M. Sheldrick, SHELXT – Integrated space-group and crystal-structure determination - *Acta Crystallographica Section A*, **2015**, *71*, 3.) and refined on F^2 with full-matrix least squares (SHELXL-2014) (G. M. Sheldrick, *Acta Crystallogr., Sect. A: Found. Crystallogr.*, **2008**, *64*, 112), using the OLEX2 software package (O.V. Dolomanov, L. J. Bourhis, R. J. Gildea, J. A. K. Howard, H. Puschmann, *"OLEX2: a complete structure solution, refinement and analysis program". J. Appl. Cryst,* **2009**, *42,* 339).

In $[Pd(PPh_3)_2(PhS)Cl][Pd(PPh_3)_2Cl_2]$ (**25**) the asymmetric unit comprises two co-crystallized Pd complexes, namely $[Pd(PPh_3)_2(PhS)Cl]$ and $[Pd(PPh_3)_2Cl_2]$, which are disordered over a center of symmetry. In both structures, all non-hydrogen atoms were refined anisotropically, whereas the hydrogen atoms were placed at their calculated positions. Graphical material was prepared with the Mercury 3.8 program (C. F., Macrae, P. R. Edgington, P. McCabe, E. Pidcock, G. P. Shields, R. Taylor, M. Towler, J. van de Streek, *J. Appl. Crystallogr.*, **2006**, *39*, 453).

- **Complex 25**

Crystal data and structure refinement

CCDC number	1542232	
Identification code	shelx	
Empirical formula	C78 H65 Cl3 P4 Pd2 S	
Formula weight	1477.39	
Temperature	296(2) K	
Wavelength	0.71073 Å	
Crystal system	Monoclinic	
Space group	P 21/n	
Unit cell dimensions	a = 11.7800(10) Å	α= 90°.
	b = 18.711(2) Å	β= 106.133(2)°.
	c = 16.383(2) Å	γ = 90°.
Volume	3468.9(6) $Å^3$	
Z	2	
Density (calculated)	1.414 Mg/m^3	
Absorption coefficient	0.799 mm^{-1}	
F(000)	1504	
Crystal size	0.26 x 0.19 x 0.16 mm^3	
Theta range for data collection	1.691 to 25.597°.	
Index ranges	-14<=h<=14, -22<=k<=22, -19<=l<=19	
Reflections collected	39070	
Independent reflections	6504 [R(int) = 0.0716]	
Completeness to theta = 25.242°	100.0 %	
Absorption correction	Semi-empirical from equivalents	
Max. and min. transmission	0.745 and 0.653	
Refinement method	Full-matrix least-squares on F2	
Data / restraints / parameters	6504 / 1 / 424	

Goodness-of-fit on F2	1.038
Final R indices [I>2sigma(I)]	R1 = 0.0497, wR2 = 0.1241
R indices (all data)	R1 = 0.0802, wR2 = 0.1387
Extinction coefficient	n/a
Largest diff. peak and hole	0.626 and -0.524 e.Å^{-3}

Atomic coordinates (x 10^4) and equivalent isotropic displacement parameters (Å^2 x 10^3). U(eq) is defined as one third of the trace of the orthogonalized U^{ij} tensor

	x	y	z	U(eq)
Pd	5363(1)	3321(1)	7812(1)	48(1)
P(2)	3395(1)	3213(1)	7859(1)	45(1)
P(1)	7383(1)	3421(1)	7900(1)	42(1)
Cl(1)	5705(1)	2121(1)	8061(1)	63(1)
S(1)	5036(7)	4486(4)	7422(3)	50(1)
Cl(2)	5066(8)	4570(4)	7740(4)	77(2)
C(131)	7982(4)	2652(2)	7484(3)	44(1)
C(11)	7952(4)	4172(2)	7423(3)	44(1)
C(132)	2993(4)	2384(3)	8306(3)	48(1)
C(61)	7840(4)	4864(3)	7703(3)	57(1)
C(71)	8231(4)	3461(2)	9020(3)	48(1)
C(181)	9013(5)	2326(3)	7917(3)	59(1)
C(12)	3019(4)	3910(2)	8508(3)	50(1)
C(21)	8512(5)	4075(3)	6795(3)	60(1)
C(142)	3033(4)	1741(3)	7891(3)	59(1)
C(72)	2315(4)	3285(3)	6833(3)	50(1)
C(141)	7401(5)	2394(3)	6679(3)	55(1)
C(51)	8288(5)	5431(3)	7356(3)	63(1)
C(121)	9259(5)	3843(3)	9292(3)	66(2)

C(182)	2658(5)	2367(3)	9039(3)	61(1)
C(62)	1983(5)	4289(3)	8270(4)	65(1)
C(22)	3824(5)	4076(3)	9276(3)	69(2)
C(122)	1303(5)	2875(3)	6591(4)	72(2)
C(151)	7865(6)	1840(3)	6326(4)	69(2)
C(152)	2755(5)	1104(3)	8215(4)	73(2)
C(111)	9901(6)	3845(4)	10148(4)	79(2)
C(81)	7849(5)	3073(3)	9606(3)	68(2)
C(112)	514(5)	2938(4)	5804(4)	77(2)
C(162)	2443(5)	1098(3)	8955(5)	81(2)
C(161)	8880(6)	1521(3)	6779(4)	78(2)
C(31)	8971(6)	4649(3)	6465(4)	80(2)
C(41)	8847(6)	5321(3)	6741(4)	75(2)
C(172)	2391(6)	1726(4)	9371(4)	79(2)
C(32)	3539(7)	4610(4)	9797(4)	87(2)
C(52)	1719(6)	4820(3)	8754(5)	83(2)
C(101)	9508(6)	3453(3)	10706(4)	80(2)
C(42)	2508(7)	4974(4)	9526(5)	92(2)
C(171)	9462(6)	1757(3)	7571(4)	77(2)
C(91)	8509(7)	3076(3)	10449(4)	83(2)
C(102)	715(7)	3401(4)	5232(4)	93(2)
C(82)	2500(7)	3770(4)	6256(4)	107(3)
C(43)	4823(9)	4712(5)	4716(5)	131(4)
C(92)	1663(8)	3831(5)	5458(4)	129(3)
C(13)	5124(9)	4561(5)	6360(6)	55(2)
C(23)	4862(11)	3990(7)	5780(7)	77(3)
C(33)	4775(13)	4053(8)	4959(8)	96(4)
C(53)	5330(11)	5200(6)	6029(9)	74(3)

- **Complex 26**

Crystal data and structure refinement

CCDC number	1542233	
Identification code	shelx	
Empirical formula	C43 H36 Cl6 P2 Pd2 S	
Formula weight	1072.22	
Temperature	296(2) K	
Wavelength	0.71073 Å	
Crystal system	Monoclinic	
Space group	P 21/n	
Unit cell dimensions	a = 18.199(2) Å	α= 90°.
	b = 10.8051(9) Å	β= 107.6240(10)°.
	c = 23.415(2) Å	γ = 90°.
Volume	4388.3(7) $Å^3$	
Z	4	
Density (calculated)	1.623 Mg/m^3	
Absorption coefficient	1.336 mm^{-1}	
F(000)	2136	
Crystal size	0.29 x 0.17 x 0.16 mm^3	
Theta range for data collection	1.250 to 26.600°.	
Index ranges	-22<=h<=22, -13<=k<=13, -29<=l<=29	
Reflections collected	52792	
Independent reflections	9170 [R(int) = 0.0528]	
Completeness to theta = 25.242°	100.0 %	
Absorption correction	Semi-empirical from equivalents	
Max. and min. transmission	0.745 and 0.606	
Refinement method	Full-matrix least-squares on F2	
Data / restraints / parameters	9170 / 0 / 487	

Goodness-of-fit on F2	1.023
Final R indices [I>2sigma(I)]	R1 = 0.0443, wR2 = 0.1142
R indices (all data)	R1 = 0.0661, wR2 = 0.1261
Extinction coefficient	n/a
Largest diff. peak and hole	0.737 and -0.745 e.Å^{-3}

Atomic coordinates (x 10^4) and equivalent isotropic displacement parameters (Å^2 x 10^3). U(eq) is defined as one third of the trace of the orthogonalized U^{ij} tensor

	x	y	z	U(eq)
Pd(1)	7731(1)	4861(1)	4358(1)	40(1)
Pd(2)	7839(1)	4814(1)	5865(1)	42(1)
S(1)	7739(1)	3443(1)	5095(1)	42(1)
P(1)	7593(1)	3470(1)	3616(1)	41(1)
P(2)	7708(1)	3374(1)	6523(1)	43(1)
Cl(3)	7992(1)	6266(1)	6618(1)	62(1)
Cl(2)	7946(1)	6359(1)	5149(1)	64(1)
Cl(1)	7834(1)	6362(1)	3682(1)	64(1)
Cl(24)	4572(2)	6513(3)	5227(1)	173(1)
Cl(34)	6037(2)	6786(3)	5003(2)	220(2)
Cl(14)	4961(2)	8728(4)	4764(2)	213(2)
C(13)	8707(3)	2891(4)	5261(2)	48(1)
C(11)	6769(2)	3680(4)	2949(2)	47(1)
C(72)	8421(3)	3529(4)	7251(2)	47(1)
C(12)	7786(2)	1761(4)	6326(2)	44(1)
C(132)	6760(3)	3438(5)	6644(2)	54(1)
C(131)	7466(2)	1854(4)	3794(2)	44(1)
C(181)	6838(3)	1550(4)	3987(2)	53(1)
C(62)	8365(3)	993(4)	6645(2)	60(1)

C(63)	8813(3)	1634(5)	5223(2)	62(1)
C(71)	8453(2)	3496(4)	3381(2)	46(1)
C(61)	6573(3)	2725(5)	2537(2)	60(1)
C(81)	8439(3)	3708(5)	2796(2)	66(1)
C(82)	9188(3)	3693(5)	7282(2)	60(1)
C(22)	7212(3)	1257(5)	5834(2)	58(1)
C(141)	7935(3)	910(4)	3712(2)	58(1)
C(122)	8222(3)	3418(5)	7780(2)	67(1)
C(142)	6448(3)	2374(6)	6809(2)	70(2)
C(151)	7779(4)	-305(5)	3823(2)	70(2)
C(111)	9827(3)	3325(5)	3653(2)	72(2)
C(23)	9337(3)	3694(5)	5399(2)	60(1)
C(171)	6682(3)	355(5)	4090(2)	64(1)
C(101)	9815(3)	3539(6)	3074(3)	78(2)
C(32)	7241(4)	32(5)	5686(2)	72(2)
C(121)	9159(3)	3306(5)	3808(2)	66(1)
C(51)	5949(3)	2847(6)	2023(2)	75(2)
C(161)	7167(4)	-589(5)	4009(2)	77(2)
C(42)	7842(4)	-701(5)	6011(3)	80(2)
C(53)	9549(4)	1201(6)	5310(2)	84(2)
C(33)	10056(3)	3242(7)	5474(2)	78(2)
C(91)	9122(4)	3721(6)	2650(3)	87(2)
C(21)	6339(3)	4758(5)	2839(2)	78(2)
C(43)	10168(4)	1987(8)	5424(2)	94(2)
C(182)	6361(3)	4541(6)	6573(2)	73(2)
C(102)	9554(3)	3639(6)	8352(2)	78(2)
C(52)	8389(4)	-230(5)	6484(3)	76(2)
C(112)	8802(4)	3471(6)	8327(2)	85(2)
C(92)	9750(3)	3747(5)	7837(2)	72(2)
C(41)	5528(3)	3916(7)	1928(2)	84(2)
C(152)	5725(4)	2402(7)	6896(3)	92(2)
C(172)	5636(4)	4555(7)	6670(3)	90(2)

C(31)	5719(4)	4859(7)	2326(3)	100(2)
C(162)	5315(4)	3482(8)	6812(3)	99(2)
C(14)	5096(4)	7114(9)	4780(4)	125(3)

Chapter 2

SEMIHYDROGENATION OF INTERNAL ALKYNES WITH ZWITTERIONIC CLUSTERS

2.1 Introduction

2.1.1 Catalysis with all-metal aromatic clusters

Peculiar features of all-metal aromatic clusters let to suppose they could find interesting applications in catalysis as well. So far most of the examples involve our Pd_3^+ clusters, while previously just Bertrand and co-workers attempted a catalytic carbonylation of amines using complex **3** as catalyst.[26] Pd_3^+ complexes recently proved to be active catalysts for the cycloisomerizations of terminal 1,6-enynes and internal dienynes under mild conditions.[44] Highly decorated tricycles with a central cyclohexene could be readily obtained with two different sequences, depending on the substrate employed *(Scheme 8)*.

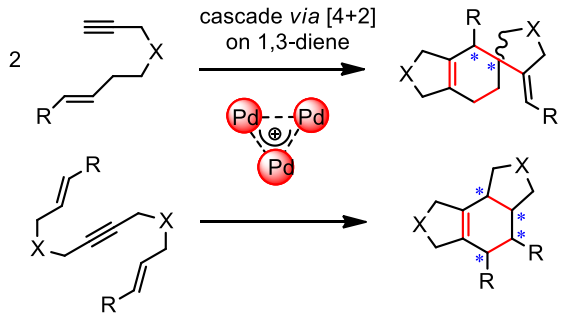

Scheme 8: Distinct reactivity of terminal 1,6-enynes and internal dienynes with Pd_3^+ clusters

Further satisfying results came from the semihydrogenation of internal alkynes to cis-alkenes, reaction on which we will focus in this chapter.

[44] M. Lanzi, T. Cañeque, L. Marchiò, R. Maggi, F. Bigi, M. Malacria, G. Maestri, *ACS Catal.*, **2018**, *8*, 144.

2.1.2 Semihydrogenation of alkynes

Semihydrogenation of alkynes has a great synthetic interest and in last decades several methods have been reported. In 1952 Lindlar proposed the first catalyst, palladium supported on $CaCO_3$ and doped with lead and/or quinoline.[45] This catalytic method employed gaseous hydrogen to reduce alkynes to alkenes, $Pb(OAc)_2$ and a large amount of quinoline. Moreover, low reproducibility and selectivity lowered the efficiency of the reaction, since the formed alkene could undergo over-reduction to alkane in hydrogen atmosphere. Since then, considerable progress has been made in order to attain complete chemo and stereo control, both in homogeneous and in heterogeneous conditions. Our attention will focus on two remarkable examples among the recent methodologies based on palladium.

Elsevier proposed a catalytic method based on a mononuclear complex of Pd(0), which was generated in situ from the Pd precursor in *Scheme 9* and 1,3-bis(2,4,6-trimethylphenyl)imidazol-2-ylidene.[46] Reasoning on the fact that alkynes semireductions catalyzed by Pd(NHC) of type **35** formed in situ proved more active than well-defined $[Pd(IMes)(MA)_2]$, they selected conditions in order to obtain a complex with a free coordination site.

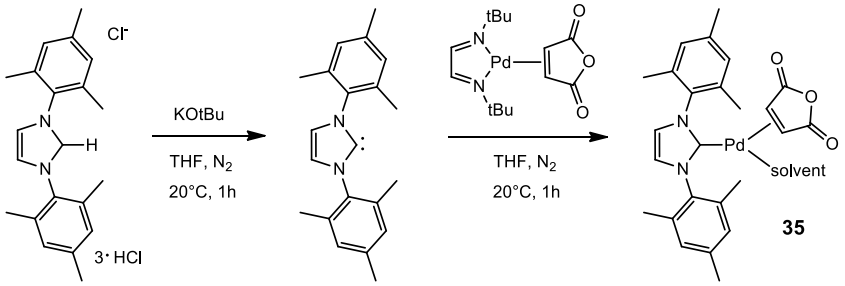

Scheme 9: Synthesis of Elsevier's Pd(0) complex

[45] H. Lindlar, *Helv. Chim. Act.*, **1952**, *57*, 446.
[46] P. Hauwert, G. Maestri, J. W. Sprengers, M. Catellani, P. J. Elsevier, *Angew. Chem.*, **2008**, *120*, 3267.

In addition, they chose milder conditions, replacing H_2 with triethylammonium formate as hydrogen donor. Several aromatic and aliphatic alkynes were successfully semireduced using 1 mol % of catalyst and a fivefold excess of $HCOOH/NEt_3$ in refluxing THF or MeCN. However, percentages of alkane were detected for some examples, especially those bearing electron-withdrawing groups lowering the LUMO of olefinic protons, which thus became better ligands for the low-valent mononuclear complex. Further studies on 1-phenyl-1-propyne led to a better understanding of the mechanism of the reaction. Both hydrogens of formic acid are transferred to the substrate in two different rate-determining steps with similar activation energy.[47] In the proposed catalytic cycle, hydrogen transfer from the formate anion, which is coordinated to the zerovalent palladium(NHC)(MA)(alkyne)-complex, is followed by the migratory insertion of the hydride. Finally, the formed alkene is released by proton transfer from the triethylammonium cation.

In 2017 Studer obtained high stereoselectivity to cis-alkenes using palladium nanoparticles. Nanoparticles with a diameter of 2.8 mm were obtained through a light-mediated synthesis mixing $Pd(OAc)_2$ and a bisacylphosphine oxide as photoinitiator in DMF. They developed a one-step methodology using just commercial reagents. Nineteen internal alkynes were semireduced in good yields (85-99%) and cis/trans ratio (up to 99/1). However, catalyst loading varied between 1 and 2% depending on the substrate and explosive H_2 was still the hydrogen source.[48]

[47] P. Hauwert, R. Boerleider, S. Warsink, J. J. Weigand, C. J. Elsevier, *J. Am. Chem. Soc.*, **2010**, *132*, 16900.
[48] F. Mäsing, H. Nüsse, J. Klingauf, A. Studer, *Org. Lett.*, **2017**, *19*, 2658.

2.1.3 First generation catalytic system with Pd_3^+

Metal aromatic Pd_3^+ complexes are prototypical subnanometric metal surfaces that represent the ideal connection between discrete homogeneous mononuclear complexes and heterogeneous metallic nanoparticles. Considering issues that commonly affect the semihydrogenation of alkynes, such as low selectivity and unpredictable formation of over-reduction products, the group thought that this reaction could be a challenging playground to test the consequences of delocalized metal-metal bonds.[49]

1-phenyl-1-propyne was employed as model substrate and mixed with 1 mol% of Pd_3^+ and 5 equivalents of triethylammonium formate in refluxing THF *(Scheme 10)*. An initial screening of available complexes ended up with relevant considerations about properties that ligands should have to provide the best catalytic performance *(Table 7)*.

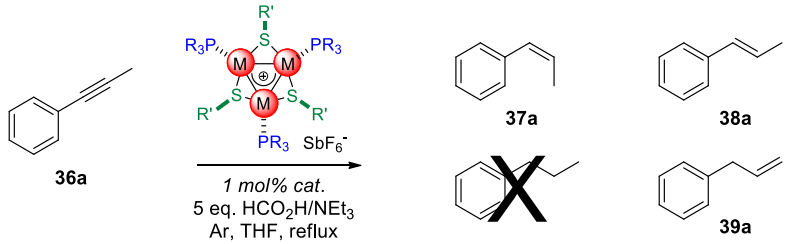

Entry	M	R	R'	t (h)	Conv. of 36a (%)	Sel. to 37a (%)
1	Pd	4-F-C_6H_4	4-Me-C_6H_4	96	86	92
2	Pd	4-Me-C_6H_4	4-Cl-C_6H_4	64	quant.	82
3	Pd	Ph	Ph	48	54	83
4	Pd	Et	4-Cl-C_6H_4	96	--	--
5	Pd	Et	4-Me-C_6H_4	96	--	--
6	Pd	4-F-C_6H_4	Me	64	34	82

[49] P. A. Deyris, T. Caneque, Y. Wang, P. Retailleau, F. Bigi, R. Maggi, G. Maestri, M. Malacria, *ChemCatChem*, **2015**, *7*, 3266.

7	Pd	4-Me-C_6H_4	Me	10	quant.	93
8	Pt	4-Me-C_6H_4	Me	96	--	--

Scheme 10: Catalytic semihydrogenation of 1-phenyl-1-propyne with M_3^+ clusters

Table 7: M_3^+ clusters tested for the catalytic semihydrogenation of 1-phenyl-1-propyne

Clusters with aromatic ligands gave modest results both in terms of conversion of the substrate and selectivity towards cis-alkene, depending on their electronic and steric features. Complex with *p*-tolyl groups on bridging thiolates and fluorinated triarylphosphines showed a fairly low activity and conversion ceased at 86% after four days (entry 1). Scrambling electron-donating and electron-withdrawing groups led to a faster reaction but to a worst selectivity (entry 2). Complex with phenyl substituents on phosphines and thiolates provided similar results regarding selectivity, but became inactive after two days (entry 3). Pd_3^+ bearing aliphatic phosphines were surprisingly inactive (entries 4 and 5), while the combination with methyl thiolates and tri(*p*-tolyl)phosphines provided the best results, namely complete conversion upon 10 hours and 93% selectivity towards cis-alkene. It is worth noting that in all these cases no traces of over-reduced alkane were detected, even prolonging heating for 24 additional hours. On the contrary, the corresponding Pt_3^+ cluster did not show any activity, even if its structure, which is nearly identical to that of Pd_3^+, let us predict a similar behaviour (entry 8). A vast array of aromatic and aliphatic alkynes was next examined. Good selectivity to cis-alkene was obtained for aromatic substrates (70-100%), noting a longer reaction time as the length of the aliphatic arm increased. Aliphatic alkynes provided on the contrary a higher percentage of trans-alkene compared to the aromatic counterparts, providing cis-alkene in 29-99% yields. A small amount of terminal alkene was detected in several cases (up to 40%). Further investigation with deuterium-labeled formic acid suggested that

hydride transfer might be the rate-determining step, while proton transfer has a lower impact on the catalytic cycle. As the matter of fact, a high deuterium incorporation on the terminal carbon atom of phenylpropyne was observed, which could derive from the formation of phenylallene as reaction intermediate. These preliminary studies indeed suggested that Pd_3^+ clusters operate with a mechanism that differ from those commonly observed with traditional palladium complexes.

2.2 Results and discussion

2.2.1 Second generation catalytic system for the semihydrogenation of internal alkynes to *cis*-alkenes

The catalytic activity of the new zwitterionic clusters was tested in the semihydrogenation of internal alkynes. In analogy to the first generation catalytic system with Pd_3^+ salts,[49] we firstly chose 1-phenyl-1-propyne as model substrate to do a screening of available complexes.[42] We performed the reaction using 1 mol% of catalyst loading and a five-fold excess of triethylammonium formate as hydrogen donor *(Scheme 11)*. This excess ensures that the chemoselectivity towards the semireduction of alkynes is due to the catalytic system rather than to a shortage of hydrogen donor.[47-50]

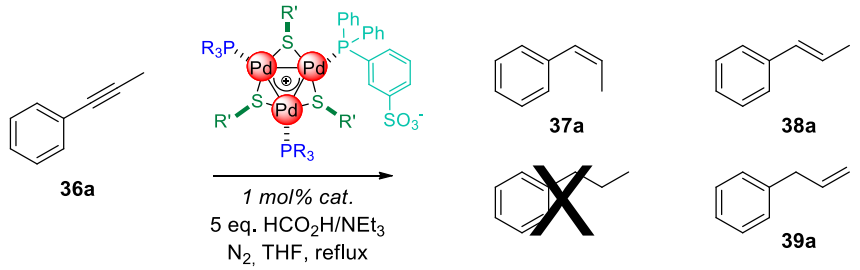

Entry	Complex	R	R'	t (h)	Conv. of 36a (%)	Sel. to 37a (%)
1	27	4-F-C_6H_4	4-Me-C_6H_4	8	97	85
2	28	4-F-C_6H_4	Me	5	quant.	87
3	29	4-Me-C_6H_4	Ph	6	quant.	78
4	30	4-Me-C_6H_4	Me	3	quant.	77
5	31	$Ph_2C_6H_4SO_3Na$	Me	3	quant.	77

Scheme 11: Catalytic semihydrogenation of 1-phenyl-1-propyne with zwitterionic clusters

*Table 8: Zwitterionic clusters tested for the catalytic semihydrogenation of **36a***

[50] a) R. Shen, T. Chen, Y. Zhao, R. Zhou, S. Yin, X. Wang, M. Goto, L. B. Han, *J. Am. Chem. Soc*, **2011**, *133*, 17037; b) J. Broggi, V. Jurcik, O. Songis, A. Poater, L. Cavallo, A. M. Z. Slawin, C. S. J. Cazin, *J. Am. Chem. Soc*, **2013**, *135*, 4588.

Complexes with fluorinated phosphines proved active with both aromatic and aliphatic bridging thiolates (*Table 8*, entries 1 and 2). Complex **28** gave a better performance since it provided complete conversion of the substrate in 5 hours. However, cis-selectivity resulted lower compared to the analogues cationic complexes tested in the first generation catalytic system (85 and 87% respectively). We were nevertheless delighted that no traces of alkane were detected. Trans-alkene **38a** and allylbenzene **39a** formed in a comparable amount, 6 and 8% respectively. Complexes with tri(*p*-tolyl)phosphine proved to be more active (entries 3 and 4), **36a** completely converted in 6 hours with the aromatic thiolate and upon 3 hours with the aliphatic one. Despite the higher activity, complexes **29** and **30** led to a worse selectivity towards **37a** (78 and 77%) **38a** and **39a** formed in a discrete amount, 10 and 13% respectively. The same trend was observed with complex **32** (entry 5), which provided a complete conversion of **36a** in 3 hours with a 77% selectivity towards **37a**. This behaviour could result from a trans-like effect[51] of the anionic ligand that would make the phosphine on the opposite edge of the metal core much more labile. It could rationalize the higher activity of the clusters bearing the phosphine with electron-withdrawing substituents compared to the first generation system (entries 1 and 2). Their Pd_3^+ analogues proved indeed to be fairly active for the semihydrogenation of **36a** (*Table 7,* entries 1 and 8). Previously described DFT modelling on **17** and **30** supported this hypothesis, because Pd-P distance with the anionic phosphine shortens in the zwitterionic complex compared to the corresponding Pd_3^+, while those with the neutral ones are slightly longer.

In all cases no traces of over-reduced alkane were detected, even prolonging warming after full conversion. In this condition we could indeed observe just a partial isomerisation of **37a** to **38a** and **39a** (below 5% upon 24 hours).

[51] a) B. J. Coe, S. J. Glenwright, *Coord. Chem. Rev*, **2000**, *203*, 5; b) B. Pinter, V. Van Speybroeck, M. Waroquier, P. Geerlings, F. De Proft, *Phys. Chem. Chem. Phys*., **2013**, *15*, 17354.

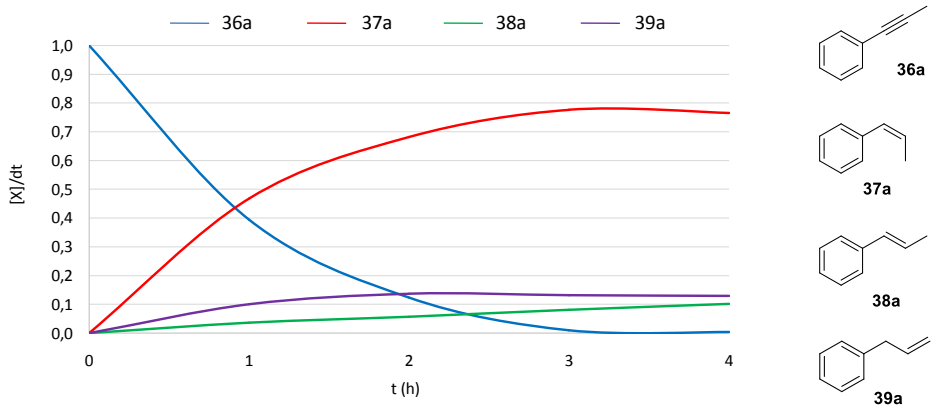

*Graph 1: Selectivity to alkenes **36a-39a** obtained with complex **30***

Graph 1 shows the pattern of selectivity obtained with complex **30** (entry 4). It highlights that after the full conversion of **36a** upon 3 hours, prolonging warming in the next hour results in an increase of **39a** at the expense of **37a**.

In all these tests we noticed the formation of traces of Pd black when the conversion of the substrate passed 70%, suggesting that zwitterionic complexes could be less robust in these reaction conditions compared to the symmetric Pd_3^+ clusters. Taken together, these results suggested that isomerisation of **37a** could be catalysed by Pd species derived from the decomposition of our cluster in the reducing reaction medium.[52]

[52] a) R. M. Drost, V. Rosar, S. Dalla Marta, M. Lutz, N. Demitri, R. Milani, B. de Bruin, C. J. Elsevier, *ChemCatChem*, **2015**, *7*, 2095; b) N. T. S. Phan, M. Van Der Sluys, C. W. Jones, *Adv. Synth. Catal.*, **2006**, *348*, 609.

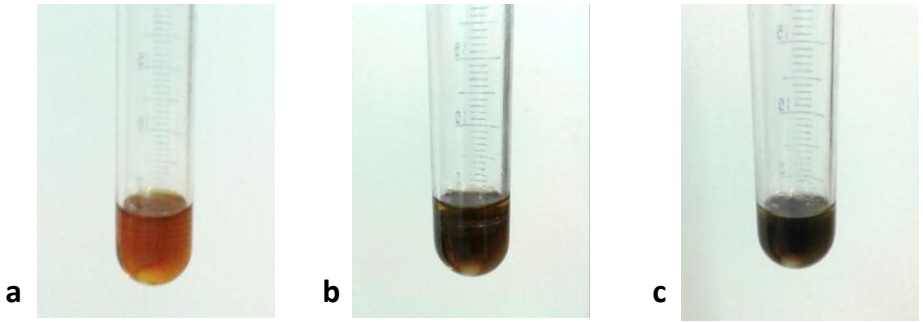

Fig. 12: Crude mixture of the semihydrogenation of 1-phenyl-1-propyne at the starting point (a), upon 2 hours (b) and upon the complete conversion of the substrate (c)

Figure 12 shows pictures of the crude mixture throughout the 3 hours of reaction. At the beginning the solution appears orange in colour (a), but 2 hours later (70% conversion of **36a**) traces of Pd black are clearly visible in the flask. Upon complete conversion of the alkyne (c), the mixture turns definitely to black.

We wondered if the addition of a suitable ligand could prevent these undesired processes and slow down the deactivation of the catalyst without quenching its activity *(Scheme 12)*.

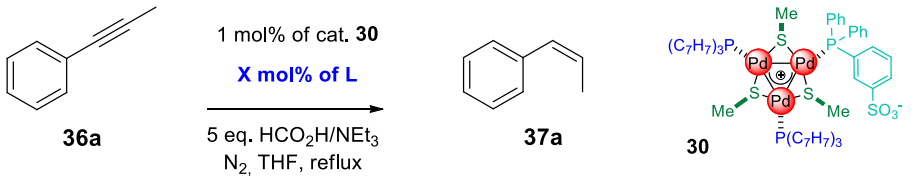

Entry	L	mol %	t (h)	Conv. of 36a (%)	Sel. to 37a (%)
1	P(4-Me-C_6H_4)$_3$	3	4	quant.	96
2	P(4-Me-C_6H_4)$_3$	10	24	quant.	96
3	$PPh_2C_6H_4SO_3Na$	3	4	quant.	96
4	dba	6	24	quant.	92

*Scheme 12: Semihydrogenation of **36a** with complex **30** and the additional ligand*

Table 9: Additional ligands tested for the semihydrogenation of 1-phenyl-1-propyne

The addition of 3 mol% of tri(*p*-tolyl)phosphine proved decisive (*Table 9*, entry 1). Full conversion of **36a** was obtained upon 3 hours and selectivity to **37a** increased significantly (from 77 to 96%). Isomers **38a** and **39a** formed in 2% yield each. Moreover, the homogeneous orange solution of complex **30** did not show any trace of Pd black metal colloids before the complete conversion of **36a** *(Fig. 13)*.

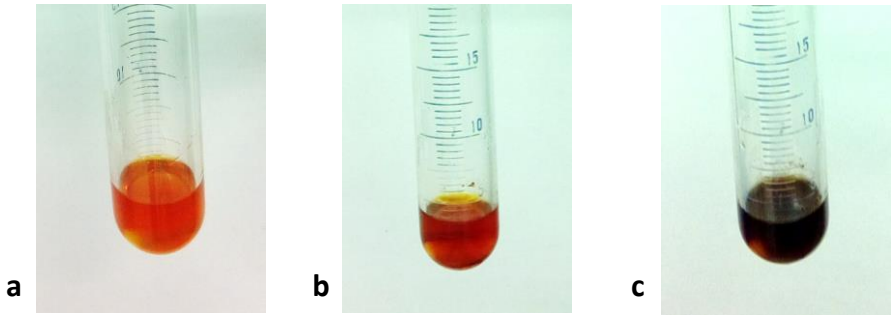

*Fig. 13: Crude mixture of the semihydrogenation of 1-phenyl-1-propyne with complex **30** and the additional ligand at the starting point (a), upon 2 hours (b) and upon the complete conversion of the substrate (c)*

We then added 10 mol% of the same phosphine (entry 2), but complete conversion of the alkyne required 24 hours. This seems to be reasonable if we think about a competition between substrates and ligands for the coordination site. No traces of visible black heterogeneous aggregates were found even in this longer experiment.

In both cases we observed a little decrease in the initial rate of the reaction (*Graph* 2), that is even more evident when a higher amount of ligand is used (violet line). Anyway, this does not interfere with the high selectivity of the process (96%).

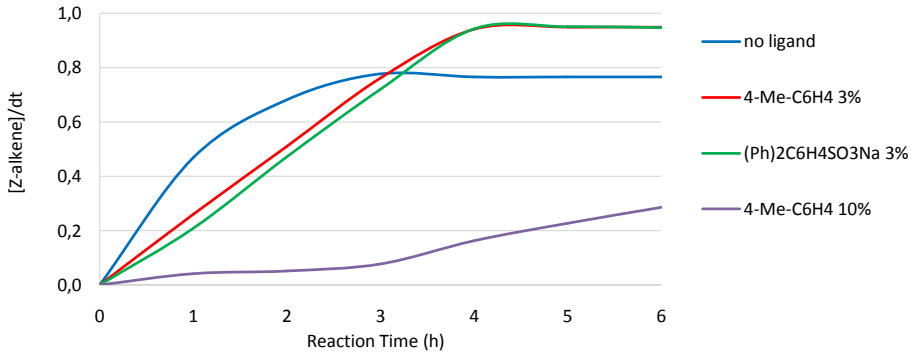

Graph 2: Z-alkene formation through time with different additional ligands

Addition of 3 mol% of a sodium sulfonate phosphine (entry 3) provided results comparable to entry 1, since complete conversion of **36a** was achieved in 4 hours with a 96% selectivity to **37a**. Again, the reaction mixture remained orange in colour. Finally, we moved to an electron-poor olefin, namely dibenzylideneacetone (dba), which gave slightly worse results. Conversion of the substrate required 24 hours and alkenes **38a** and **39a** formed in 4% yield each, stopping selectivity to **37a** at 92%.

We performed ESI$^+$-MS analysis on sample collected at regular intervals to check the stability of cluster **30** throughout the reaction. This tool proved useful to detect a fading concentration of the first generation Pd_3^+ catalysts during the reaction, in agreement with the formation of Pd black.[49] However, the difficulty in the ionization of zwitterion **30** hampered the application of the same approach. Despite the absence of visible traces of metal colloids, we did not detect neither the protonated cation of **30** or any other species showing an isotopic distribution compatible with the presence of Pd atoms in the ion. This outcome was observed with all samples collected, from 0 min before warming up to the complete conversion of the substrate.

We then came back to the ESI$^+$-MS spectra of the pure clusters to better understand the reason of this behaviour. We noticed that ESI$^+$-MS spectra of

Pd_3^+ *(Fig. 14)* and zwitterion **30** *(Fig. 15)* provided very different values of the detected total ion current.

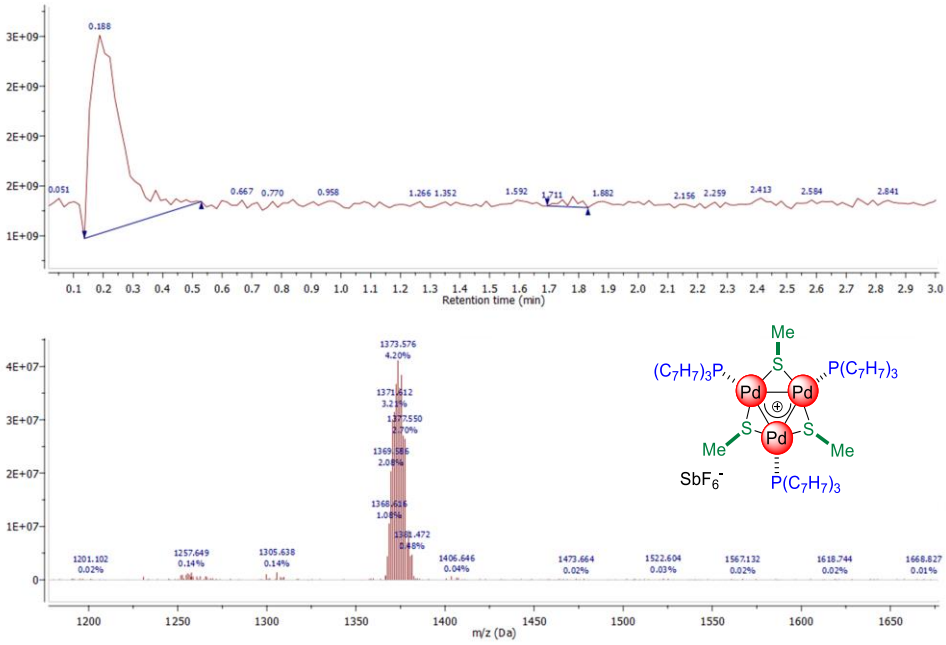

*Fig. 14: ESI⁺-MS analysis of Pd_3^+ cluster **17***

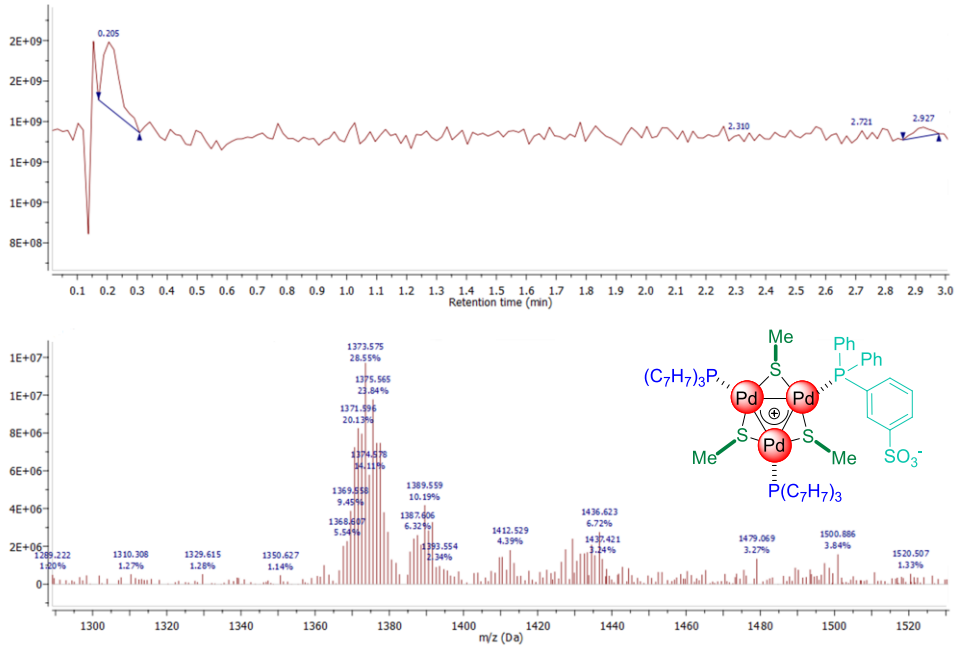

*Fig. 15: ESI⁺-MS analysis of zwitterionic cluster **30***

Preparing samples at the same concentration of both pure complexes (0.1 mg/mL), the intensity of the most abundant isotopic signal of **17** is almost two orders of magnitude higher compared to that observed with **30**, $3 \cdot 10^9$ and $1 \cdot 10^9$ respectively. Different values observed for the two complexes can be related to their different capability to ionize under ESI^+ conditions. While zwitterionic complex **30** needs protonation, complex **17** is already a cationic species.

We confirmed this result analysing a 1:1 mixture of **17** and **30**. As expected from previous tests on pure clusters, mixing a sample of **17** (0.1 mg/mL) with a sample of **30** (0.1 mg/mL), the resulting TIC of $4 \cdot 10^9$ can be almost totally referred to the cation **17**. The protonated zwitterionic complex (1412 m/z) is indeed barely visible *(Fig. 16).*

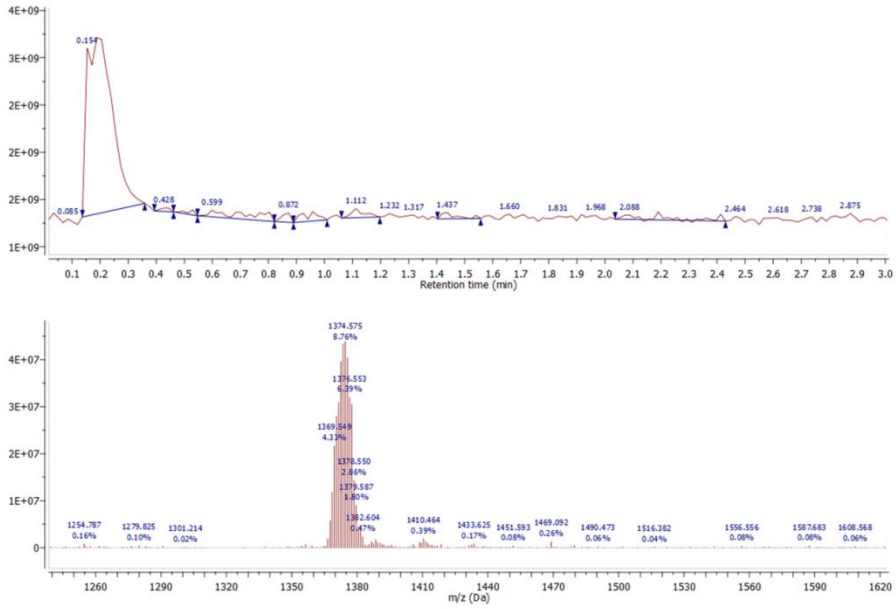

*Fig. 16: ESI⁺-MS analysis of a 1:1 mixture of Pd_3^+ cluster **17** and zwitterionic cluster **30***

To overcome this issue, we moved to another strategy. Reasoning that the complex is the unique species in solution that shows a significant absorbance in the visible region, we monitored reaction samples by UV-Vis spectroscopy *(Fig. 17)*. Complex **30** shows a broad and almost flat band between 340 and 380 nm, followed by a smaller one around 450 nm (light blue curve on the right). No significant differences were observed adding 3 mol% of tri(*p*-tolyl)phosphine (green curve on the right).

100 µl samples were then taken from the crude mixture at regular intervals and diluted with 4.9 ml of THF prior to analysis. Just small changes were detected through the reaction, both in the position and in the relative intensity of bands, which is slightly lower upon hours at reflux.

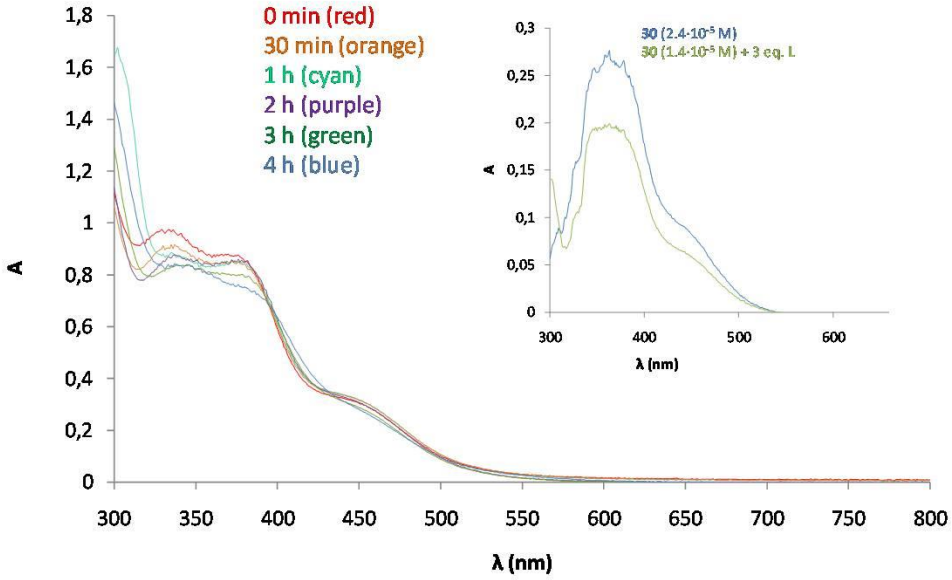

*Fig. 17: UV-Vis spectra of zwitterionic cluster **30** and a mixture of **30** and tri(p-tolyl)phosphine (top right); UV-Vis spectra of crude samples taken from the semihydrogenation of **36a** (bottom left)*

These observations combined with catalysis results confirm the stability of the catalyst during the semireduction of 1-phenyl-1-propyne. Apparent ε values barely shift throughout the experiment. Small variations in the shape and position of the bands compared to the spectra of pure clusters are likely due to the presence of variating concentrations of substrate, products and triethylammonium formate during the reaction course.

Taken together these results suggest that the addition of a suitable ligand could be an efficient tool to stabilize the cluster in the reaction medium and to make the process highly selective to cis-alkene.

Furthermore, these UV-vis experiments strongly suggest that the trinuclear complex is actually the catalyst of the semi-reduction.

Our next purpose was to exploit these hypotheses by reducing the catalyst loading *(Table 10)*. We decided to fix the concentration of complex **30** to 0.001

M, reducing progressively the amount of THF to hold for a higher amount of alkyne. For this reason, entries 4-6 became formal solvent-free experiments. The increased solubility of zwitterionic complexes in apolar media compared to their analogue Pd_3^+ made this possible. By the way, this approach ensures the minimization of the production of wastes.

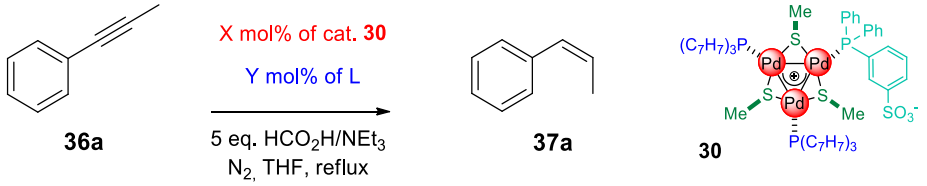

Entry	X (mol %)	Y (mol %)	t (h)	Conv. of 36a (%)	Sel. to 37a (%)	TOF (h^{-1})
1	1	--	3	quant.	77	18
2	0.3	--	4	quant.	90	137
3	0.1	--	7	quant.	96	329
4	0.05	--	6	77	98	582
5	0.05	0.15	5	quant.	98	1026
6	0.03	0.09	6	quant.	98	1242

Table 10: Reduction of catalyst loading on semihydrogenation of 1-phenyl-1-propyne

Experiments were planned in order to change the [propyne]/[cat] ratio from 100 up to 2000.

Reducing the catalyst loading to 0.3 mol% (entry 2) proved beneficial for selectivity, which increased by 13%, and full conversion was obtained upon 4 hours, keeping the reaction time practical. Further reduction to 0.1 mol% (entry 3) resulted in a selectivity to **37a** of 96%, but it took 7 hours to obtain full conversion of the alkyne. On the contrary, the reaction with 0.05 mol% of **30** (entry 4) did not reach full conversion, since only 77% reacted upon 6

hours. In all these cases we noticed the formation of Pd black. Anyway, this represented a great improvement compared to the first generation catalytic system, since Pd_3^+ was no more active before the full conversion of the alkyne at catalyst loadings lower than 1 mol%.

Keeping in mind our previous findings about the addition of a ligand, we repeated the experiment with 0.05 mol% with 0.15 mol% of tri(*p*-tolyl)phosphine (entry 5). The solution remained homogeneous and orange in colour and **36a** was completed converted in 5 hours delivering almost exclusively **37a** (98%). We further reduced the catalyst loading to 300 ppm (entry 6), observing a comparable result.

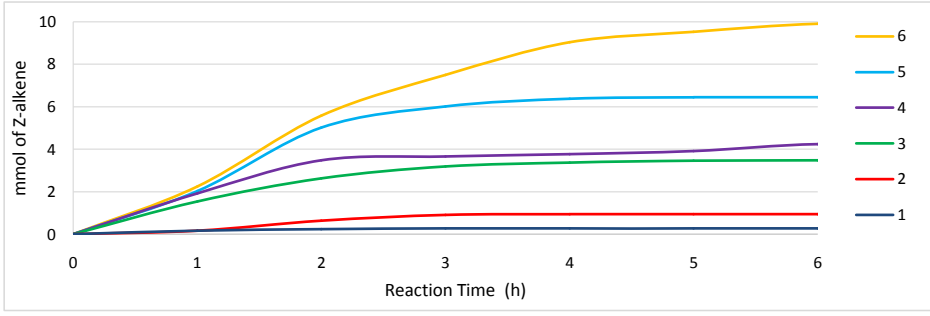

Graph 3: Z-alkene formation through time for entries 1-6 of table 10

Graph 3 shows the plot of alkene production/time reducing the catalyst loading for the six entries. The comparison of the curves underlines an increased apparent rate throughout the series. The linear part of the slope was used to calculate the TOF of each reaction presented in the table, assuming that the amount of complex corresponds to the amount of active species. This approach likely gives an underestimation of the actual TOF.

Finally, we tried to scale up the reaction presented in entry 6 to test if the method could find a broader application. 1.2 g of **1** were successfully converted to **37** with a 98% selectivity upon 6 hours, using commercially available

reagents without any previous purification. Pure cis-alkene was easily recovered filtering the crude mixture on a 2 cm pad of silica gel and washing with 5 ml of pentane (1.15 g, 96% yield).

This highlights the practical and environmental viability of the present catalytic system.

In order to check the generality of the reported method, we repeated the model reaction with various combinations of complexes **30**, **32** and **34** with additional ligands. We also tested mononuclear complex **25** and two dinuclear Pd complexes, namely **26** and its analogue with two thiolates as bridgind ligands, $[Pd_2(PPh_3)_2(PhS)_2]$ (**40**) *(Scheme 13, Table 11)*.

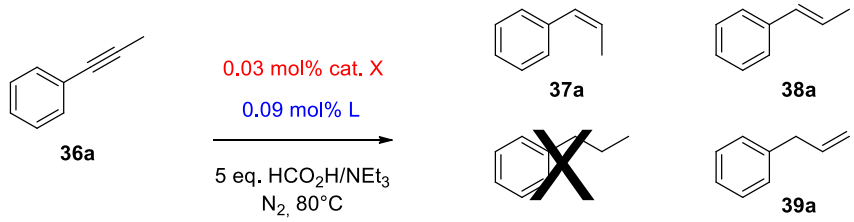

Entry	X	L	t (h)	Conv. of 36 (%)	Sel. to 37 (%)
1	30	$P(4\text{-Me-}C_6H_4)_3$	6	quant.	98
2	30	$C_6H_5\text{-SNa}$	5	36	100
3	32	$P(4\text{-Me-}C_6H_4)_3$	6	quant.	94
4	32	$PPh_2C_6H_4SO_3Na$	6	94	97
5	34	$P(4\text{-Me-}C_6H_4)_3$	8	96	96
6	25	$P(4\text{-Me-}C_6H_4)_3$	8	72	92
7	26	$P(4\text{-Me-}C_6H_4)_3$	8	24	98
8	40	$P(4\text{-Me-}C_6H_4)_3$	6	45	94

Scheme 13: Semihydrogenation of 1-phenyl-1-propyne in optimized reaction conditions

Table 11: Screening of catalysts in optimized reaction conditions

The combination of complex **30** and tri(*p*-tolyl)phosphine (entry 1), provided the best result, confirming the outcome obtained in the previous optimization. On the contrary, the replacement of the phosphine with sodium benzenethiolate quenched the reactivity (entry 2), and conversion of **36a** stopped at 36% upon 5 hours. This finding let to suppose that a phosphine could stabilize the complex in the reducing reaction medium, while an excess of thiolate acts in the opposite direction. As the matter of fact, the apparent rate of the semireduction slows down, suggesting that the species probably competes with formate anions. The combination of complex **32** with tri(*p*-tolyl)phosphine (entry 3), afforded **37a** in 94% yield upon 6 hours, giving results comparable to those obtained in the previous optimization. Replacing the neutral phosphine with the anionic one increased the selectivity to **37a** to 97% (entry 4), but the conversion of **36a** was slightly worse (94%). We wondered if this lower conversion could derive from a lower solubility of complex **32** compared to other clusters with just one anionic phosphine. We tried to answer this question testing complex **34**, which bears tetrabutylammonium anions on the sulfonate groups instead of sodium cations (entry 5). However, this attempt did not give better results both in terms of conversion and selectivity.

We subsequently tested some possible precursors of Pd_3^+ clusters, namely monomeric and dimeric complexes **25**, **26** and **40**. Complex **25** proved to be the best among the three (entry 6), providing 72% of conversion of **36a** upon 8 hours, with 92% selectivity to *cis*-alkene. Dinuclear complexes **26** and **40** showed as well a high selectivity towards **37a**, but the consumption of the alkyne ceased at 24 and 45% respectively (entry 7 and 8). No further changes were observed prolonging warming for 24 additional hours. In these experiments metal colloids started forming after few minutes from the beginning of the reaction despite a high concentration of the substrate.

Anyway, they are probably fairly active only in the isomerisation of **37a** to **38a** and **39a** in these conditions.

Taken together, these results confirm that zwitterionic Pd_3 complexes with delocalized metal-metal bonds are efficient catalysts for solvent-free semireduction of internal alkynes to cis-alkenes.

To prove the generality of the system we tested the scope of the reaction.[40]

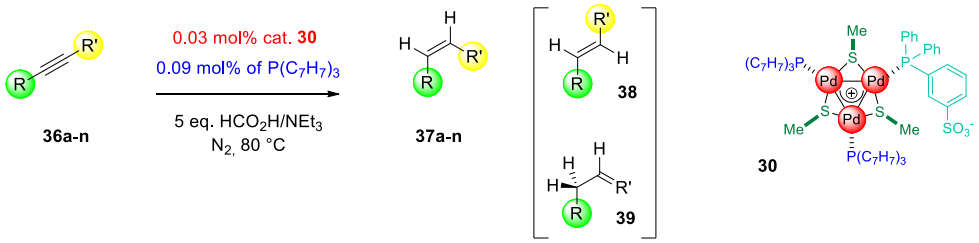

Entry	Alkyne	t (h)	Sel. to 37 (%)	Yield (%)
1	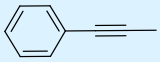 **36a**	6	98	98
2	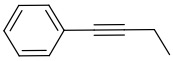 **36b**	15	90	99
3	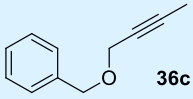 **36c**	6	93	99
4	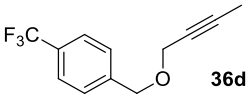 **36d**	4	96	99
5	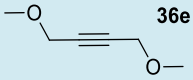 **36e**	13	100	94
6	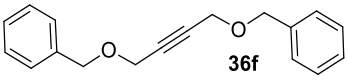 **36f**	5	100	99
7	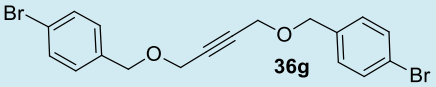 **36g**	5	100	99
8	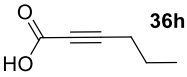 **36h**	6	100	99

9	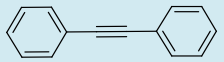 **36i**	3	100	99
10	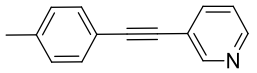 **36j**	7	100	87
11	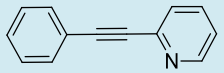 **36k**	15	100	95
12	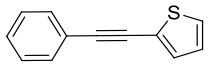 **36l**	6	100	99
13	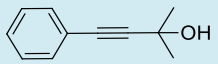 **36m**	4	100	99
14	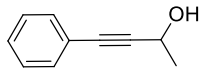 **36n**	6	94	85

Table 12: Scope of the semihydrogenation of internal alkynes to cis-alkenes

As shown in *Table 12* a vast array of internal alkynes could be converted to the corresponding cis-alkenes in excellent to quantitative yields. Apart from our model substrate **36a** (entry 1), the introduction of some hindrance close to the triple bond made the reaction much slower, since 15 hours were required to completely convert alkyne **36b** to alkenes **37**-**38b** (entry 2, 90/10 ratio). This result represents nonetheless an improvement over the first generation catalytic system, in which alkyne **36b** delivered a 78/21/1 ratio of **37b**-**39b** upon 24 hours. In addition, various propargylic ethers with benzylic substituents could be easily converted (entries 3-4, 93 and 96% selectivity to **37c** and **37d** respectively). Substitution of 2-butyne-1,4-diol with various fragments enabled to access *cis*-diethers **37e**-**37g** in quantitative yields (entry 5-7). We found particularly interesting that the C-Br bond in **36g** remained untouched, leaving a handle for further functionalization. All these ethers present propargylic C-H bonds that could easily undergo homolytic cleavage. They indeed require purification on silica gel or distillation prior to use to prevent the poisoning of the small amount of catalyst employed and to guarantee the best performance. This protocol is no longer required with

higher catalyst loadings (1 mol%), indicating that the purity of the reagent can become an important issue to preserve chemical stability over several thousand of turnovers. Substituted propiolic acids could be completely converted (entry 8), showing that carboxylic acids did not hamper the reaction. Diarylacetylenes, including heteroaryl ones, were then tested (**37i-l**, entries 9-12). Diphenylacetylene completely converted in 3 hours, proving to be the most active upon the substrates employed (entry 9). Pyridyl fragments were tolerated, and remarkably both 3- and 2-pyridyl moieties afforded exclusively the *cis*-alkene. Conversion stopped at 87% with the former (entry 10), while the latter delivered 95% of **37k** upon 15 hours (entry 11). Thiophene ring gave a comparable performance, since it exclusively converted to **37l** in 6 hours (entry 12). It is worth noting that these results show a further original element compared to popular heterogenous palladium catalysts, such as the Lindlar system, for which aromatic aza- and thio-heterocycles are known poisons. Hindered propargylic alcohols are good substrates too. **36m** was smoothly converted to **37m** in few hours (entry 13), while conversion of **36n** was stuck at 94%, giving anyway alkene **37n** almost exclusively (entry 14).

The present scope clearly shows that the zwitterionic complex displays chemical stability for at least 3000 turnovers over an ample mix of substrates with different organic fragments, together with high activity and often complete selectivity.

In all these cases the reaction mixture remained clear until the full conversion of the substrate thanks to the addition of 0.09 mol% of the phosphine. This outcome perfectly reproduces what we observed during the optimization with 1-phenyl-1-propyne.

Figure 18 presents the series of ^{1}H NMR spectra collected at regular intervals during the semihydrogenation of **36f** (purple line).

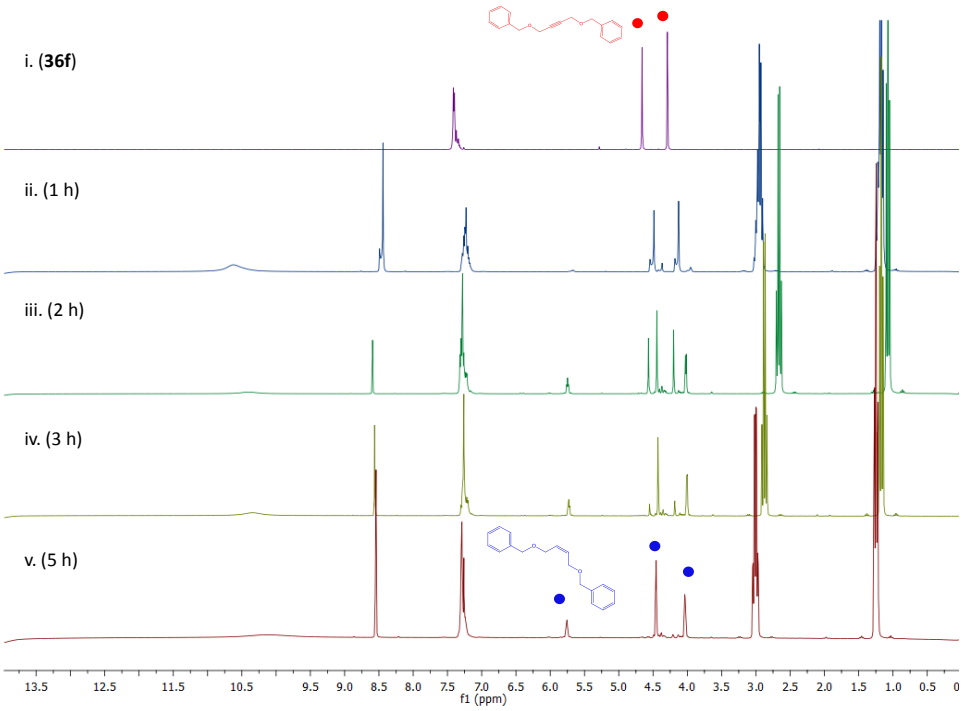

*Fig.18: ^{1}H NMR spectra of crude samples from the semihydrogenation of alkyne **36f***

Beside triethylammonium formate, no other organic species appear throughout the experiment. Comparing samples collected upon 1 (blue line), 2 (green), 3 (yellow) and 5 hours (red), it is worth noting that upon full conversion of the alkyne the crude is essentially a solution of **37f**. These results confirm again that the zwitterionic complex **30** does not catalyse any alkene isomerisation.

To further support this statement, we performed deuterium labelling experiments. A similar test was conducted with the first generation catalytic system conditions, with 1 mol% of Pd_3^+ complex **17** without the phosphine as additional ligand *(Scheme 14)*.[49]

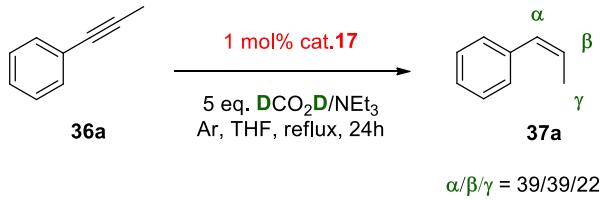

*Scheme 14: Deuterium-labeling experiment with Pd_3^+ catalyst **17***

Deuterium was non selectively retrieved on the three non-aromatic carbons of **37a** in 2:2:1 ratio, using DCOOD as deuterium source. Traces of **38a** and **39a** behave similarly. However, the replacement of formic acid with the deuterated one resulted in a much longer reaction time, from 10 to 24 hours to reach the complete conversion of the alkyne. This is consistent with a relevant primary kinetic isotope effect and, in turn, likely caused partial complex decomposition over the longer experiment, which we speculate as the reason of both double bonds isomerisation and H/D scrambling.[53] We then repeated the reaction in the new conditions with 0.03 mol% of complex **30** and 0.09 mol% of additional ligand *(Scheme 15)*. **36a** converted in 9 hours instead of 6, combining with the higher selectivity towards the *cis*-alkene (**37a**-*d*, 97%). The *trans*-alkene **38a** was not observed, while **39a** formed in traces (**39a**-*d*, 3%). Regarding deuterium incorporation, an average of two D nuclei for each molecule is observed. In alkene **37a**, the α and β positions are almost completely deuterated (85%), but a significant incorporation on the terminal carbon γ is also observed (18%). In **39a** the methylene group shows a high incorporation (84%), while labelling at the β carbon was 50%.

[53] T. G. Gant, *J. Med. Chem.*, **2014**, *57*, 3595.

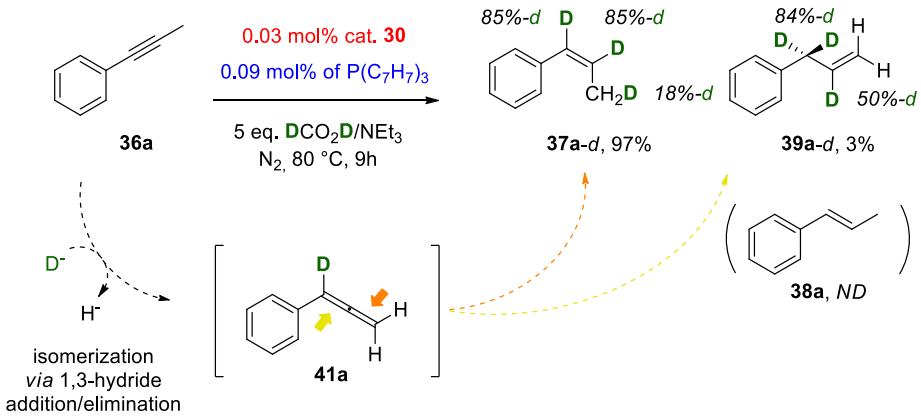

*Scheme 15: Deuterium-labeling experiment with catalyst **30** on **36a***

These findings suggest that **36a** can isomerise to phenylallene **41a** via sequential 1,3-hydride addition/elimination during the reaction.[54] This is consistent with the hypothesis that complex **30** can catalyze both alkyne/allene isomerization and reduction[55] and neither alkene isomerization nor reduction to alkane. These findings have no precedent among homogeneous Pd-based catalysts.[46-47-56] However, we could not exclude at the present stage a similar distribution of olefins resulting from hydrogenolysis of a palladium allyl intermediate, which would favour the formation of the aryl conjugated *cis*-alkene. We repeated the same experiment on alkyne **36d**, which presents a non-conjugated triple bond with a methyl and a methylene substituted by an electron donating oxygen *(Scheme 16)*. As expected, full conversion required a longer time (15 hours), confirming the impact of

[54] a) T. Cañeque, F. M. Truscott, R. Rodriguez, G. Maestri, M. Malacria, *Chem. Soc. Rev*, **2014**, *43*, 2916; b) L. Fensterbank, M. Malacria, *Acc. Chem. Res.*, **2014**, *47*, 953; c) A. Fürstner, P. W. Davies, *Angew. Chem. Int. Ed.*, **2007**, *46*, 3410.

[55] H. Guo, Z. Zheng, F. Yu, S. Ma, A. Holuigue, D. S. Tromp, C. J. Elsevier, Y. Yu, *Angew. Chem. Int. Ed.*, **2006**, *45*, 4997.

[56] a) G. Li, R. C. Jin, *J. Am. Chem. Soc.*, **2014**, *136*, 11347; b) K. Radkowski, B. Sundararaju, A. Furstner, *Angew. Chem. Int. Ed.*, **2013**, *52*, 355; c) K. Tokmic, A. R. Fout, *J. Am. Chem. Soc.*, **2016**, *138*, 13700; d) M. K. Karunananda, N. P. Mankad, *J. Am. Chem. Soc.*, **2015**, *135*, 14598; e) A. Siva Reddy, K.C. Kumara Swamy, *Angew. Chem. Int. Ed.*, **2017**, *56*, 6984; f) S. M. Fu, N. Y. Chen, X. F. Liu, Z. H. Shao, S. P. Luo, Q. Liu, *J. Am. Chem. Soc.*, **2016**, *138*, 8588.

primary kinetic isotope effect. Alkenes **37-39d** formed in a 95:2:3 ratio. Sp^2 carbons in **37d** are almost fully deuterated (90 and 88%), while the amount of **30** on the terminal methyl is 58%, even more than the 18% value observed in **37a**. We were unable to quantify the deuterium incorporation on **38d**, since it formed in a small amount. Regarding **39d**, the allylic methylene is fully deuterated.

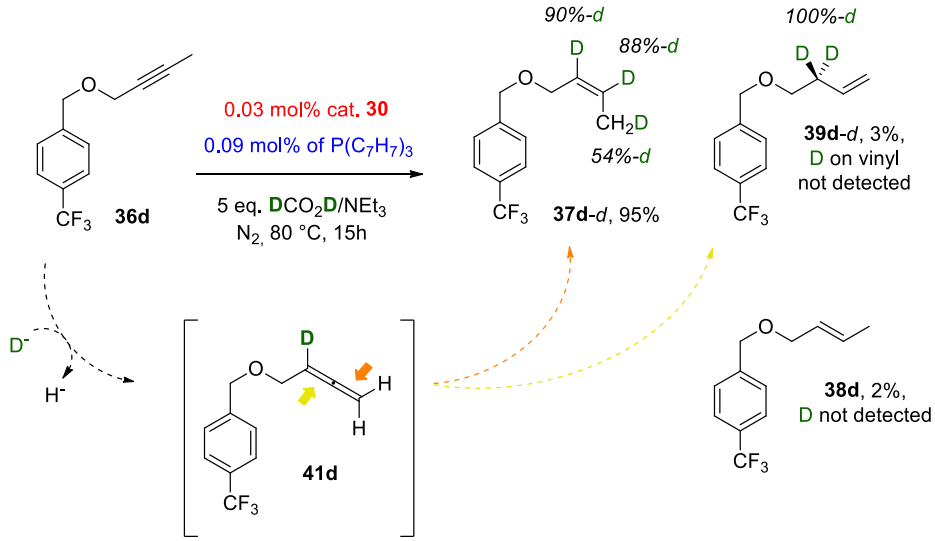

*Scheme 16: Deuterium-labeling experiment with catalyst **30** on **36d***

No deuterium incorporation on the ethereal methylene was detected in products **37-39d**. This could correlate with an unfavourable hydride 1,3-addition/elimination leading to an allene different from **41d** because of the presence of the electron donating ethereal oxygen.

Since isomerisation of **36** to **41** liberates a hydride, this could in principle contribute to catalyst decomposition. Reasoning on the fact that 1,3-hydride addition/elimination on internal alkynes requires a propargylic C-H group, we wondered if we could further push the reaction conditions using diphenylacetylene **36i** as model *(Scheme 17)*. We thus lowered the catalyst

loading to 0.01 mol% and the amount of additional ligand to 0.03 mol%. In addition, we managed to reduce the molar excess of hydrogen donor to 2 equivalents keeping a practical reaction time (6 hours) and still keep a complete selectivity to *cis*-stilbene. This contributes to minimize the consumption of chemicals and the production of waste en route to pure product.[57]

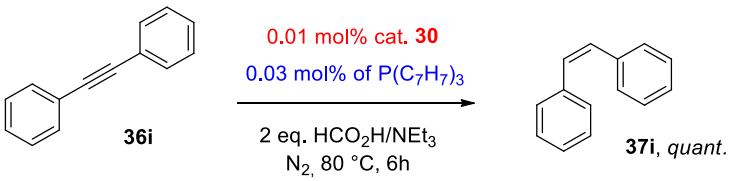

Scheme 17: Semihydrogenation of diphenylacetylene

The reaction can be performed on multi-gram scale (6.24 g, 35 mmol) employing only few milligrams of catalyst and phosphine (4.9 and 3.2 mg, respectively) and 10.3 g of hydrogen donor. To prevent overheating of large scale reaction, neutralization of formic acid with triethylamine can be carried out in advance in a separate flask with an ice bath and the resulting solution can then be syringed in the reaction flask at will. Unreacted triethylamonium formate could be in principle recovered via distillation at the end of the reaction, further minimizing production of wastes. Pure **37i** can be quantitatively recovered (6.31 g) filtering the crude on a short pad of silica gel (4 g) and washing with 12.5 g of pentane (20 ml). With this simple purification, Pd complex remains adsorbed on the silica pad. Even assuming that it quantitatively contaminates the product, this would result in a heavy metal content of 174 ppm only. It is worth noting that the zwitterionic complex could

[57] a) P. J. Dunn, *Chem. Soc. Rev*, **2012**, *41*, 1452; b) R. A. Sheldon, *Chem. Soc. Rev*, **2012**, *41*, 1437; c) R. A. Sheldon, *Chem. Commun.*, **2008**, *44*, 3352; d) I. T. Horváth, P. T. Anastas, *Chem. Rev*, **2007**, *107*, 2169; e) P. T. Anastas, M. M. Kirchoff, *Acc. Chem. Res*, **2002**, *35*, 686; f) B. M. Trost, *Angew. Chem. Int. Ed. Engl*, **1995**, *34*, 259.

be in principle recovered too, since it can be purified by flash column chromatography on silica gel. However, the tiny amount of complex used made this unfeasible in our conditions. This approach would also increase the amount of wastes. In the present reaction TON and TOF went up to 10000 and 3000 h^{-1} respectively.

Green metrics can be calculated to compare the present method with four representative ones, which employ organic solvents and require workup and chromatographic purifications *(Table 13)*.

Entry	Yield (%)	*E*-factor	PMI
this procedure	100	4.24	5.24
Furstner procedure[56b]	82	45.8	46.8
Elsevier procedure[46]	99	31.7	32.7
Copéret procedure[58]	99	24.4	25.5
Studer procedure[48]	99	52.9	53.9

Table 13: Calculated green metrics for the present catalytic method and comparison with other representative procedures for the semihydrogenation of alkynes

We calculated *E*-factor and PMI index to quantify the possible beneficial contribute deriving from the absence of unnecessary organics combined with the simple purification method in our model reaction. The use of solvents, workup extractions and column chromatography usually results in values above 20 even for the most efficient methods. On the contrary, in our case *E*-factor and PMI values are significantly lower, 4.24 and 5.24 respectively.

Taken together, these findings highlight the practical and environmental viability of the present catalytic system.

[58] A. Fedorov, H.-J. Liu, H.-K. Lo, C. Copéret, *J. Am. Chem. Soc.*, **2016**, *138*, 16502.

2.3 Conclusions

Catalytic properties of zwitterionic tripalladium complexes were tested in the semihydrogenation of internal alkynes to *cis*-alkenes. Best results were obtained with the cluster bearing two tri(*p*-tolyl)phosphines and methylthiolates as bridging ligands. Its chemical stability for several thousand tournovers led to unprecedented performances among the mononuclear palladium-based catalysts. We managed to convert a vast array of alkynes using 0.03 mol% of catalyst and 5 equivalents of triethylammonium formate as hydrogen donor. The developed method does not require any additional solvent and a simple work up delivers the pure product. In addition, we performed a multi-gram scale synthesis of *cis*-stilbene, further reducing the catalyst loading to 0.01 mol% and the amount of hydrogen donor to 2 equivalents, demonstrating the practical and environmental viability of our method.

2.4 Experimental section

2.4.1 General remarks

All chemicals whose synthesis are not reported hereafter were purchased from commercial sources and used as received. Solvents were dried and stored over molecular sieves previously activated (350°C overnight). Solvents, triethylammonium formate and liquid reagents were degassed by bubbling N_2 for at least 30 minutes prior to use. Reactions and filtrations were carried out under N_2using standard Schlenk technique.

^{1}H NMR spectra were recorded in $CDCl_3$ Bruker 300 AVANCE spectrometer fitted with a BBFO probe-head at 300 MHz, using the solvent as internal standard (7.26 ppm).

^{13}C NMR spectra were recorded in $CDCl_3$ on a Bruker 300 AVANCE spectrometer fitted with a BBFO probe-head at 75 MHz, using the solvent as internal standard (77.16 ppm).

^{19}F NMR spectra were recorded in $CDCl_3$ at 298 K on a Bruker 400 AVANCE spectrometer fitted with a BBFO probe-head at 376 MHz, using hexafluorobenzene as external standard (-164.9 ppm).

The terms m, s, d, t, q represent multiplet, singlet, doublet, triplet, quadruplet respectively, and the term br means a broad signal.

Exact mass of alkyne **36g** was recorded on a LTQ ORBITRAP XL Thermo Mass Spectrometer (electrospray source). Mass analysis were performed on an Infusion Water Acquity Ultra Performance LC HO6UPS-823M instrument (electrospray source, quadrupole analyser).

UV-Vis spectra were recorded on a Thermo Scientific Evolution 260 Bio UV Spectrophotometer.

Graph 1, *Graph 2* and *Graph 3* were obtained monitoring reactions by GC using *p*-xylene as internal standard (100 µl of crude mixture diluted with 900 µl of methanol).

2.4.2 Synthesis of alkynes

2.4.2.1 Procedure A[49]

Sodium hydride 60% w/w (440 mg, 11 mmol, 1.1 equiv.) and dry THF (0.4 mol/L) were added to an oven-dried Schlenk-type flask. The suspension was cooled to 0°C in an ice bath and then but-2-yn-1-ol (748 µl, 10 mmol, 1.0 eq.) was added dropwise. The mixture was stirred until hydrogen evolution ceased. The desired benzyl bromide (11 mmol, 1.1 eq.) was then added. The solution was allowed to warm to room temperature and stirred overnight. The mixture was quenched with 5 ml of water added dropwise and THF was removed under vacuum. The resulting suspension was extracted by MTBE (3 x 10 ml), the organic layers were collected and dried over $MgSO_4$ anhydrous. The desired product was purified by flash column chromatography on silica gel (eluent: gradient hexane/ethyl acetate).

- **((but-2-yn-1-yloxy)methyl)benzene (36c)**

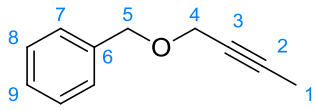

The product was obtained from benzylbromide and but-2-yn-1-ol according to the general procedure described above. NMR data are in accordance with those from the literature.[49]

Isolated as a pale yellow liquid. Yield = 73%

^{1}H NMR (300 MHz, $CDCl_3$) δ (ppm): 7.36-7.25 (m, 5H, $H_{7\text{-}9}$), 4.58 (s, 2H, H_5), 4.13 (dd, 2H, *J* = 2.3, 4.6 Hz, H_4), 1.88 (t, 3H, *J* = 2.3 Hz, H_1).

^{13}C NMR (75 MHz, $CDCl_3$) δ (ppm):137.7 (C_6), 128.4 (C_8), 128.0 (C_7), 127.7 (C_9), 82.6 (C_3), 75.1 (C_2), 71.4 (C_5), 57.7 (C_4), 3.6 (C_1).

- **1-((but-2-yn-1-yloxy)methyl)-4-(trifluoromethyl)benzene (36d)**

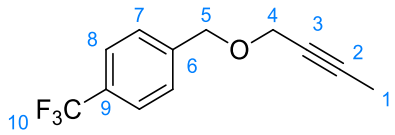

The product was obtained from 4-(trifluoromethyl)benzylbromide and but-2-yn-1-ol according to the general procedure described above. NMR data are in accordance with those from the literature.[49]

Isolated as a pale yellow liquid. Yield = 75%

^{1}H NMR (300 MHz, $CDCl_3$) δ (ppm): 7.60 (d, 2H, *J* = 8.1 Hz, H_8), 7.47 (d, 2H, *J* = 8.0 Hz, H_7), 4.63 (s, 2H, H_5), 4.17 (q, 2H, *J* = 2.3 Hz, H_4), 1.88 (t, 3H, *J* = 2.3 Hz, H_1).

^{13}C NMR (75 MHz, $CDCl_3$) δ (ppm): 141.9 (C_6), 129.7 (q, *J* = 32.5 Hz, C_9), 127.9 (C_7), 125.3 (d, *J* = 3.5 Hz, C_8), 124.2 (q, *J* = 271.7 Hz, C_{10}), 83.1 (C_3), 74.7 (C_2), 70.6 (C_5), 58.2 (C_4), 3.6 (C_1).

^{19}F NMR (376 MHz, $CDCl_3$) δ (ppm): -62.5.

2.4.2.2 Procedure B

2-Butyne-1,4-diol (5.2 g, 60 mmol, 1 eq.) was added to a Schlenk-type flask and the vessel underwent at least three vacuum/N_2 cycles. Freshly degassed dry DMSO (60 ml) was syringed under N_2 and the mixture was stirred until complete solubilization. KOH (10.1 g, 180 mmol, 3 eq.) was slowly added and the mixture was warmed to 35°C. The desired alkyl halide (180 mmol, 3 eq.) was then added and the resulting mixture was kept under magnetic stirring for 72 hours at 35°C. The reaction was quenched with water (50 ml) and the suspension was extracted by ethyl acetate (3 x 50 ml). The organic layer was washed with brine (50 ml) and dried over Na_2SO_4 anhydrous. The desired

product was purified by flash column chromatography on silica gel (eluent: gradient hexane/ethyl acetate).

- **1,4-dimethoxybut-2-yne (36e)**

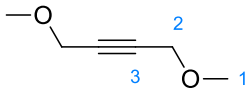

The product was obtained from 2-butyne-1,4-diol and iodomethane according to the general procedure described above. NMR data are in accordance with those from the literature.[59]

Isolated as a colourless oil. Yield = 59%

^{1}H NMR (300 MHz, $CDCl_3$) δ (ppm): 4.14 (s, 4H, H_2), 3.38 (s, 6H, H_1).

^{13}C NMR (75 MHz, $CDCl_3$) δ (ppm): 82.3 (C_3), 59.8 (C_1), 57.5 (C_2).

- **1,4-bis(benzyloxy)but-2-yne (36f)**

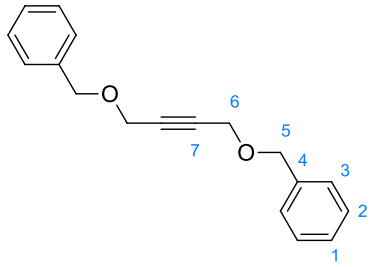

[59] K. G. M. Kou, B. X. Li, J. C. Lee, G. M. Gallego, T. P. Lebold, A. G. Di Pasquale, R. Sarpong, *J. Am. Chem. Soc.*, **2016**, *138*, 10830.

The product was obtained from 2-butyne-1,4-diol and benzyl bromide according to the general procedure described above. NMR data are in accordance with those from the literature.[60]

Isolated as a pale yellow oil. Yield = 52%

^{1}H NMR (300 MHz, $CDCl_3$) δ (ppm): 7.38 (m, 10H, $H_{1\text{-}3}$), 4.66 (s, 4H, H_6), 4.29 (s, 4H, H_5).

^{13}C NMR (75 MHz, $CDCl_3$) δ (ppm): 137.5 (C_4), 128.5 (C_3), 128.1 (C_2), 127.9 (C_1), 82.6 (C_7), 71.7 (C_5), 57.5 (C_6).

- **1,4-bis((4-bromobenzyl)oxy)but-2-yne (36g)**

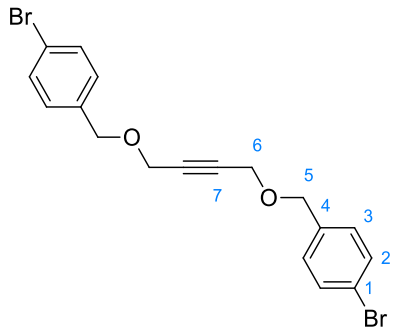

The product was obtained from 2-butyne-1,4-diol and 4-bromobenzyl bromide according to the general procedure described above.

Isolated as white crystals. Yield = 36%

HRMS calculated for $C_{18}H_{20}O_2NBr_2$ $[M+NH_4]^+$: 441.9835, found: 441.9834.

^{1}H NMR (300 MHz, $CDCl_3$) δ (ppm): 7.48 (d, *J*= 8.39 Hz, 4H, H_2), 7.23 (d, *J*= 8.46 Hz, 4H, H_3), 4.55 (s, 4H, H_6), 4.23 (s, 4H, H_5).

^{13}C NMR (75 MHz, $CDCl_3$) δ (ppm): 136.4 (C_1), 131.6 (C_2), 129.6 (C_3), 121.8 (C_4), 82.5 (C_7), 70.9 (C_5), 57.6 (C_6).

---

[60] J. S. Panek, T. Hu, *J. Org. Chem.,* **1997**, *62*, 4912.

2.4.2.3 Procedure C

The desired aryl iodide (10 mmol, 1.0 eq.), the terminal alkyne (11 mmol, 1.1 eq.) and dry THF (0.1 mol/L) were added to a Schlenk-type flask previously dried in the oven. The mixture was stirred under N_2 and $Pd(PPh_3)Cl_2$ (351 mg, 0.5 mmol, 0.05 eq.), CuI (114 mg, 0.6 mmol, 0.06 eq.) and trimethylamine (2.8 ml, 20 mmol, 2.0 eq.) were sequentially added. The resulting black mixture was stirred at room temperature until complete consumption of the starting material (monitored by TLC). The crude was diluted with 30 ml of ethyl acetate and washed with brine (3x20 ml). The organic phase was dried over $MgSO_4$ anhydrous, filtered and evaporated under vacuum. The desired product was purified by flash column chromatography on silica gel (eluent: gradient hexane/ethyl acetate).

- **3-(p-tolylethynyl)pyridine (36j)**

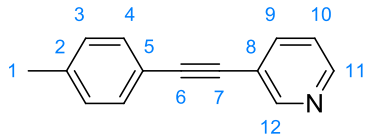

The product was obtained from 3-ethynylpyridine and 4-iodotoluene according to the general procedure described above. NMR data are in accordance with those from the literature.[49]

Isolated as a white solid. Yield = 94%

^{1}H NMR (300 MHz, $CDCl_3$) δ (ppm): 8.76 (d, 1H, *J* = 1.4 Hz, H_{12}), 8.53 (dd, 1H, *J* = 1.4, 4.9 Hz, H_{11}), 7.80 (dt, 1H, *J* = 1.9, 7.9 Hz, H_9), 7.44 (d, 2H, *J* = 8.1 Hz, H_4), 7.30-7.26 (m, 1H, H_{10}), 7.18 (d, 2H, *J* = 7.9 Hz, H_3), 2.38 (s, 3H,H_1).

^{13}C NMR (75 MHz, $CDCl_3$) δ (ppm): 152.2 (C_{12}), 148.3 (C_{11}), 139.1 (C_5), 138.4 (C_9), 131.6 (C_4), 129.2 (C_3), 123.0 (C_{10}), 120.7 (C_8), 119.4 (C_5), 92.9 (C_6), 85.3 (C_7), 21.5 (C_1).

2.4.3 Spectroscopic data of alkenes a-n

- **Table 12, entry 1**

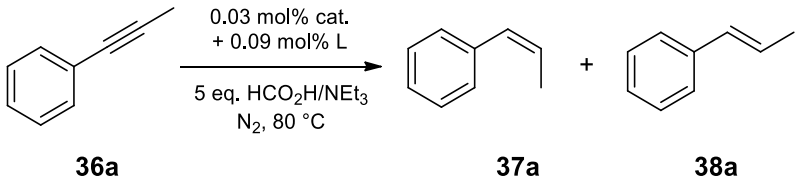

The semi-reduction of alkyne **36a** reached full conversion in 6 hours, delivering products **37a** and **38a** in quantitative yield and 98/2 ratio.

The mixture of products was isolated as a colorless liquid. NMR data are in accordance with those from the literature.[49]

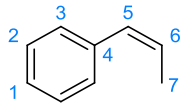

37a

^{1}H NMR (300 MHz, $CDCl_3$) δ (ppm): 7.41-7.23 (m, 5H, $H_{1\text{-}3}$), 6.49 (dd, 1H, *J* = 1.3, 11.6 Hz, H_5), 5.84 (dq, 1H, *J* = 7.2, 11.8 Hz, H_6), 1.95 (dd, 3H, *J* = 1.7, 7.2 Hz, H_7).

^{13}C NMR (75 MHz, $CDCl_3$) δ (ppm): 137.6 (C_4), 129.8 (C_5), 128.8 (C_3), 128.1 (C_2), 126.8 (C_6), 126.4 (C_1), 14.6 (C_7).

- **Table 12, entry 2**

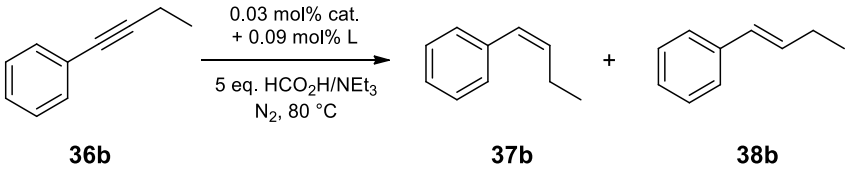

The semi-reduction of alkyne **36b** reached full conversion in 15 hours, delivering products **37b** and **38b** in quantitative yield and 90/10 ratio.
The mixture of products was isolated as a colorless liquid. NMR data are in accordance with those from the literature.[49]

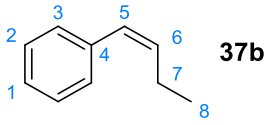

37b

^{1}H NMR (300 MHz, $CDCl_3$) δ (ppm): 7.46-7.23 (m, 5H, H_{1-3}), 6.44 (dt, 1H,*J* = 1.7, 11.8 Hz, H_5), 5.71 (dt, 1H,*J* = 7.3, 11.6 Hz, H_6), 2.40 (pentet of d, 2H, *J* = 1.8, 7.5 Hz, H_7), 1.11 (t, 3H,*J* =7.5 Hz, H_8).
^{13}C NMR (75 MHz, $CDCl_3$) δ (ppm): 137.8 (C_4), 134.7 (C_6), 128.7 (C_3), 128.2 (C_2), 128.1 (C_5), 126.4 (C_1), 21.9 (C_7), 14.4 (C_8).

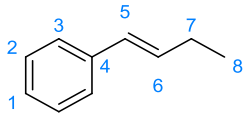

38b

^{1}H NMR (300 MHz, CDCl3) δ (ppm): 7.46-7.23 (m, 5H, H_{1-3}), 6.34 (t, 1H, *J* = 6.1 Hz, H_5), 5.66-5.58 (m, 1H,H_6), 2.31-2.26 (m, 2H,H_7), 1.15 (t, 3H, *J* =7.5 Hz, H_8).
^{13}C NMR (75 MHz, CDCl3) δ (ppm): 137.9 (C_4), 132.6 (C_6), 128.4 (C_3), 128.2 (C_2), 126.7 (C_5), 125.9 (C_1), 26.0 (C_7), 13.1 (C_8).

- **Table 12, entry 3**

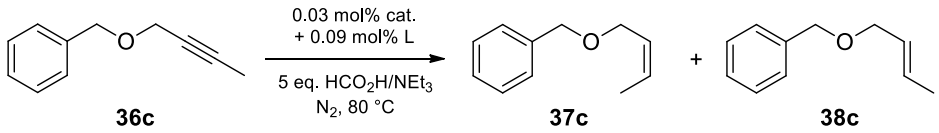

36c **37c** **38c**

The semi-reduction of alkyne **36c** reached full conversion in 6 hours, delivering products **37c** and **38c** in quantitative yield and 93/7 ratio.

The mixture of products was isolated as a pale yellow liquid. NMR data are in accordance with those from the literature.[49]

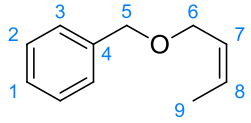

37c

^{1}H NMR (300 MHz, $CDCl_3$) δ (ppm): 7.38-7.27 (m, 5H, $H_{1\text{-}3}$), 5.74-5.58 (m, 2H, $H_{7\text{-}8}$), 4.52 (s, 2H, H_5), 4.10 (dd, 2H, *J* = 3.2, 3.4 Hz, H_6), 1.65 (dd, 3H, *J* =0.8, 6.2 Hz, H_9).

^{13}C NMR (75 MHz, $CDCl_3$) δ (ppm): 138.5 (C_4), 128.4 (C_3), 128.0 (C_1), 127.8 (C_2), 127.6 (C_7 or C_8), 126.9 (C_7 or C_8), 72.1 (C_5), 65.4 (C_6), 13.2 (C_9).

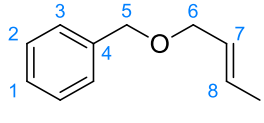

38c

^{1}H NMR (300 MHz, $CDCl_3$) δ (ppm): 7.38-7.27 (m, 5H, $H_{1\text{-}3}$), 5.74-5.58 (m, 2H, $H_{7\text{-}8}$), 4.50 (s, 2H, H_5), 3.96 (dd, 2H, *J* = 1.1, 6.0 Hz, H_6), 1.73 (dd, 3H, *J* =1.1, 6.1 Hz, H_9).

^{13}C NMR (75 MHz, $CDCl_3$) δ (ppm): 136.1 (C_4), 71.9 (C_5), 70.9 (C_6), 17.9 (C_9).

- **Table 12, entry 4**

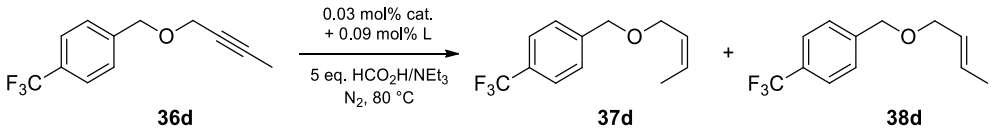

The semi-reduction of alkyne **36d** reached full conversion in 3 hours, delivering products **37d** and **38d** in quantitative yield and 96/4 ratio.

The mixture of products was isolated as a pale yellow liquid. NMR data are in accordance with those from the literature.[49]

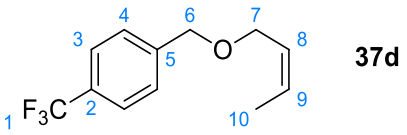

37d

^{1}H NMR (300 MHz, $CDCl_3$) δ (ppm): 7.61 (d, 2H, *J* = 8.1 Hz, H_3), 7.47 (d, 2H, *J* = 8.0 Hz, H_4), 5.74-5.58 (m, 2H, $H_{8\text{-}9}$), 4.57 (s, 2H, H_6), 4.12 (d, 2H, *J* = 6.2 Hz, H_7), 1.66 (dd, 3H, *J* = 0.8, 6.6 Hz, H_{10}).

^{13}C NMR (75 MHz, $CDCl_3$) δ (ppm): 142.7 (C_5), 129.7 (q, *J* = 32.5 Hz, C_2), 128.5 (C_8), 127.6 (C_4), 126.5 (C_9), 125.3 (q, *J* = 3.8 Hz, C_3), 124.2 (q, *J* = 272.0 Hz, C_1), 71.2 (C_6), 65.8 (C_7), 13.2 (C_{10}).

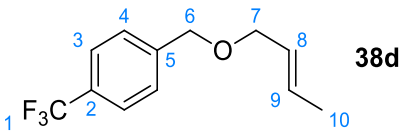

38d

^{1}H NMR (300 MHz, $CDCl_3$) δ (ppm): 4.55 (s, 2H, H_6), 3.99 (d, 2H, *J* = 6.0 Hz, H_7), 1.74 (dd, 3H, *J* = 1.2, 6.2 Hz, H_{10}).

^{13}C NMR (75 MHz, $CDCl_3$) δ (ppm): 143.0 (C_5), 129.8 (C_2), 128.5 (C_9), 126.4 (C_8), 71.5 (C_6), 71.0 (C_7), 17.7 (C_{10}).

- **Table 12, entry 5**

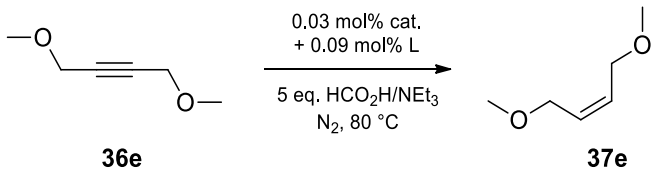

36e **37e**

The semi-reduction of alkyne **36e** reached a conversion of 95% in 13 hours, delivering product **37e** with complete selectivity.

The product was not isolated because of its volatility. Chemical shifts of **37e** in ^{1}H and ^{13}C NMR spectra of the crude mixture are listed below.

NMR data of alkene **37e** are in accordance with those from the literature.[61]

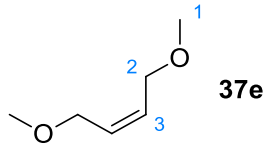

37e

^{1}H NMR (300 MHz, $CDCl_3$, crude mixture) δ (ppm): 8.51 (s, 1H, HCOOH), 5.70 (dd, J_1= 4.6, J_2= 3.7 Hz, 2H, H_3), 3.99 (d, J = 4.1 Hz, H_2), 3.22 (s, 6H, H_1), 3.05 (q, J = 7.0 Hz, $N(CH_2CH_3)_3$), 1.28 (t, J = 7.3 Hz, $N(CH_2CH_3)_3$).

^{13}C NMR (75 MHz, $CDCl_3$, crude mixture) δ (ppm): 168.31 (HCOOH), 129.3 (C_3), 68.1 (C_2), 58.0 (C_1), 44.99 ($N(CH_2CH_3)_3$), 8.50 ($N(CH_2CH_3)_3$).

[61] D. M. Hodgson, B. Štefane, T. J. Miles, J. Witherington, *J. Org. Chem.,* **2006**, *71*, 8510.

- **Table 12, entry 6**

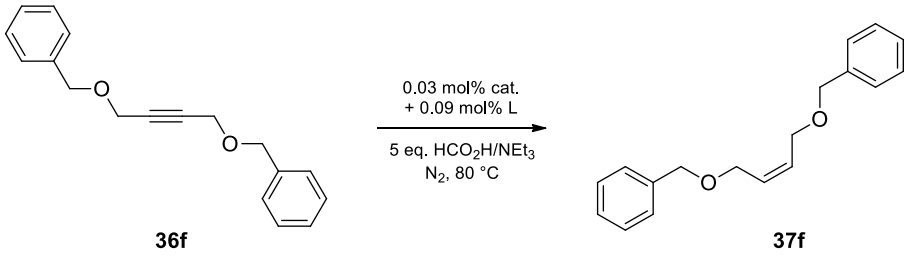

The semi-reduction of alkyne **36f** reached full conversion in 5 hours, delivering product **37f** in quantitative yield and complete selectivity.

The product was isolated as a pale yellow oil.

NMR data of alkene **37f** are in accordance with those from the literature.[62]

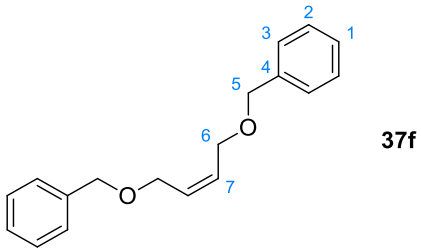

^{1}H NMR(300 MHz, $CDCl_3$) δ (ppm): 7.32 (m, 10H, $H_{1\text{-}3}$), 5.81 (t, *J*= 3.82 Hz, 2H, H_7), 4.50 (s, 4H, H_5), 4.08 (d, *J*= 4.69 Hz, 4H, H_6).

^{13}C NMR (75 MHz, $CDCl_3$) δ (ppm): 138.2 (C_4), 129.5 (C_3), 128.4 (C_2), 127.8 (C_2), 127.7 (C_7), 72.3 (C_5), 65.8 (C_6).

[62] J. M. Schomaker, S. Bhattacharjee, J. Yan, B. Borhan, *J. Am. Chem. Soc.*, **2007**, *129*, 1996.

- **Table 12, entry 7**

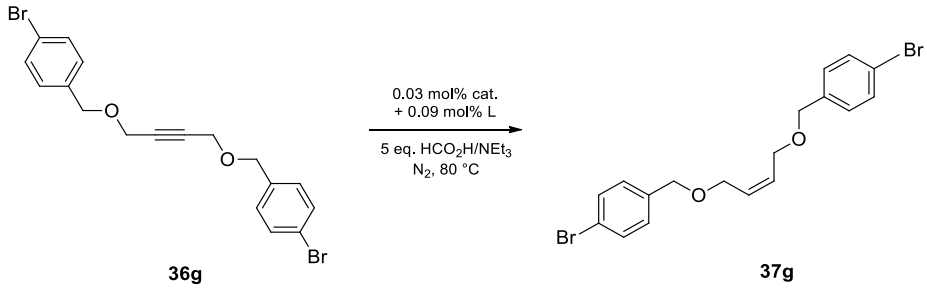

The semi-reduction of alkyne **36g** reached full conversion in 5 hours, delivering product **37g** in quantitative yield and complete selectivity.
Isolated as white crystals.
NMR data of alkene **37g** are in accordance with those from the literature.[63]

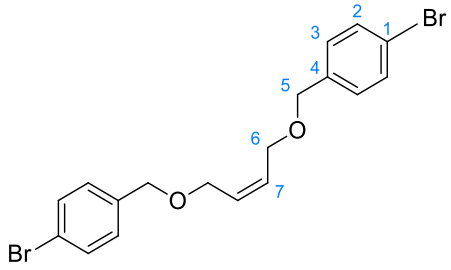

37g

^{1}H NMR (300 MHz, $CDCl_3$) δ (ppm): 7.47 (d, *J*= 8.34 Hz, 4H, H_2), 7.19 (d, *J* = 8.30 Hz, 4H, H_3), 5.78 (t, *J* = 3.86 Hz, 2H, H_7), 4.43 (s, 4H, H_5), 4.05 (d, *J* = 4.66 Hz, 4H, H_6).

^{13}C NMR (75 MHz, $CDCl_3$) δ (ppm): 137.1 (C_1), 131.5 (C_2), 129.4 (C_3), 129.3 (C_4), 121.6 (C_7), 71.5 (C_5), 65.8 (C_6).

[63] C. Y. Chuang, V. C. Vassar, Z. Ma, R. Geney, I. Ojima, *Chirality,* **2002**, *14*, 151.

- **Table 12, entry 8**

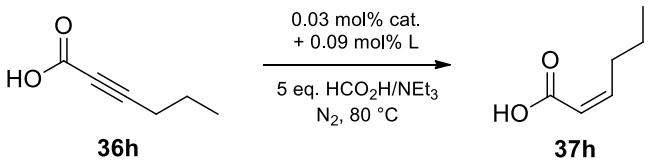

36h **37h**

The semi-reduction of alkyne **36h** reached full conversion in 6 hours, delivering product **37h** in quantitative yield and complete selectivity.
The product was isolated as a colorless oil. NMR data are in accordance with those from the literature.[64]

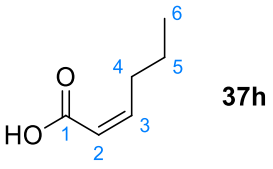

37h

^{1}H NMR (300 MHz, $CDCl_3$) δ (ppm): 6.35 (dt, 1H, *J* = 7.5, 11.6 Hz, H_3), 5.80 (dt, 1H, *J* = 1.5, 11.5 Hz, H_2), 2.64 (qd, 2H, *J* = 1.6, 7.5 Hz, H_4), 1.54-1.42 (m, 2H, H_5), 0.95 (t, 3H, *J* = 7.4 Hz, H_6).
^{13}C NMR (75 MHz, $CDCl_3$) δ (ppm): 171.8 (C_1), 153.2 (C_3), 119.2 (C_2), 31.1 (C_4), 22.2 (C_5), 13.7 (C_6).

[64] P. M. Savu, J. A. Katzenellenbogen, *J. Org. Chem.,* **1981**, *46*, 239.

- **Table 12, entry 9**

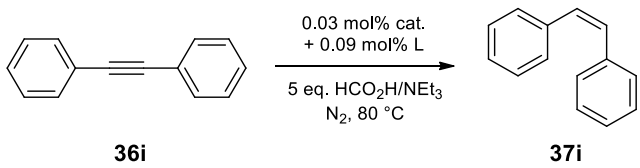

The semi-reduction of alkyne **36i** reached full conversion in 3 hours, delivering the product **37i** in quantitative yield and complete selectivity.

The product was isolated as a white solid. NMR data are in accordance with those from the literature.[49]

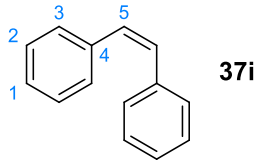

^{1}H NMR (300 MHz, $CDCl_3$) δ (ppm): 7.31-7.26 (m, 10H, $H_{1\text{-}3}$), 6.69-6.67 (m, 2H, H_5).

^{13}C NMR (75 MHz, $CDCl_3$) δ (ppm): 137.2 (C_4), 130.2 (C_5), 128.9 (C_3), 128.2 (C_2), 127.1 (C_1).

- **Table 12, entry 10**

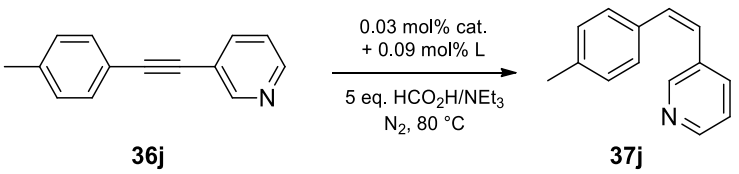

36j **37j**

The semi-reduction of alkyne **36j** reached full conversion in 7 hours, delivering product **37j** in quantitative yield and complete selectivity.

The product was isolated as a colorless oil. NMR data are in accordance with those from the literature.[49]

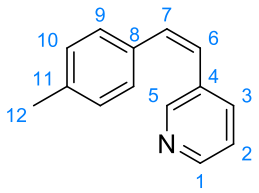

37j

^{1}H NMR (300 MHz, $CDCl_3$) δ (ppm): 8.48 (s, 1H, H_5), 8.41 (d, 1H, *J* = 3.8 Hz, H_1), 7.53 (dt, 1H, *J* = 1.6, 7.9 Hz, H_3), 7.14-7.03 (m, 5H, H_2, H_9, H_{10}), 6.71 (d, 1H, *J* = 12.2 Hz, H_7), 6.49 (d, 1H, *J* = 12.2 Hz, H_6), 2.31 (s, 3H, H_{12}).

^{13}C NMR (75 MHz, $CDCl_3$) δ (ppm): 150.1 (C_5), 147.9 (C_1), 137.4 (C_{11}), 135.8 (C_3), 133.5 (C_4), 133.2 (C_8), 132.6 (C_7), 129.2 (C_{10}), 128.6 (C_9), 125.7 (C_6), 122.9 (C_2), 21.2 (C_{12}).

- **Table 12, entry 11**

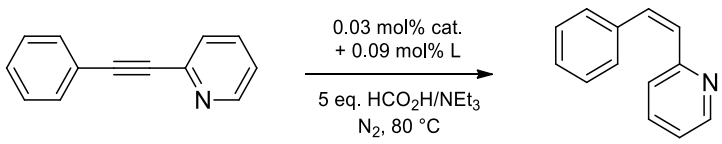

36k **37k**

The semi-reduction of alkyne **36k** reached full conversion in 15 hours, delivering product **37k** in quantitative yield and complete selectivity.

The product was isolated as a brown oil. NMR data are in accordance with those from the literature.[65]

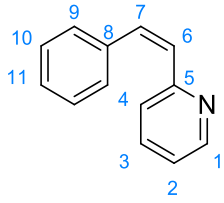

37k

^{1}H NMR (300 MHz, $CDCl_3$) δ (ppm): 8.60 (d, 1H, *J* = 5.3 Hz, H_1), 7.68-7.08 (m, 9H, $H_{2\text{-}4}$,$H_{9\text{-}11}$), 6.85 (d, 1H, *J* = 12.5 Hz, H_6), 6.71 (d, 1H, *J* = 12.5 Hz, H_7).

^{13}C NMR (75 MHz, $CDCl_3$) δ (ppm): 156.3 (C_5), 149.5 (C_1), 136.6 (C_3), 135.6 (C_8), 133.3 (C_7), 130.4 (C_{11}), 128.9 (C_{10}), 128.3 (C_9), 127.6 (C_6), 125.7 (C_6), 123.8 (C_4), 121.7 (C_2).

[65] D.-J. Dong, H.-H. Li, S.-K. Tian, *J. Am. Chem. Soc.*, **2010**, *132*, 5018.

- **Table 12, entry 12**

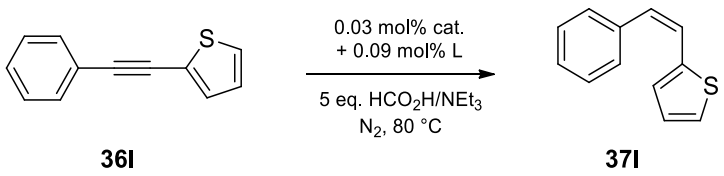

36l **37l**

The semi-reduction of alkyne **36l** reached full conversion in 6 hours, delivering product **37l** in quantitative yield and complete selectivity.

The product was isolated as a orange oil. NMR data are in accordance with those from the literature.[66]

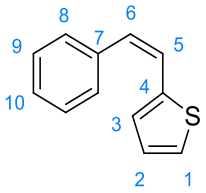

37l

^{1}H NMR (300 MHz, $CDCl_3$) δ (ppm): 7.37-7.30 (m, 5H, $H_{8\text{-}10}$), 7.10 (d, 1H, *J* = 5.1 Hz, H_1), 6.98 (d, 1H, *J* = 3.5 Hz, H_3), 6.89 (dd, 1H, *J* = 3.7, 5 Hz, H_2), 6.71 (d, 1H, *J* = 12.0 Hz, H_5), 6.59 (d, 1H, *J* = 12.0 Hz, H_6).

^{13}C NMR (75 MHz, $CDCl_3$) δ (ppm): 139.8 (C_4), 137.3 (C_7), 128.9 (C_6), 128.8 (C_9), 128.5 (C_8), 128.1 (C_3), 127.5 (C_{10}), 126.4 (C_2), 125.5 (C_1), 123.3 (C_5).

[66] J. Li, R. Hua, T. Liu, *J. Org. Chem.*, **2010**, *75*, 2966.

- **Table 12, entry 13**

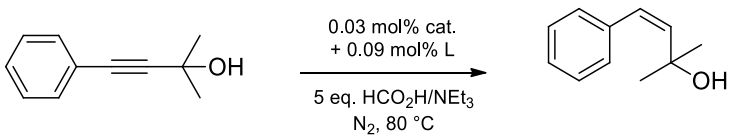

36m **37m**

The semi-reduction of alkyne **36m** reached full conversion in 4 hours, delivering product **37m** in quantitative yield and complete selectivity.
The product was isolated as a yellow liquid. NMR data are in accordance with those from the literature.[67]

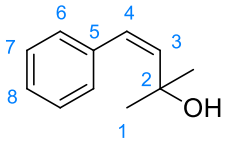

37m

^{1}H NMR (300 MHz, $CDCl_3$) δ (ppm): 7.37-7.24 (m, 5H, H_{6-8}), 6.46 (d, 1H, *J* = 12.7 Hz, H_4), 5.76 (d, 1H, *J* = 12.7 Hz, H_3), 1.36 (s, 6H, H_1).
^{13}C NMR (75 MHz, $CDCl_3$) δ (ppm): 139.3 (C_3), 137.5 (C_5), 129.0 (C_6), 128.1 (C_7), 127.8 (C_4), 126.9 (C_8), 72.0 (C_2), 31.1 (C_1).

[67] Z. Q. Liu, L. Sun, J. G. Wang, J. Han, Y. K. Zhao, B. Zhou, *Org. Lett.*, **2009**, *11*, 1437.

- **Table 12, entry 14**

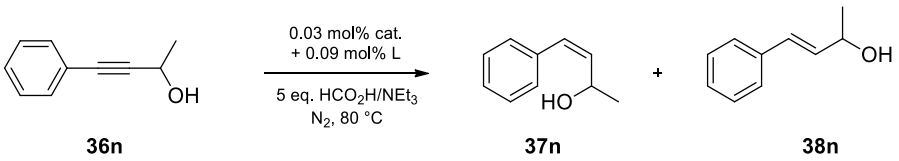

36n **37n** **38n**

The semi-reduction of alkyne **36n** reached a conversion of 85% in 6 hours, delivering product **37n** in 94% selectivity with traces of **38n**.

The crude was diluted with EtOAc (10 ml) and the organic phase washed three times with brine (3x10 ml). Upon evaporation of solvent the product was recovered as a yellow liquid. NMR data are in accordance with those from the literature.[67]

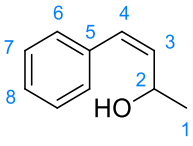

37n

^{1}H NMR (300 MHz, $CDCl_3$) δ (ppm): 7.35-7.26 (m, 5H, $H_{6\text{-}8}$), 6.51 (d, 1H, *J* = 11.6 Hz, H_4), 5.70 (dd, 1H, *J* =9.1, 11.6 Hz, H_3), 4.84-4.72 (m, 1H, H_2), 1.36 (s, 6H, H_1).

^{13}C NMR (75 MHz, $CDCl_3$) δ (ppm): 136.6 (C_5), 135.6 (C_4), 130.1 (C_3), 128.8 (C_7), 128.3 (C_6), 127.2 (C_8), 64.2 (C_2), 23.6 (C_1).

Chapter 3

SYNTHESIS OF MIXED METAL CLUSTERS OF PALLADIUM, PLATINUM AND RUTHENIUM

3.1 Introduction

3.1.1 Mixed metal clusters of palladium and platinum

Reasoning on the fact that palladium and platinum are isoelectronic and that Pd_3^+ and Pt_3^+ clusters can be easily obtained using commercial reagents, the group investigated the possibility to combine the two transition metals in a single species. Applying the standard methodology, Pd and Pt precursors were mixed in chloroform in a 2 : 1 or 1 : 2 ratio, together with 1 equivalent of 4-fluorophenyl phosphine and 0.5 equivalents of 4-chlorophenyl disulfide. The formation of the desired products was observed via HRMS analyses, confirming the possibility to obtain heteronuclear aromatic clusters. However, the selectivity was low *(Fig. 19)*.[30]

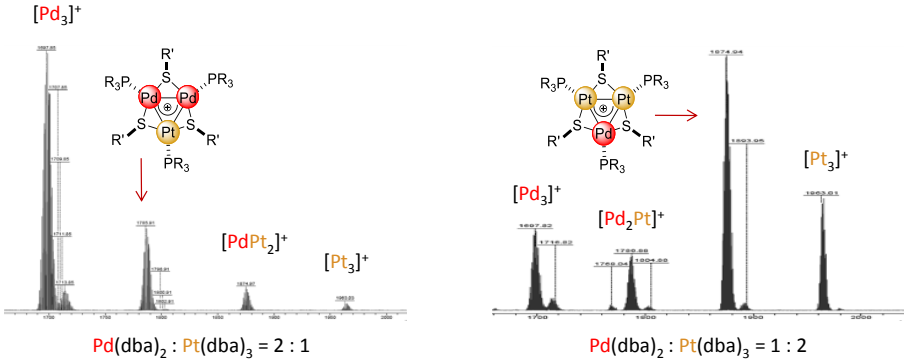

Fig.19: HRMS analysis of crude mixtures of reactions with 2:1 and 1:2 ratio of $Pd(dba)_2$ and $Pt(dba)_3$

In both the two cases the reaction led to the formation of the four possible complexes. While with a Pd : Pt ratio of 1 : 2 the $[Pt_2Pd]^+$ complex was the major product, with a Pd : Pt ratio of 2 : 1 the $[Pd_2Pt]^+$ complex formed in just 21% yield. This behaviour could be due to the lower reactivity of $Pt(dba)_3$, which should lose one more ligand compared to $Pd(dba)_2$.

3.2 Results and discussion

We wondered if information acquired on the mechanism of formation of the trinuclear complexes presented in the first chapter could have enabled us to the selectivity of the process.[40] We speculated that the delocalized three-center two-electron bond might result from the formal addition of a Pd(0) fragment onto a coordinatively unsaturated Pd(II) dimer. We chose Pd(II) dimer **40** as target, thinking that it could represent an intermediate in the reaction of formation of Pd_3^+ species. This dimer featured two benzenethiolates as bridging ligands, a triphenylphosphine and a chloride anion as ligands on each palladium atom. We mixed 1 equivalent of **40** with 1 equivalent of $Pd(dba)_2$, 1 equivalent of PPh_3 and 1 equivalent of sodium thiophenate. All reagents were allowed to dissolve in a redox-neutral solvent, namely C_6D_6, then we added 1 equivalent of $AgSbF_6$ as halogen scavenger.

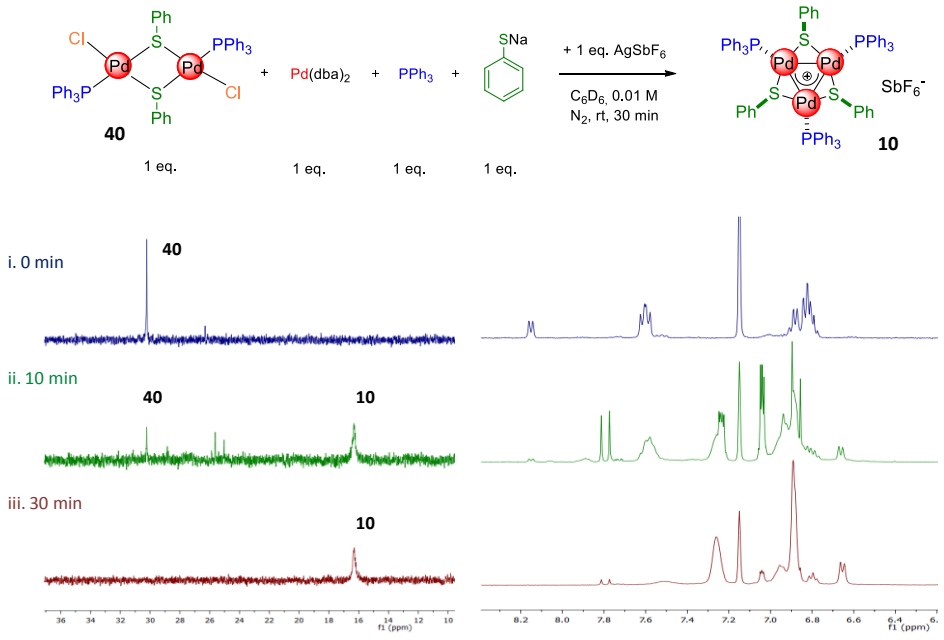

*Fig. 20: Synthesis of complex **10** from a dimer **40** and a $Pd(dba)_2$*

Multinuclear NMR analysis showed that dimer **40** completely converted into Pd_3^+ complex within 30 minutes *(red line, Fig. 20)*, witnessing the selectivity of the process.

This new synthetic strategy is thus complementary to those existing in literature,[20-25-27-68] which exclusively rely on the addition of an oxidized mononuclear complex, such as Au(I) or Zn(II) fragments, on a reduced metal dimer that formally provides two electrons to the metal-aromatic complex, like Au(0) or Zn(I) respectively. This could eventually extend the panel of readily available prototypical metal surfaces.

We thus tried to exploit this new strategy in the synthesis of mixed-metal clusters of palladium and platinum.

We added 1 equivalent of $Pt(dba)_3$ to the Pd(II) dimer **40**, followed by 1 equivalent of PPh_3 and 1 equivalent of sodium thiophenate. 1 hour upon the addition of 1 equivalent of $AgSbF_6$ the crude mixture in toluene had the composition showed in *Figure 21*. The reaction seemed to be selective towards the formation of heteronuclear complexes. The major product was the desired $[Pd_2Pt]^+$ cluster **42**, which formed with a 57% yield (estimated from HRMS), while $[Pt_2Pd]^+$ formed with a 25% yield. On the contrary, homonuclear species Pd_3^+ and Pt_3^+ formed in very low quantity, 10 and 5% respectively. The yield of the desired complex significantly increased, proving that this could be a valuable strategy to obtain new metal surfaces.

[68] F. Fu, J. Xiang, H. Cheng, L. Cheng, H. Chong, S. Wang, P. Li, S. Wei, M. Zhu, Y. Li, *ACS Catal.*, **2015**, *44*, 6519.

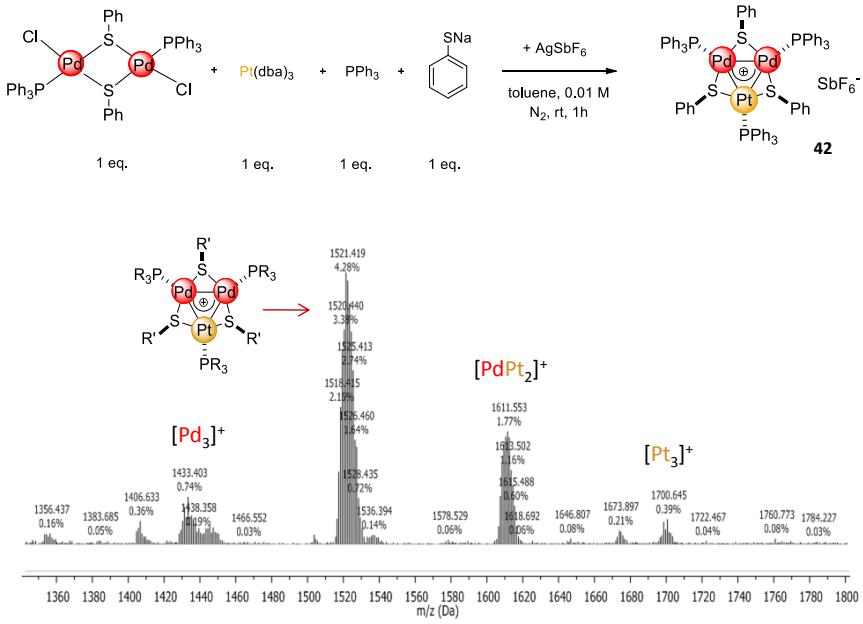

*Fig. 21: HRMS analysis of the synthesis of mixed-metal cluster **42** from a dimer of Pd(II) and a monomer of Pt(0)*

3.2.1 Synthesis of Pd_2Ru clusters

We previously demonstrated that Pd_3^+ clusters can be obtained from the formal addition of a Pd(0) fragment onto a coordinatively unsaturated Pd(II) dimer.[40] This new strategy proved useful to synthesize mixed-metal clusters of palladium and platinum too, by adding a Pt(0) precursor to a Pd(II) dimer. Intrigued by the improved selectivity of this process compared to previous attempts, we supposed we could in principle extend the number of available structures replacing palladium and platinum with other metals. We thus met this challenge and we made the first attempt with ruthenium. We mixed dichloro(*p*-cymene)ruthenium(II) dimer with 1 equivalent of $Pd(dba)_2$, 1 equivalent of triphenylphosphine, 3 equivalents of sodium thiophenate and 3 equivalents of $AgSbF_6$, which should act as halogen scavenger *(Scheme 18)*. We

performed the reaction in a redox-neutral solvent, namely toluene, to avoid any competitive reaction.

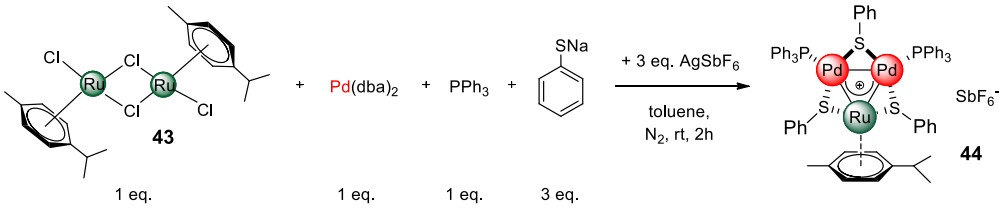

*Scheme 18: Synthesis of the first Pd_2Ru cluster (**44**)*

The crude mixture appeared deep red in colour few minutes upon the complete solubilization of all reagents, but it interestingly turned to green two hours later. Analysis on TLC revealed the presence of a green spot among others, suggesting that the selectivity of the reaction was pretty low. Species obtained proved stable on silica gel and we could indeed isolate the major products by flash column chromatography. Combination of multinuclear NMR analysis, mass spectrometry and X-Ray diffraction let us to identify three complexes, namely a mixed-metal cluster with a triangular core made up of two atoms of palladium and one atom of ruthenium (**44**), a dimer of Ru(II) with three thiolates as bridging ligands and a *p*-cymene on each ruthenium atom (**45**), and Pd_3^+ cluster **10** *(Fig. 22)*.

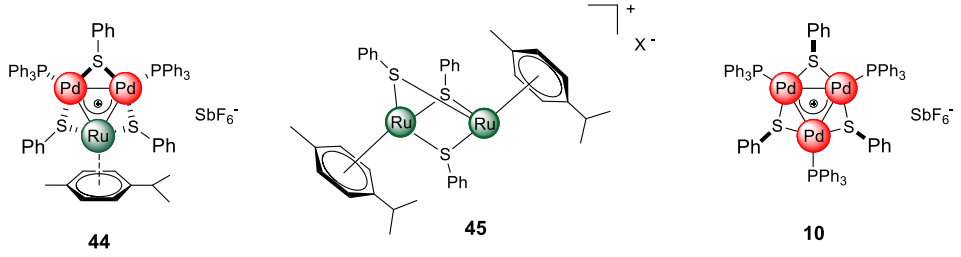

Fig. 22: Products of reaction 18

Surprisingly, we did not detect the mixed-metal cluster with two ruthenium and a palladium atom, suggesting that dimer **43** preferentially broke to release a reactive monomeric fragment. Complex **45** likely formed upon ligand exchange on dichloro(*p*-cymene)ruthenium(II) dimer, while the formation of Pd_3^+ cluster probably occurred upon a redox reaction promoted by the excess of silver salt.

Crystals of **44** suitable for X-Ray analysis were obtained upon cristallization by vapour diffusion using CH_2Cl_2/hexane *(Fig. 23)*. The present complex has a metal core composed by two palladium and a ruthenium atoms, which coordinate two phosphines and a *p*-cymene respectively, while thiolates act as bridging ligands between metal atoms. It has an overall positive charge balanced by a non-coordinating counterion. Pd_2Ru is smaller compared to Pd_3^+ and loses its perfectly equilateral arrangement. Pd-Ru distances are 2.7430(6) and 2.7692(7) Å, while Pd-Pd one is slightly shorter, 2.7379(7) Å. The three angles of the triangular core are 59.56(2)°, 59.74(2)° and 60.69(2)°, while Ru-S-Pd and Pd-S-Pd angles are 73.52(5)°, 73.68(5)° and 72.45(5)° respectively. The arrangement of ligands is in sharp contrast with that observed in Pd_3^+ complexes, where all the heteroatoms which complete the first sphere of coordination of palladium atoms are coplanar to the metal core. In Pd_2Ru instead, thiolates between ruthenium and palladium and between the two palladium atoms point above and below the plane of the triangle, with dihedral angles of 95.27(4)°, 97.33(4)° and 96.88(4)° respectively. Phosphines remain essentially coplanar to the metal core, with dihedral angles of 150.15(5)° and 157.66(5)°.

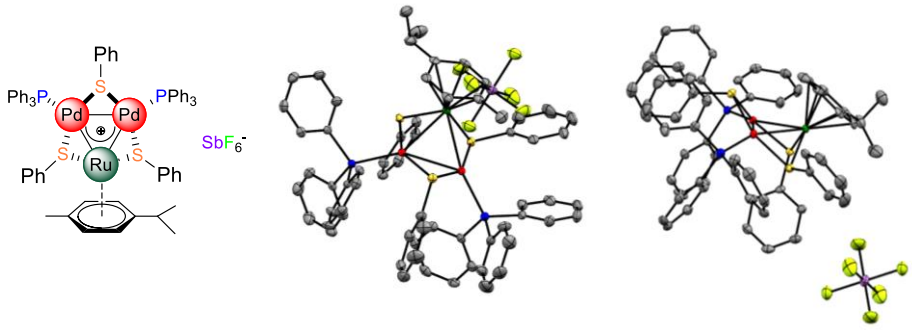

*Fig. 23: X-Ray structure of Pd_2Ru cluster **44***

Unfortunately, we managed to obtain the pure compound just by crystallization. As the matter of fact, we found really hard to isolate the Pd_2Ru complex from byproducts by chromatography, since the present cluster and ruthenium dimer **45** have a similar retention factor with most of eluents.
Nonetheless, **44** is the first example of a mixed Ru-Pd trinuclear cluster.
We then tried to overcome purification issues optimizing reaction conditions in the hope to obtain a higher yield of Pd_2Ru. We firstly diluted the reaction mixture from 0.01 M to 0.005 M, but this dramatically lowered the yield and promoted the formation of complexes **45** and Pd_3^+ (*Table 14*, entry 2). The same outcome was obtained switching from toluene to THF and CH_3CN (entries 3 and 4).

Entry	Solvent	Conc. (M)	Yield (%)
1	toluene	0.01	26,[a] mixture with **45**
2	toluene	0.005	<10,[a] mixture with **45** and **10**
3	THF	0.01	<10,[a] mixture with **45** and **10**
4	CH_3CN	0.01	<10,[a] mixture with **45** and **10**

[a] Yield obtained by NMR

Table 14: Optimization of reaction conditions: solvent and concentration

Considering that no improvements resulted from the variation of the reaction medium, we tuned stoichiometric ratios. We lowered the amount of sodium thiophenate to avoid the formation of complex **45**, but the reaction did not provide any cluster (*Table 15*, entry 2).

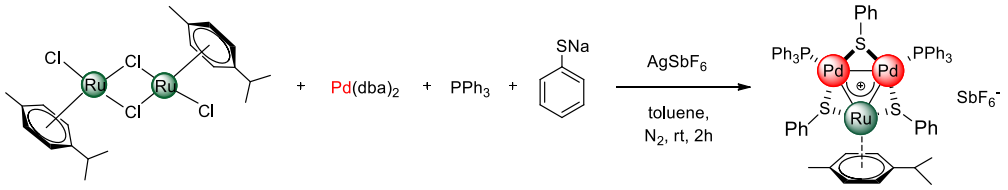

Entry	Ru	Pd	PPh_3	PhSNa	$AgSbF_6$	Yield (%)
1	1	1	1	3	3	26,[a] mixture with **45**
2	1	1	1	1	3	--
3	1	4	4	6	12	--
4	1	4	4	6	6	<10,[a] mixture with **10**
5	1	4	4	6	2	<10,[a] mixture with **10**

[a] Yield obtained by NMR

Table 15: Optimization of reaction conditions: stoichiometric ratios

Switching to a Pd:Ru ratio of 2:1 was fruitless too, since just traces of Pd_2Ru were detected with 6 and 2 equivalents of silver salt (entries 4 and 5), while no formation occurred with a large excess of $AgSbF_6$ (entry 3).

We wondered if the low solubility of sodium thiophenate in toluene could hamper the feasibility of this reaction. We thus replaced Na^+ with a larger counterion, namely Ag^+, which could in addition act as halogen scavenger. Unfortunately, this promoted the formation of complex **45** at the expense of Pd_2Ru (*Table 16*, entry 2). No reaction was observed using diphenyldisulfide instead of the sodium salt, since it could not react in these reaction conditions (entry 3).

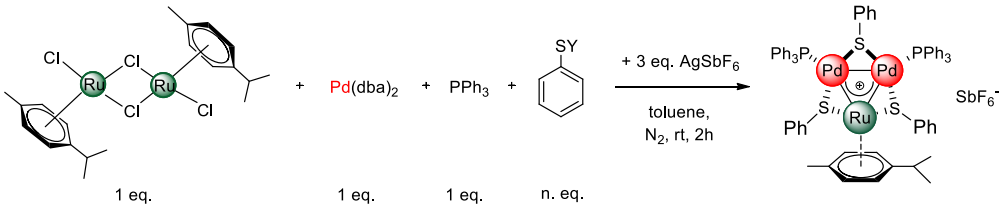

Entry	Y	n	Yield (%)
1	Na^+	3	26,[a] mixture with **45**
2	Ag^+	3	--
3	-SPh	1.5	--

[a] Yield obtained by NMR

Table 16: Optimization of reaction conditions: thiolate source

We next examined different ruthenium and palladium precursors. We replaced $Pd(dba)_2$ with dimer **40**, which bears two thiolates as bridging ligands and two phosphines on each palladium atom (*Table 17*, entry 1). Complex **40** remained unreacted and the same outcome was obtained with cocrystallized monomers of palladium **25** (entry 2). Concerning ruthenium, the formation of the desired cluster was not detected even using the analogue of dimer **43** with iodides instead of chlorides (**46**) (entry 3). We then tried to mix $Pd(dba)_2$ with complex **45** in order to verify if it could have been an intermediate in the formation of Pd_2Ru. As expected, no reaction was observed between **45** and palladium(0) (entry 4). In addition, we tested two monomeric complexes of ruthenium with a *p*-cymene and three molecules of acetonitrile coordinated, with BF_4^- or SbF_6^- as counterions.[69] Just complex **48** with SbF_6^- gave Pd_2Ru complex in low yields with a Ru:Pd ratio of 2:1 and 3:1.

[69] M. A. Bennet, A. K. Smith, *J. Chem. Soc., Dalton. Trans.*, **1974**, *0*, 233.

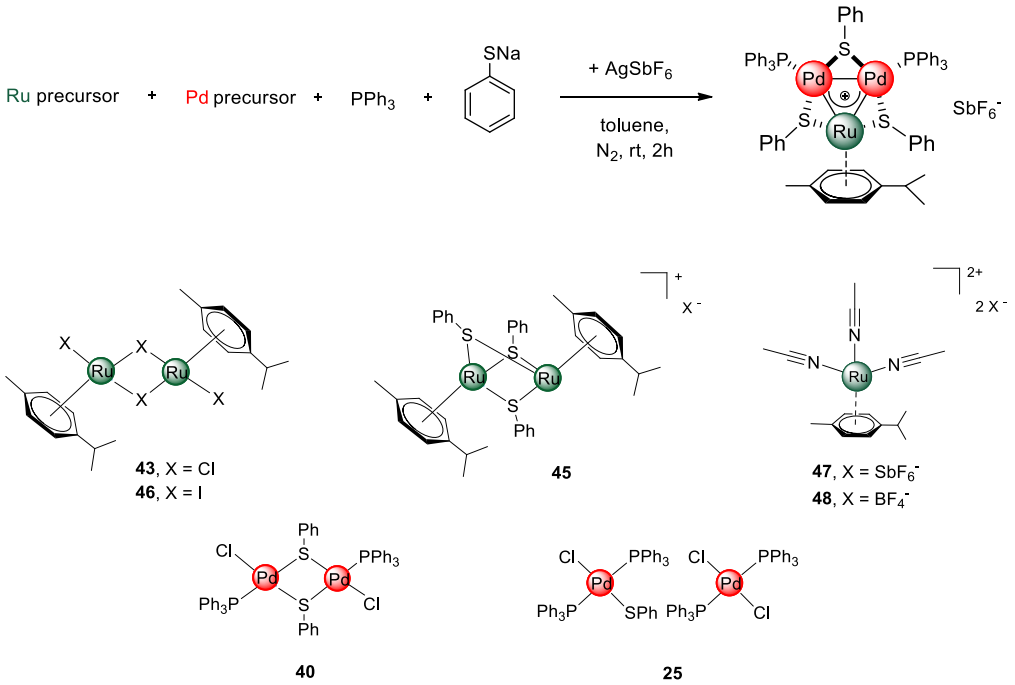

Entry	Ru / eq.	Pd / eq.	PPh_3	PhSNa	$AgSbF_6$	Yield (%)
1	43 / 1	40 / 1	--	1	2	--
2	43 / 1	25 / 1	--	--	2	--
3	46 / 1	$Pd(dba)_2$ / 1	1	3	3	--
4	45 / 1	$Pd(dba)_2$ / 2	2	--	2	--
5	47 / 2	$Pd(dba)_2$ / 1	1	3	3	--
6	48 / 1	$Pd(dba)_2$ / 1.3	1.3	4	4	--
7	48 / 1	40 / 1	--	1	2	--
8	48 / 2	$Pd(dba)_2$ / 1	1	3	3	<10[a]
9	48 / 3	$Pd(dba)_2$ / 1	1	3	3	<10[a]

[a] Yield obtained by NMR

Table 17: Optimization of reaction conditions: ruthenium and palladium precursors

None of our efforts led to better yields and selectivity. We nevertheless decided to extend the scope of this reaction replacing triphenylphosphine and the phenyl group on the thiolate *(Table 18)*.

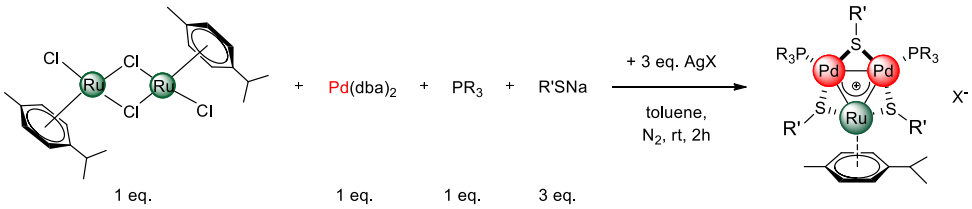

Entry	Complex	R	R'	X	Yield (%)
1	44	Ph	Ph	SbF_6	26[a]
2	49	4-Me-C_6H_4	Ph	SbF_6	32
3	50	4-F-C_6H_4	Ph	PF_6	16
4	51	4-Me-C_6H_4	4-Me-C_6H_4	SbF_6	6
5	52	4-Me-C_6H_4	4-Br-C_6H_4	SbF_6	20
6	53	4-F-C_6H_4	4-Cl-C_6H_4	SbF_6	14
7	54	4-Me-C_6H_4	4-Cl-C_6H_4	SbF_6	36

[a] Yield obtained by NMR

Table 18: Scope of the synthesis of Pd_2Ru complexes

We managed to obtain seven Pd_2Ru complexes with different combinations of electron-donating and electron-withdrawing fragments. The present method is nevertheless limited to aromatic substituents, attempts with aliphatic thiolates proved unsuccessful. The worst result was obtained with *p*-tolyl groups both on the phosphine and on the thiolate, suggesting that the presence of electron-donating groups on all ligands could hamper the formation of the cationic complex (entry 4, 6%). The replacement of *p*-tolyl with phenyl group on the thiolate proved indeed beneficial, since complex **49** formed in 32% yield (entry 2). Thiolates with chlorine and bromine in para position were also

tested, giving comparable results (entries 5-7, 14-36%). The replacement of SbF_6^- with PF_6^- as counterion did not make any relevant improvement (entry 3). Beside complex **44**, the introduction of different functional groups on phosphines and thiolates increased the difference in polarity between Pd_2Ru cluster and complex **45**, allowing to isolate the pure clusters by column chromatography. Nevertheless, yields stuck around 15-30% even changing electronic and steric features.

Clusters **44**, **49-54** were characterized by MS analysis, multinuclear NMR experiments, UV-Vis spectroscopy and IR spectrometry.

Similarly to Pd_3^+ clusters, the cationic core of Pd_2Ru complexes is readily visible under ESI^+ conditions.

However, lack of symmetry makes NMR spectra more complicated. Phosphines generate two different doublets in ^{31}P NMR, as well as two patterns of signals in ^1H NMR. Thiolates show the same behaviour, since ligands between palladium and ruthenium give resonances that are downfield shifted compared to those of the thiolate between palladium nuclei.

Regarding UV-Vis, the spectrum of Pd_2Ru presents an interesting band of low intensity around 600 nm with an ε value of $3.98 \cdot 10^3$ $M^{-1}cm^{-1}$ *(Fig. 24, right)*, which has no precedent among Pd_3^+ complexes.

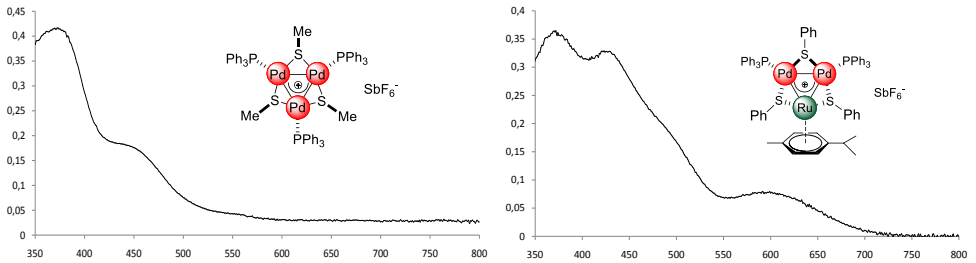

*Fig.24: Comparison between UV-Vis spectra of Pd_3^+ **20** (left) and Pd_2Ru **44** (right)(samples concentration = $2 \cdot 10^{-5}$ M)*

It could correspond to a d-d transition, being ε values one order of magnitude lower compared to the other bands at 372 and 423 nm ($\varepsilon = 1.82 \cdot 10^4$ $M^{-1}cm^{-1}$ and $1.64 \cdot 10^4$ $M^{-1}cm^{-1}$ respectively), which are likely charge transfer ones.

3.3 Conclusions

We demonstrated that tripalladium clusters can be accessed from the formal addition of a Pd(0) fragment onto a Pd(II) dimer. This synthetic strategy is complementary to those reported in literature, which deal with the addition of an oxidized mononuclear complex on a reduced metal dimer. The present method allowed to extend the panel of available prototypical metal surfaces and we successfully synthesized mixed metal clusters of palladium and platinum increasing the selectivity obtained with the standard synthetic strategy. In addition, we replaced platinum with ruthenium, obtaining a new family of trinuclear aromatic clusters with a metal core composed by a ruthenium and two palladium atoms.

3.4 Experimental section

3.4.1 General remarks

$Pd(dba)_2$, $Pt(dba)_3$, ruthenium dimers, phosphines and Ag salts were purchased from commercial sources and used as received. Sodium thiolates were obtained reducing the corresponding thiols with sodium hydride. Solvents were degassed by bubbling N_2 for at least 30 minutes prior to use. Reactions and filtrations were carried out under N_2 using standard Schlenk technique.

^1H NMR spectra were recorded in $CDCl_3$ or C_6D_6 at 298 K on Bruker 400 AVANCE and Bruker 300 AVANCE spectrometers fitted with a BBFO probe-head at 400 and 300 MHz respectively, using the solvent as internal standard (7.26 ppm for $CDCl_3$ and 7.16 ppm for C_6D_6).

^{13}C NMR spectra were recorded in $CDCl_3$ at 298 K on a Bruker 400 AVANCE spectrometer fitted with a BBFO probe-head at 101 MHz, using the solvent as internal standard (77.16 ppm).

^{31}P NMR spectra were recorded in $CDCl_3$ or C_6D_6 at 298 K on a Bruker 400 AVANCE spectrometer fitted with a BBFO probe-head at 162 MHz, using 85% H_3PO_4 as external standard (0 ppm).

^{19}F NMR spectra were recorded in $CDCl_3$ at 298 K on a Bruker 400 AVANCE spectrometer fitted with a BBFO probe-head at 376 MHz, using hexafluorobenzene as external standard (-164.9 ppm).

The terms m, s, d, t, q represent multiplet, singlet, doublet, triplet, quadruplet respectively, and the term br means a broad signal.

Exact masses of complexes **44**, **49**, **50** were recorded on a LTQ ORBITRAP XL Thermo Mass Spectrometer (electrospray source). Mass analysis on complexes **51**-**54** were performed on an Infusion Water Acquity Ultra Performance LC HO6UPS-823M instrument (electrospray source, quadrupole analyser).

UV-Vis spectra were recorded on a Thermo Scientific Evolution 260 Bio UV Spectrophotometer.
IR spectra were collected with a Thermo Scientific Nicolet 5PCFT-IR-ATR spectrometer equipped with diamond crystal (3400-400 cm^{-1} interval).

3.4.2 Synthesis of complex 40

$Pd(PPh_3)_4$ (1 eq., 0.17 mmol, 200 mg) and diphenyl disulfide (0.5 eq., 0.086 mmol, 19 mg) were added to a 50 ml schlenk and the vessel underwent at least three vacuum/N_2 cycles. 20 ml of freshly degassed $CHCl_3$ were immediately syringed under N_2 to obtain a deep red solution. The crude mixture was kept under magnetic stirring at room temperature for 3 hours, then the solvent was removed under vacuum. The resulting solid was purified by $CHCl_3$/hexane washings (1/60 v/v, 3x30 ml). Evaporation of volatiles afforded a deep red solid. Crystals of **40** were obtained upon crystallization by vapour diffusion using $CHCl_3$/hexane.

3.4.3 Synthesis of Pd_2Ru complexes 44, 49-54

$Pd(dba)_2$ (1 eq., 0.16 mmol, 92 mg), $Ru_2(p\text{-cymene})_2Cl_4$ (1 eq., 0.16 mmol, 98 mg), sodium thiophenate (3 eq., 0.48 mmol, 64 mg) and the desired phosphine (1 eq. , 0.16 mmol) were added to a 50 ml schlenk and the vessel underwent at least three vacuum/N_2 cycles. Freshly degassed toluene (16 mL) was immediately syringed under N_2. 10 minutes later a deep red solution was formed, then $AgSbF_6$ (3 eq., 0.48 mmol, 164 mg) was added under N_2. The reaction mixture was stirred at room temperature and it gradually turned to green. Two hours later the crude was filtered under N_2 through a short pad of celite to remove traces of black metals. Toluene was evaporated under vacuum and the resulting solid was purified by flash column chromatography on silica gel using hexane/acetone or hexane/ethyl acetate as eluent. The green solid obtained was then triturated three times with pentane and dried under

vacuum to afford a crystalline powder. Clusters **44**, **49-54** were characterized by ^{1}H, ^{31}P, ^{19}F, ^{13}C NMR spectroscopy, HRMS or MS analysis, UV-Vis spectroscopy and IR spectrometry.

3.4.4 Spectroscopic data of complex 40

- **Complex 40**

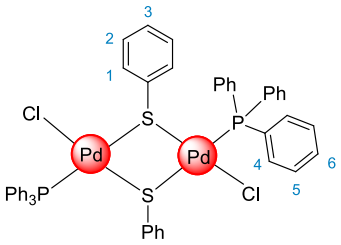

Isolated as deep red crystals obtained upon crystallization by vapour diffusion using $CHCl_3$/hexane.

Crystals of **40** provided under ESI-*positive* analysis a main ion current deriving from the corresponding Pd_3^+ cation (centered at *m/z* 1433), which is likely generated during ionization. This suggests that the reactivity observed in solution can be exerted under MS conditions as well.

^{1}H NMR (400 MHz, C_6D_6) δ (ppm): 8.15 (d, *J*= 7.16 Hz, 4H, H_1), 7.60 (m, 12H, H_4), 6.84 (m, 24H, $H_{2\text{-}3}$, $H_{5\text{-}6}$).

^{31}P NMR (162 MHz, C_6D_6) δ (ppm): 30.23.

3.4.5 Spectroscopic data of complexes 44, 49-54

- **Complex 44**

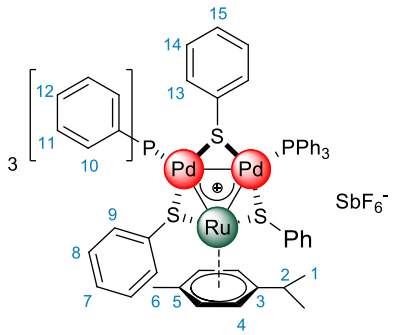

Isolated as deep green crystals obtained upon crystallization by vapour diffusion using CH_2Cl_2/hexane. Yield obtained by NMR = 26%

HRMS calculated for $C_{64}H_{59}P_2Pd_2RuS_3$ $[M]^+$: 1300.0400, found: 1300.0422.

^{1}H NMR (400 MHz, $CDCl_3$) δ (ppm): 7.35 (m, 18H, $H_{11\text{-}12}$), 7.18 (m, 6H, H_{10}), 7.11 (m, 6H, H_{10}), 6.98 (m, 4H, H_8), 6.93 (m, 4H, H_9), 6.85 (m, 2H, H_7), 6.68 (t, *J* = 6.9 Hz, 1H, H_{15}), 6.64 (d, *J* = 7.7 Hz, 2H, H_{13}), 6.42 (t, *J* = 7.9 Hz, 2H, H_{14}), 5.08 (d, *J* = 5.8 Hz, 1H, H_4), 4.84 (d, *J* = 4.9 Hz, 1H, H_4), 4.75 (d, *J* = 6.4 Hz, 1H, H_4), 4.55 (d, *J* = 6.4 Hz, 1H, H_4), 2.55 (m, 1H, H_2), 2.24 (s, 3H, H_6), 1.25 (m, 6H, H_1).

^{31}P NMR (162 MHz, $CDCl_3$) δ (ppm): 21.76 (d, *J* = 103.0 Hz, 1P), 19.98 (d, *J* = 103.0 Hz, 1P).

IR (ATR) ν (cm^{-1}): 3061, 2923, 2854, 1474, 1434, 1178, 1094, 1025, 999, 740, 689, 653, 520, 505.

UV-Vis (c = $2\cdot10^{-5}$ M): λ_{max1} = 372 nm, ε_{max1} = $1.82\cdot10^4$ $M^{-1}cm^{-1}$; λ_{max2} = 423 nm, ε_{max2} = $1.64\cdot10^4$ $M^{-1}cm^{-1}$; λ_{max3} = 599 nm, ε_{max3} = $3.98\cdot10^3$ $M^{-1}cm^{-1}$.

- **Complex 49**

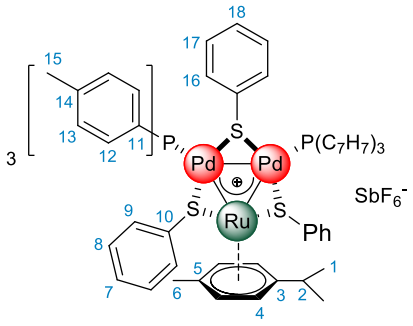

Isolated as deep green crystalline solid. Yield = 32%

HRMS calculated for $C_{70}H_{71}P_2Pd_2RuS_3$ $[M]^+$: 1384.1341, found: 1384.1384.

^{1}H NMR (400 MHz, $CDCl_3$) δ (ppm): 7.22 (dd, J_1= 10.8, J_2= 8.2 Hz, 6H, H_{12}), 7.06 (d, J_1= 11.0, J_2= 8.2 Hz, 6H, H_{12}), 7.01 (d, J = 7.8 Hz, 6H, H_{13}), 6.96 (m, 8H, $H_{8\text{-}9}$), 6.88 (d, J = 7.5 Hz, 6H, H_{13}), 6.83 (d, J = 7.6 Hz, 2H, H_7), 6.70 (t, J = 7.4 Hz, 1H, H_{18}), 6.63 (d, J = 7. 6 Hz, 2H, H_{16}), 6.42 (t, J = 7.6 Hz, 2H, H_{17}), 5.04 (d, J = 5.8 Hz, 1H, H_4), 4.85 (d, J = 6.0 Hz, 1H, H_4), 4.65 (d, J = 5.7 Hz, 1H, H_4), 4.53 (d, J = 5.9 Hz, 1H, H_4), 2.58 (dt, J_1= 13.5, J_2= 6.7 Hz, 1H, H_2), 2.31 (s, 9H, H_{15}), 2.27 (s, 9H, H_{15}), 2.22 (s, 3H, H_6), 1.25 (m, 6H, H_1).

^{13}C NMR (101 MHz, $CDCl_3$) δ (ppm): 141.0 (C_{14}), 140.6 (C_{14}), 138.3 (C_{10}), 136.3 (C_{10}), 133.6 (d, $^2J_{CP}$ = 12.2 Hz, C_{12}), 133.4 (d, $^2J_{CP}$ = 12.5 Hz, C_{12}), 133.1 ($C_{7or8or9}$), 132.7 ($C_{7or8or9}$), 132.4 ($C_{7or8or9}$), 129.4 (d, $^3J_{CP}$ = 10.6 Hz, C_{13}), 129.0 (d, $^3J_{CP}$ = 10.2 Hz, C_{13}), 127.3-126.8 (C_{11}), 107.9 (C_{3or5}), 100.6 (C_{3or5}), 87.7 (C_4), 86.8 (C_4), 85.4 (C_4), 81.7 (C_4), 53.17, 30.8 (C_2) , 24.2 (C_1), 33.3 (C_1), 21.5 (C_{15}), 21.3 (C_6).

^{31}P NMR (162 MHz, $CDCl_3$) δ (ppm): 20.37 (d, J = 103.2 Hz, 1P), 18.47 (d, J = 103.0 Hz, 1P).

IR (ATR) ν (cm^{-1}): 2967, 2918, 2872, 1696, 1405, 1095, 1021, 855, 744, 657, 521.

UV-Vis (c = 2·10^{-5}M, THF): λ_{max1} = 368 nm, ε_{max1} = 6.45·10^{3} M^{-1}cm^{-1}; λ_{max2} = 428 nm, ε_{max2} = 5.65·10^{3} M^{-1}cm^{-1}; λ_{max3} = 581 nm, ε_{max3} = 1.28·10^{3} M^{-1}cm^{-1}.

- **Complex 50**

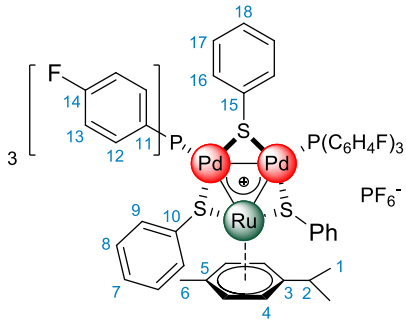

Isolated as deep green crystalline solid. Yield = 16%

HRMS calculated for $C_{64}H_{53}F_6P_2Pd_2RuS_3$ $[M]^+$: 1407.9835, found: 1407.9857.

^{1}H NMR (400 MHz, $CDCl_3$) δ (ppm): 7.28 (m, 6H, H_{13}), 7.15 (m, 6H, H_{13}), 7.00 (t, J = 7.8 Hz, 4H, H_8), 6.96 (m, 12H, $H_{7,9,12}$), 6.81 (t, J = 8.2 Hz, 6H, H_{12}), 6.76 (d, J = 7.4 Hz, 1H, H_{18}), 6.67 (d, J = 7.4 Hz, 2H, H_{16}), 6.50 (t, J = 7.7 Hz, 2H, H_{17}), 5.42 (d, J = 5.9 Hz, 1H, H_4), 5.30 (d, J = 6.0 Hz, 1H, H_4), 4.83 (d, J = 6.1 Hz, 1H, H_4), 4.48 (m, J = 6.1 Hz, 1H, H_4), 2.40 (m, 1H, H_2), 2.24 (s, 3H, H_6), 1.27 (d, J = 6.8 Hz, 3H, H_1), 1.19 (d, J = 6.8 Hz, 3H, H_1).

^{13}C NMR (101 MHz, $CDCl_3$) δ (ppm): 164.1 (d, $^1J_{CF}$ = 254 Hz, C_{14}), 163.9 (d, $^1J_{CF}$ = 252 Hz, C_{14}), 140.8 (C_{10or15}), 138.3 (C_{10or15}), 136.3 (m, C_{12}), 133.3 ($C_{7\text{-}9or16\text{-}18}$), 132.7 ($C_{7\text{-}9or16\text{-}18}$), 132.6 ($C_{7\text{-}9or16\text{-}18}$), 131.8 ($C_{7\text{-}9or16\text{-}18}$), 128.7 ($C_{7\text{-}9or16\text{-}18}$), 127.9 ($C_{7\text{-}9or16\text{-}18}$), 127.3 (d, J_{CP} = 6.6 Hz, C_{11}), 116.3 (d, $^2J_{CF}$ = 21.2 Hz, C_{13}), 116.2 (d, $^2J_{CF}$ = 21.2 Hz, C_{13}), 115.8 (d, $^2J_{CF}$ = 21.4 Hz, C_{13}), 115.7 (d, $^2J_{CF}$ = 21.5 Hz, C_{13}), 107.7 (C_{3or5}), 102.0 (C_{3or5}), 90.7 (C_4), 87.0 (C_4) , 85.6 (C_4), 83.2 (C_4), 31.8 (C_2), 23.2 (C_1), 23.0 (C_1), 21.5 (C_6).

^{31}P NMR (162 MHz, $CDCl_3$) δ (ppm): 17.72 (d, J = 105.0 Hz, 1P), 16.64 (d, J = 105.8 Hz, 1P), -144.17 (d, J_{PF} = 718.8 Hz, PF_6).

^{19}F NMR (377 MHz, $CDCl_3$) δ (ppm): -71.81, -73.70, -107.83, -108.61.

IR (ATR) ν (cm^{-1}): 2953, 2918, 2856, 1586, 1495, 1438, 1394, 1231, 1161, 1092, 827, 742, 691, 556, 527, 447.

UV-Vis (c = $2\cdot10^{-5}$M, THF): λ_{max1} = 368 nm, ε_{max1} = $1.23\cdot10^{4}$ $M^{-1}cm^{-1}$; λ_{max2} = 411 nm, ε_{max2} = $8.45\cdot10^{3}$ $M^{-1}cm^{-1}$; λ_{max3} = 604 nm, ε_{max3} = $1.47\cdot10^{3}$ $M^{-1}cm^{-1}$.

- **Complex 51**

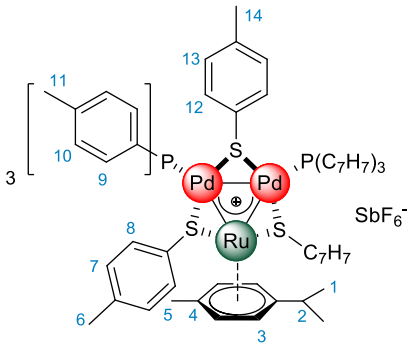

Isolated as deep green crystalline solid. Yield = 6%

MS calculated for $C_{73}H_{77}P_2Pd_2RuS_3$ $[M]^+$: 1425.1770, found: 1426.795.

^{1}H NMR (400 MHz, $CDCl_3$) δ (ppm): 7.16 (dd, J_1= 10.8, J_2= 8.1 Hz, 6H, H_9), 7.07 (dd, J_1= 10.8, J_2= 8.1 Hz, 6H, H_9), 6.99 (d, J = 7.2 Hz, 6H, H_{10}), 6.88 (d, J = 7.3 Hz, 6H, H_{10}), 6.82 (m, 4H, H_7), 6.76 (d, J = 8.0 Hz, 2H, H_8), 6.63 (d, J = 7.8 Hz, 2H, H_8), 6.50 (d, J = 7.9 Hz, 2H, H_{13}), 6.20 (d, J = 7.9 Hz, 2H, H_{12}), 4.99 (d, J = 5.8 Hz, 1H, H_3), 4.83 (d, J = 5.8 Hz, 1H, H_3), 4.59 (d, J = 5.7 Hz, 1H, H_3), 4.54 (d, J = 5.7 Hz, 1H, H_3), 2.62 (m, 1H, H_2), 2.31 (s, 9H, H_{11}), 2.29 (s, 9H, H_{11}), 1.28 (m, 6H, H_1).

^{31}P NMR (162 MHz, $CDCl_3$) δ (ppm): 20.32 (d, J = 101.3 Hz, 1P), 18.54 (d, J = 101.5 Hz, 1P).

IR (ATR) ν (cm^{-1}): 2926, 2848, 1602, 1471, 1397, 1094, 1010, 801, 655, 549, 498.

UV-Vis (c = 2·10^{-5}M, THF): λ_{max1} = 377 nm, ε_{max1} = 2.17·10^{4} M^{-1}cm^{-1}; λ_{max2} = 412 nm, ε_{max2} = 1.96·10^{4} M^{-1}cm^{-1}; λ_{max3} = 581 nm, ε_{max3} = 4.28·10^{3} M^{-1}cm^{-1}.

- **Complex 52**

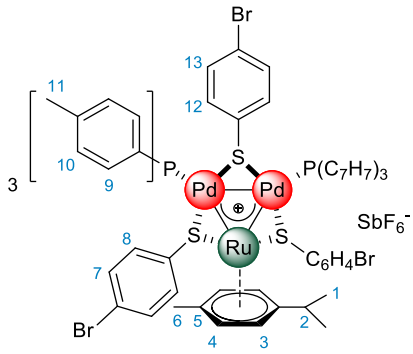

Isolated as deep green crystalline solid. Yield = 20%

MS calculated for $C_{70}H_{68}Br_3P_2Pd_2RuS_3$ $[M]^+$: 1620.838, found: 1620.417.

^{1}H NMR (400 MHz, $CDCl_3$) δ (ppm): 7.13 (dd, J_1= 11.0, J_2= 8.1 Hz, 6H, H_9), 7.05 (m,16H, $H_{9\text{-}10}$, H_7), 6.98 (d, J = 6.6 Hz, 4H, H_8), 6.94 (d, J = 8.0 Hz, 6H, H_{10}), 6.81 (d, J = 8.3 Hz, 2H, H_7), 6.75 (d, J = 8.3 Hz, 2H, H_8), 5.26 (d, J = 6.0 Hz, 1H, $H_{3\text{-}4}$), 4.91 (d, J = 6.1 Hz, 1H, $H_{3\text{-}4}$), 4.88 (d, J = 6.0 Hz, 1H, $H_{3\text{-}4}$), 4.55 (d, J = 5.8 Hz, 1H, $H_{3\text{-}4}$), 2.56 (m, 1H, H_2), 2.33 (s, 18H, H_{11}), 2.28 (s, 3H, H_6), 1.29 (d, J = 6.8 Hz, 3H, H_1), 1.24 (m, 3H, H_1).

^{31}P NMR (162 MHz, $CDCl_3$) δ (ppm): 20.64 (d, J = 100.8 Hz, 1P), 18.76 (d, J = 100.5 Hz, 1P).

IR (ATR) ν (cm^{-1}): 2926, 2852, 1465, 1375, 1260, 1093, 1005, 801, 707, 654, 629, 610, 518, 489, 418.

UV-Vis (c = 2·10^{-5} M, THF): λ_{max1} = 370 nm, ε_{max1} = 1.74·10^{4} M^{-1}cm^{-1}; λ_{max2} = 431 nm, ε_{max2} = 1.38·10^{4} M^{-1}cm^{-1}; λ_{max3} = 597 nm, ε_{max3} = 3.38·10^{3} M^{-1}cm^{-1}.

- **Complex 53**

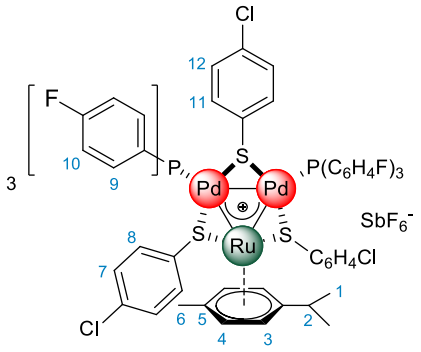

Isolated as deep green crystalline solid. Yield = 14%

MS calculated for $C_{64}H_{50}Cl_3F_6P_2Pd_2RuS_3$ $[M]^+$: 1511.464, found: 1512.380.

^{1}H NMR (400 MHz, $CDCl_3$) δ (ppm): 7.26 (m, 6H, H_{10}), 7.18 (m, 6H, H_{10}), 7.02 (t, *J* = 8.0 Hz, 6H, H_9 + 4H, H_7), 6.96 (m, 6H, $H_{7\text{-}8}$), 6.90 (t, *J* = 8.4 Hz, 6H, H_9), 6.85 (d, *J* = 8.3 Hz, 2H, H_8), 6.59 (d, *J* = 8.3 Hz, 2H, H_{12}), 6.46 (d, *J* = 8.3 Hz, 2H, H_{11}), 5.52 (d, *J* = 6.1 Hz, 1H, $H_{3\text{-}4}$), 5.39 (d, *J* = 6.0 Hz, 1H, $H_{3\text{-}4}$), 4.87 (d, *J* = 6.1 Hz, 1H, $H_{3\text{-}4}$), 4.54 (m, *J* = 6.1 Hz, 1H, $H_{3\text{-}4}$), 2.44 (m, 1H, H_2), 2.28 (s, 3H, H_6), 1.29 (d, *J* = 6.9 Hz, 3H, H_1), 1.22 (d, *J* = 6.9 Hz, 3H, H_1).

^{31}P NMR (162 MHz, $CDCl_3$) δ (ppm): 17.59 (d, *J* = 104.2 Hz, 1P), 16.78 (d, *J* = 103.8 Hz, 1P).

^{19}F NMR (377 MHz, $CDCl_3$) δ (ppm): -107.05, -107.61.

IR (ATR) ν (cm^{-1}): 2921, 1588, 1495, 1470, 1392, 1231, 1160, 1088, 1010, 825, 658, 527, 495, 488, 449, 440.

UV-Vis (c = $2\cdot10^{-5}$ M, THF): λ_{max1} = 377 nm, ε_{max1} = $1.90\cdot10^4$ $M^{-1}cm^{-1}$; λ_{max2} = 427 nm, ε_{max2} = $1.58\cdot10^4$ $M^{-1}cm^{-1}$; λ_{max3} = 596 nm, ε_{max3} = $3.23\cdot10^3$ $M^{-1}cm^{-1}$.

- **Complex 54**

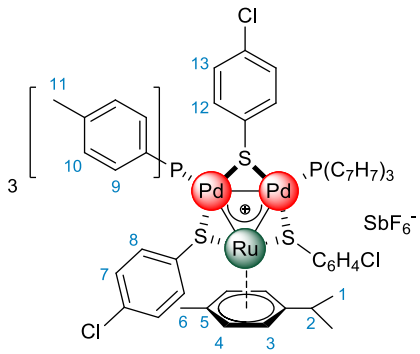

Isolated as deep green crystalline solid. Yield = 36%

MS calculated for $C_{70}H_{68}Cl_3P_2Pd_2RuS_3$ $[M]^+$: 1487.046, found: 1487.591.

^{1}H NMR (400 MHz, $CDCl_3$) δ (ppm): 7.14 (d, J_1= 11.0, J_2= 8.0 Hz, 6H, H_9), 7.06 (dd, J_1= 11.0, J_2= 8.0 Hz, 6H, H_9), 7.02 (d, J = 9.0 Hz, 6H, H_{10}), 6.93 (m, 8H, H_{10}, H_7), 6.88 (d, J = 8.4 Hz, 2H, H_7), 6.81 (m, 4H, H_8), 6.51 (d, J = 8.5 Hz, 2H, H_{13}), 6.29 (d, J = 8.5 Hz, 2H, H_{12}), 5.26 (d, J = 6.0 Hz, 1H, $H_{3\text{-}4}$), 4.90 (d, J = 6.4 Hz, 2H, $H_{3\text{-}4}$), 4.55 (d, J = 5.9 Hz, 1H, $H_{3\text{-}4}$), 2.56 (m, 1H, H_2), 2.32 (s, 18H, H_{11}), 2.28 (s, 3H, H_6), 2.56 (m, 1H, H_2), 1.29 (d, J = 6.9 Hz, 3H, H_1), 1.24 (d, J = 7.0 Hz, 3H, H_1).

^{31}P NMR (162 MHz, $CDCl_3$) δ (ppm): 20.68 (d, J = 100.6 Hz, 1P), 18.79 (d, J = 100.7 Hz, 1P).

IR (ATR) ν (cm^{-1}): 2962, 2919, 2857, 1595, 1470, 1392, 1092, 1011, 801, 658, 516.

UV-Vis (c = $2\cdot10^{-5}$M, THF): λ_{max1} = 371 nm, ε_{max1} = $2.04\cdot10^4$ $M^{-1}cm^{-1}$; λ_{max2} = 432 nm, ε_{max2} = $1.73\cdot10^4$ $M^{-1}cm^{-1}$; λ_{max3} = 588 nm, ε_{max3} = $4.26\cdot10^3$ $M^{-1}cm^{-1}$.

3.4.6 Summary of X-Ray diffraction analysis on complex 44

X-ray single crystal data collections was performed at Elettra Sincrotrone (Trieste, Italy) on beamline XRD1. The beamline spectra (produced by a NdBFe multipole wiggler) was monochromatized to 17.71 KeV (0.700Å) through a Si(111) double crystal monochromator and focused to obtain a beam size of 0.2 × 0.2 mm FWHM at the sample (photon flux 1012-1013 ph·sec-1). Crystals were dipped in NHV oil (Jena Bioscience GmbH) and mounted on the goniometer head with a nylon loop (0.05-0.3 mm). Complete datasets were collected at 100 K (nitrogen stream supplied through an Oxford Cryostream 700) through the rotating crystal method. For triclinic crystals complete datasets have been obtained merging two different data collections done on the same crystal, mounted with different orientations. Data were acquired using a monochromatic wavelength of 0.700 Å on a Pilatus 2M hybrid-pixel area detector. The diffraction data were indexed and integrated using XDS. Scaling have been done using CCP4-Aimless code. The structures were solved by the dual space algorithm implemented in the SHELXT code in OLEX2. Fourier analysis and refinement were performed by the full-matrix least-squares methods based on F^2 implemented in SHELXL-2014. For all the structures, anisotropic displacement parameters were refined except for hydrogen atoms.

Crystal data and structure refinement

Identification code	am230v-bis_1_
Empirical formula	C64 H59 P2 Pd2 Ru S3, 2(F3 Sb0.5), 0.5(C Cl3)
Formula weight	1595.03
Temperature	100 K
Wavelength	0.700 Å
Crystal system	Triclinic

Space group	P -1
Unit cell dimensions	a = 11.9921(3) Å α= 94.5180(16)°.
	b = 12.28439(18) Å β= 91.0356(18)°.
	c = 21.7330(5) Å γ = 101.5240(16)°.
Volume	3125.45(11) $Å^3$
Z	2
Density (calculated)	1.695 Mg/m^3
Absorption coefficient	1.467 mm^{-1}
F(000)	1581
Crystal size	0.15 x 0.10 x 0.10 mm^3
Theta range for data collection	1.7060 to 32.8820°
Index ranges	-14<=h<=14, -15<=k<=15, -27<=l<=27
Reflections collected	35985
Independent reflections	11869 [R(int) = 0.0152]
Max. and min. transmission	1.00000 and 0.69180
Refinement method	Full-matrix least-squares on F2
Data / restraints / parameters	11869 / 316 / 803
Goodness-of-fit on F2	1.329
Final R indices [I>2sigma(I)]	R1 = 0.0504, wR2 = 0.1275
R indices (all data)	R1 = 0.0515, wR2 = 0.1279
Extinction coefficient	n/a

Atomic coordinates (x 10^4) and equivalent isotropic displacement parameters ($Å^2$ x 10^3). U(eq) is defined as one third of the trace of the orthogonalized U^{ij} tensor

	x	y	z	U(eq)
Pd2	6281.7(4)	4851.3(4)	2186.2(2)	13(1)
Pd1	6788.1(4)	3155.2(4)	2814.2(2)	14(2)
Ru1	8473.4(4)	4450.5(4)	2203.3(2)	14(2)
S2	7352.1(13)	4587.7(13)	1342.1(7)	15(2)
S3	7917.5(13)	2525.5(13)	2101.8(7)	16(1)
S1	6011.6(13)	4622.9(14)	3225.1(7)	17(1)
P2	4993.7(13)	5849.4(14)	1871.3(7)	14(2)
P1	5757.4(14)	1573.6(14)	3165.4(7)	16(1)
C12	4241(5)	6412(5)	2503(3)	15(2)
C132	3929(5)	5067(5)	1310(3)	15(1)
C14	6797(6)	3315(6)	882(3)	18(1)
C64	7559(6)	2738(6)	601(3)	20(2)
C22	4910(5)	7074(6)	2973(3)	18(2)
C182	3187(6)	4122(6)	1481(3)	21(2)
C32	4405(6)	7567(6)	3460(3)	21(2)
C26	1011.1(5)	4550(6)	2697(3)	23(2)
C71	6496(5)	442(5)	3273(3)	19(2)
C65	9134(6)	1806(6)	3049(3)	23(2)
C161	2939(6)	-27(6)	1721(3)	25(1)
C72	5632(5)	7119(5)	1515(3)	16(2)
C11	5094(6)	1808(6)	3895(3)	22(1)
C36	1032.7(5)	4931(6)	2101(3)	23(2)
C82	5069(6)	7999(6)	1506(3)	19(1)
C24	5637(6)	2992(6)	743(3)	20(2)
C34	5251(6)	2066(6)	333(3)	24(2)
C141	4483(6)	1477(6)	2069(3)	21(1)

C62	3064(5)	6250(6)	2532(3)	22(2)
C13	4582(6)	4283(6)	3432(3)	24(1)
C42	3255(6)	7397(6)	3491(3)	25(1)
C81	6810(6)	160(6)	3843(3)	27(2)
C142	3928(6)	5305(6)	694(3)	24(2)
C16	9428(6)	5023(6)	3116(3)	22(1)
C46	9855(5)	5826(6)	1915(3)	22(2)
C181	3929(6)	-91(6)	2680(3)	24(1)
C172	2458(6)	3421(6)	1048(3)	25(1)
C151	3622(6)	974(6)	1633(3)	24(2)
C52	2557(6)	6730(6)	3023(3)	26(2)
C76	9257(7)	4668(7)	3764(3)	33(2)
C15	8959(5)	1864(6)	2421(3)	19(1)
C63	4258(7)	4740(7)	4000(4)	34(2)
C131	4632(5)	937(6)	2595(3)	19(2)
C54	7156(6)	1815(6)	193(3)	25(1)
C33	2624(6)	3346(7)	3249(4)	29(2)
C112	7237(6)	8233(6)	1048(3)	28(1)
C92	5584(6)	8991(6)	1274(3)	22(1)
C23	3732(6)	3567(6)	3061(3)	27(1)
C86	1005.0(6)	6296(7)	1295(3)	32(2)
C122	6720(6)	7232(6)	1282(3)	24(1)
C162	2481(7)	3652(7)	437(4)	33(1)
C171	3085(6)	-568(6)	2247(3)	25(2)
C21	5790(6)	2433(7)	4365(3)	29(1)
C25	9563(6)	1322(7)	1998(4)	31(1)
C44	6000(7)	1466(6)	60(3)	26(1)
C35	1035.2(7)	735(8)	2210(5)	45(1)
C121	6848(6)	108(6)	2734(3)	25(2)
C111	7492(6)	-894(6)	2786(4)	27(2)
C102	6672(6)	9108(6)	1051(3)	25(2)
C55	9919(6)	1224(7)	3258(4)	33(1)

C56	9133(6)	6282(6)	2331(3)	24(1)
C91	7484(7)	-625(7)	3885(4)	33(2)
C61	3959(6)	1454(8)	4001(3)	33(2)
C152	3222(7)	4598(7)	261(3)	32(1)
C66	8892(6)	5875(6)	2913(3)	22(1)
C101	7837(6)	-1156(6)	3356(4)	30(2)
C43	2327(7)	3799(8)	3802(4)	38(1)
C51	3522(7)	1716(9)	4568(4)	44(1)
C31	5364(7)	2683(8)	4931(4)	38(2)
C45	1053.6(7)	693(7)	2830(5)	41(2)
C96	1089.7(7)	7411(8)	1387(4)	39(2)
C53	3155(8)	4484(8)	4178(4)	45(2)
C106	1046.5(9)	5524(9)	808(4)	51(2)
C41	4209(7)	2331(8)	5031(4)	38(2)
Sb1	1000.0	0	0	24(2)
F0AA	1158.4(6)	434(7)	155(5)	38(2)
F1AA	9819(7)	1401(7)	320(5)	52(3)
F3	9864(8)	-523(9)	780(4)	56(3)
Sb2	424.5(12)	8083.0(17)	4662.3(6)	44(1)
F52	1066(13)	6863(12)	4369(11)	157(9)
F22	496(19)	759(2)0	5428(7)	166(9)
F32	-175(15)	9204(14)	4973(13)	155(8)
F62	1881(9)	8838(12)	4786(7)	86(4)
F72	-1044(13)	736(2)0	4512(12)	118(8)
F42	42(2)0	866(4)0	3935(13)	212(12)
F3A	9055(13)	300(14)	618(7)	57(5)
F1A	1125.2(14)	286(14)	552(8)	53(5)
F2A	1026.9(12)	1515(11)	-173(8)	47(4)
Cl5	1454(5)	7808(7)	5049(3)	78(2)
Cl1	683(7)	8436(9)	3882(3)	78(3)
Cl3	-949(6)	7475(8)	4777(4)	71(2)
C5	445(17)	824(4)0	4673(4)	90(2)

Chapter 4

TRIPALLADIUM AROMATIC CLUSTERS AS DONOR LIGANDS FOR LEWIS ACIDIC CATIONS

4.1 Introduction

4.1.1 Non-covalent cation-π interactions

Peculiar features of aromatics gave rise to several applications. Delocalized molecular orbitals allow them to interact with ions and to consequently act as ligands for organometallic compounds. Thanks to their quadrupolar moment, neutral arenes can coordinate Lewis acids. Few examples of coordination compounds of π-acidic group XI elements were reported. Munakata and co-workers obtained η^2-coordinated silver (I) complexes of polycyclic aromatic hydrocarbons with the purpose of obtaining new supramolecular architectures.[70] Regarding gold, in 2007 a gold (I) complex with toluene entered the scene,[71] while more recently Rekhroukh et al. synthesized the first gold (III)-arene complex by insertion of olefins into gold-aryl bonds.[72] Non covalent cation-π interactions are as well documented for neutral main-group aromatic and play a key role in chemistry and biology.[73] Cations usually form these bonding interactions with arenes having a negative quadrupolar moment perpendicular to their plane, while anions with those that have a positive one *(Fig. 25)*.[74]

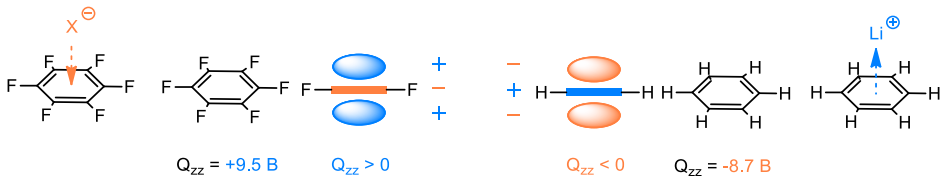

Fig.25: Examples of non-covalent ion-arene interactions

[70] M Munakata, L. P. Wu, T. Kuroda-Sowa, M. Maekava, Y. Suenaga, G. L. Ning, T. Kojima, *J. Am. Chem. Soc*., **1998**, *120*, 8618.
[71] V. Lavallo, G. D. Frey, S. Kousar, B. Donnadieu, G. Bertrand, *PNAS*, **2007**, *104*, 13569.
[72] F. Rekhroukh, C. Blons, L. Estévez, S. M. Ladeira, K. Miqueu, A. Amgoune, D. Bourissou, *Chem. Sci*., **2017**, *8*, 4539.
[73] a) J. C. Ma, D. A. Dougherty, *Chem. Rev*., **1997**, *97*, 1303; b) A. S. Mahadevi, G. N. Sastri, *Chem. Rev*., **2013**, *113*, 2100.
[74] R. E. Dawson, A. Hennig, D. P. Weimann, D. Emery, V. Ravikumar, J. Montenegro, T. Takeuchi, S. Gabutti, M. Mayor, J. Mareda, C. A. Schalley, S. Matile, *Nat. Chem*., **2010**, *2*, 533.

Since suitably delocalized molecular orbitals can be found in structures that involve metal atoms in their core as well, we wondered if our $[M_3]^+$ clusters could behave the same way as regular aromatics.

4.1.2 Synthesis and characterization of $[Pd_3M]^{++}$ clusters[75]

Computational studies previously performed on Pd_3^+ complexes provided unexpected data in term of quadrupolar moment, which resulted largely negative. This should be, in principle, a diagnostic feature of electron rich, neutral or anionic molecules.[73a-74-76] Calculated Q_{zz} of $[M_3]^+$ were higher than those of benzene, by four to seven times depending on the model. The trend was the same among different levels of theory (HF and DFT), functionals (exchange-correlation and orthodox hybrid ones) and basis sets (both double and triple-ζ for metal atoms). The largely negative values of $[M_3]^+$ aromatic clusters let us to speculate about a possible interaction with other cations. A seek to trap a molecule featuring a bonding cation-cation interaction could seem counterintuitive, because of the effects of electrostatic repulsion. However, computational studies suggest that this repulsive effect, being inherently a long-range one, could potentially be trumped by covalency, which is a essentially a short-range attractive force.[77]

The projects started modelling a naked Li^+ 6.0 Å above the planar metal core of our cationic complex. Reasonable expectations suggested that the electrostatic repulsion should have pushed the two cations away without constraints,[38] but the outcome was unexpected since the optimization converged living Li^+ 2.11-2.13 Å above the center of $[M_3]^+$ (M = Pd, Pt). M-M distances remained basically untouched, around 2.9 Å, and the three M-Li ones were nearly identical at 2.4 Å. Each one of the tetrahedral structures obtained is thus an irregular pyramid

[75] Y. Wang, A. Monfredini, P.-A. Deyris, F. Blanchard, E. Derat, G. Maestri, M. Malacria, *Chem. Sci.*, **2017**, *8*, 7394.
[76] A. S. Mahadevi, G. N. Sastri, J. C. Ma, D. A. Dougherty, *Chem. Rev.*, **2013**, *113*, 2100.
[77] F. Weinhold, *Angew. Chem. Int. Ed.*, **2017**, *56*, 14577.

with an equilateral triangular homonuclear base and a shorter height. Li^+ complexation by $[Pt_3]^+$ cation has a ΔG of -15.0 kcal/mol. The ΔG value decreases to -43.2 kcal/mol adding BF_4^- as non-coordinating counterion. The large increase in calculated ΔG reflects a lower destabilizing electrostatic contribution and highlights the meaningful calculated metal aromatic-lithium cation bonding interaction. Comparable results were obtained modelling homo- and heteronuclear $[M_3]^+$ complexes although ΔG values became slightly less negative, -41.4, -39.3 and -37.9 kcal/mol for $[Pt_2Pd]^+$, $[PtPd_2]^+$ and $[Pd_3]^+$ respectively. For comparison, calculated ΔG for Li^+ complexation by neutral ligands such as water and benzene were -32.4 and -25.9 respectively. The delocalized bonding HOMO of $[M_3]^+$ has a sigmoid symmetry that overlaps with the LUMO of Li^+, which is an empty 2s atomic orbital. The calculated HOMO of $[M_3Li]^{++}$ remains similar and its central lobe slightly expands towards the Li atom *(Fig. 26)*.

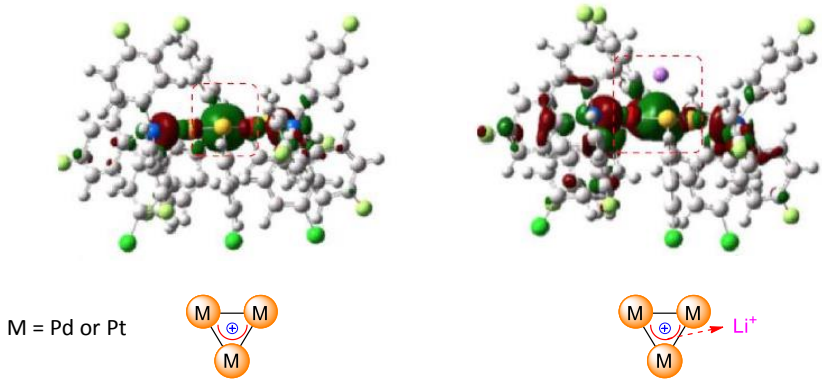

Fig. 26: Comparison of bonding HOMO of $[M_3]^+$ and $[M_3Li]^{++}$ obtained at the M06/Def2-SVP level

Li^+ complexation was previously observed just by an anionic mixed organo-lead aromatic,[78] thus the present bonding mode has limited experimental analogies.

The next step was to translate this interesting modelling into an experimental evidence. Crystals of $[Pd_3]^+$ complex bearing 4-chlorothiolate and tri(4-fluoro)phosphine were prepared with different non-coordinating counterions, namely SbF_6^- (**13**), BF_4^- (**55**) and $CF_3SO_3^-$ (**56**). Each of them have been mixed with various amounts of the corresponding lithium salt in dry THF at room temperature *(Scheme 19)*. NMR spectrum run upon 1 hour showed that thiolate resonances in **56** appeared splitted upon treatment with four equivalents of lithium triflate *(Fig. 27, red line)*. Two apparent dd centered at 6.88 and 6.52 ppm, namely 0.01-0.02 ppm downfield shifted, were thus observed. On the contrary, no shift was observed for aromatic protons on the phosphine. The reaction with ten equivalents of LiOTf showed a single pattern of resonances instead.

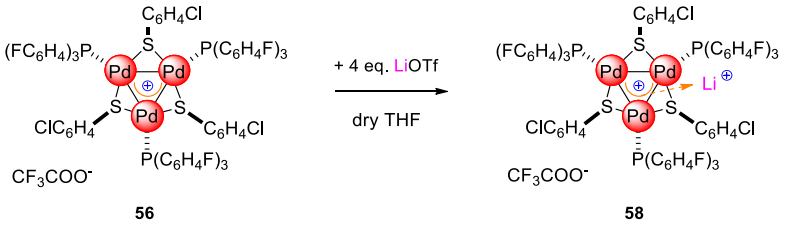

*Scheme 19: Synthesis of $[Pd_3Li]^{++}$ complex **58***

[78] M. Saito, M. Sakaguchi, T. Tajima, K. Ishimura, S. Nagase, M. Hada, *Science*, **2010**, *328*, 339.

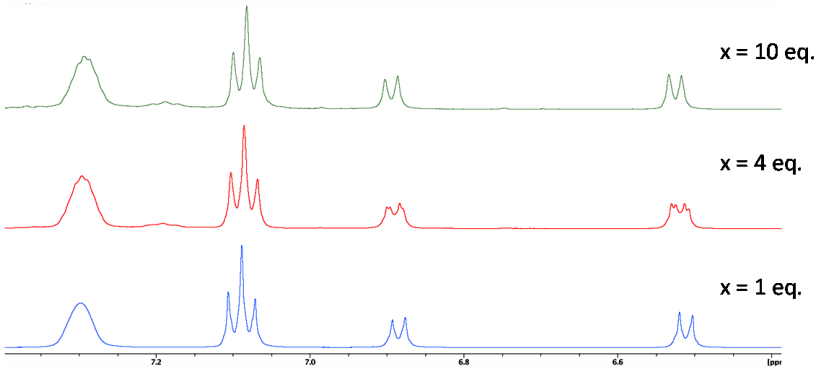

*Fig. 27: ^{1}H NMR spectra of **56** upon treatment with LiOTf*

Complex **55** showed a similar behaviour upon the addition of four and ten equivalents of $LiBF_4$. Mass spectrometry proved however fruitless, since only the diagnostic pattern of the starting material was detected. In this case, metal-lithium interaction was probably too labile for electrospray ionization conditions. Crystallization was unsuccessful too.

To overcome these issues, an increase in atomic number that could contribute to reduce the Coulomb density and consequently limit the electrostatic repulsion was tested. Cations of group XI seemed to be a good choice, since these M(I) species have metal-centered LUMOs of sigmoid symmetry that can overlap with the HOMO of $[Pd_3]^+$. Firstly, copper was tried by mixing $[Pd_3]^+$ with four and ten equivalents of the commercial reagent $(CuOTf)_2{\cdot}PhCH_3$. Both experiments gave the same result mentioned above for the lithium salts, and a slight downfield shift of thiolate protons could be observed in ^{1}H NMR spectrum (0.02 ppm). In addition, the $[Pd_3Cu]$ isotopic pattern was detected by ESI-HRMS analysis, giving a proof of the formation of a tetranuclear species. Switching to silver, $[Pd_3]^+$ was mixed with the corresponding silver salt (SbF_6^-, BF_4^- and $CF_3SO_3^-$), isolating a solid with high mass recovery (71-76%). The solubility of these species proved significantly lower in chlorinated solvents, probably because of the increased polarity of the dicationic molecule. Even in

this case modest shifts were observed in ^{1}H NMR spectra and the isotopic fingerprint of a species containing the tripalladium cluster with its counterion together with a silver atom was detected with HRMS analysis *(Fig. 28)*.

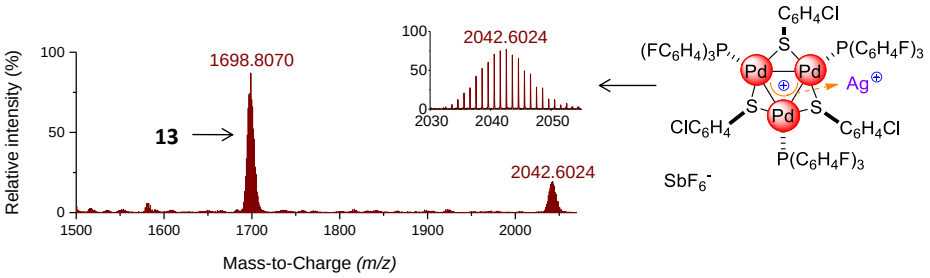

*Fig. 28: HRMS analysis of complex **59***

Finally, gold has been tested, choosing as Au precursor PPh_3AuSbF_6, in combination with a Pd_3^{+} complex with ancillary PPh_3 in order to avoid any scrambling of phosphorous ligands. Results were comparable to those obtained with copper and silver.

Beside these encouraging data, the clear-cut experimental evidence of the formation of the tetranuclear species required the isolation of $[Pd_3M]^{++}$ as a crystalline solid. Slow crystallization by vapour diffusion using $CHCl_3$/hexane afforded single crystals of $[Pd_3Ag]^{++}$ with BF_4^- as counterion (**60**), while crystals of $[Pd_3Ag]^{++}$ with SbF_6^- (**59**) were recovered replacing $CHCl_3$ with THF *(Fig. 29)*. Taking **60** as example, the silver atom lies 2.4 Å above the center of the planar palladium triangle. Its first coordination sphere is fulfilled through oxygen atoms of two water molecules and a fluorine atom of a tetrafluoroborate anion. Such a coordination pattern is in accordance to that commonly observed for mononuclear Ag(I) complexes, which are 18-electron species with a tetrahedral geometry ensured by four ligands on the formal *d*-10 metal center. Interestingly, the palladium triangle remains almost equilateral upon coordination, since Pd-Pd distances are just slightly different from the starting

complex, being 2.909(1), 2.882(1) and 2.874(1) Å instead of 2.8731(8) Å. The three Pd-Ag distances are 2.819(1), 2.804(1) and 2.793(1) Å. These structural features are similar to complexes with regular π-aromatics and can mimic a η^3-coordination by a 2 electron donor. Phosphorous and sulphur atoms remained coplanar with the palladium core, dihedral angles remained below 5°. The same observations were made for crystals of **59**. In both cases all metal-metal distances are significantly shorter than the sum of Van der Waals radii of palladium and silver (3.26 and 3.30 respectively). This finding further supports the hypothesis of the presence of a bonding interaction between these nuclei.
By the way, complexes **59** and **60** are the first examples of mixed Pd/Ag tetranuclear clusters.

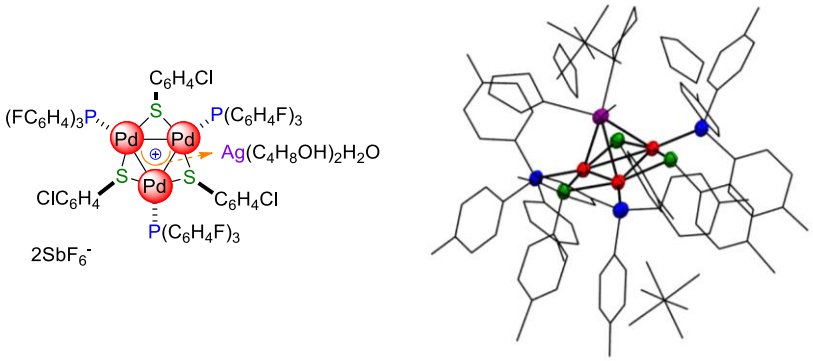

*Fig. 29: X-Ray structure of $[Pd_3Ag]^{++}$ complex **59***

4.2 Results and discussion

4.2.1 Studies on the nature of the bonding mode of Pd_3^+ clusters towards Lewis acidic cations[75]

Structures of $[Pd_3M]^{++}$ previously obtained let us speculate about the nature of this bonding mode. We wondered if our tripalladium cluster could really coordinate a metal cation miming a π-donor ligand, rather than forming a covalent bond which is fully delocalized among the four metal nuclei of the pyramid. Regarding the latter possibility, an example of three-dimensional aromaticity was reported in literature when Pyykkö and Runeberg described a tetranuclear cluster of gold whose bonding HOMO represented a four-center two-electron bond of a perfect tetrahedral symmetry.[79] The fact that the heteroatoms that complete the first coordination sphere of the palladium did not tilt and remained almost coplanar with the trinuclear metal core suggested a coordination-like bonding mode. This represented indeed a great structural difference between $[Pd_3Ag]^{++}$ and $[Au_4]^{++}$ complex. We thus planned a clear-cut experiment to discriminate between these two possibilities and to gain a proof of the relative lability of this coordination compound. We tested the effect of water, which might indeed revert complexation equilibria stabilizing the aquo complex of the Ag^+ cation. We prepared crystals of complex **20**, which has a methyl group on the bridging thiolate that resonates as a sharp diagnostic singlet at 1.0 ppm in ^1H NMR spectrum (red line). We dissolved them in $CDCl_3$, then added 4 equivalents of previously dried $AgSbF_6$ and finally put the mixture in an unsealed NMR tube. This enables moisture to slowly diffuse through time from the rubber septum *(Scheme 20)*.

[79] P. Pyykkö, N. Runeberg, *Chem. Commun*., **1993**, *0*, 1812.

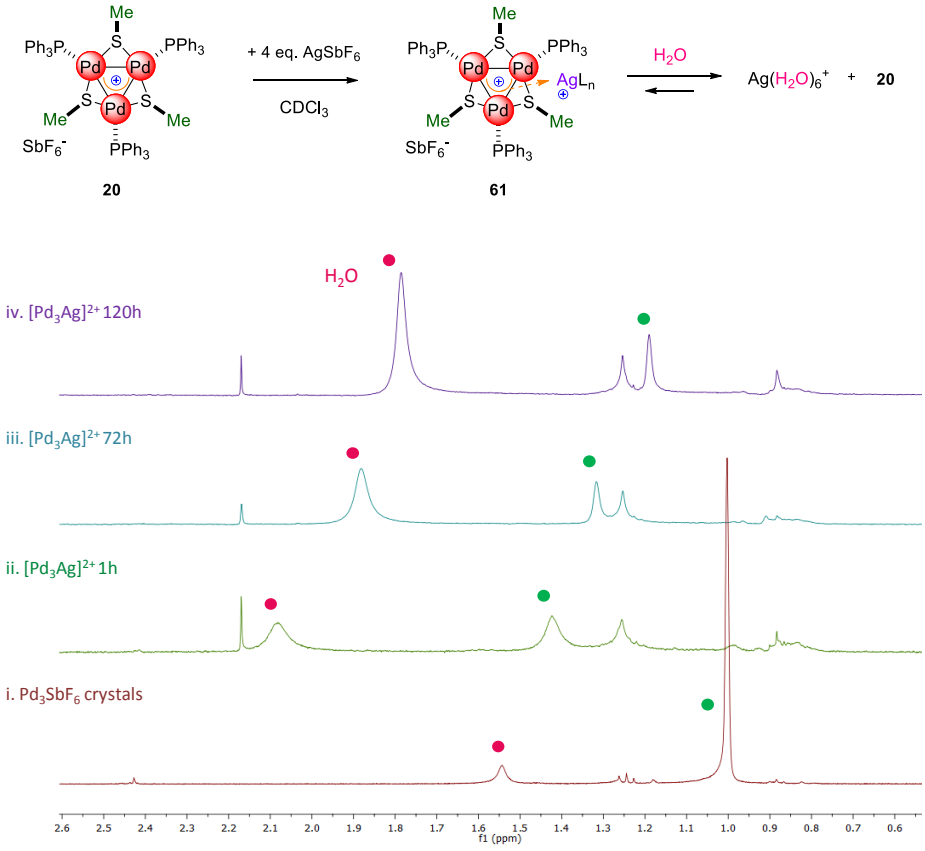

*Scheme 20: Synthesis of complex **20** and equilibrium with the aquo complex of Ag^+*

Fig. 30: ^1H NMR spectra of reaction 20 highlighting water (purple) and methyl (green) resonances

^1H NMR spectrum run upon 1 hour upon the addition of the silver salt shows meaningful chemical shifts of methyl protons (Δ=0.45 ppm) and a slightly increased resonance of the residual water, which moved from 1.56 to 2.1 ppm *(Fig. 30, green line)*. Upon 24 hours, the shift of the methyl resonance is reduced, while the peak of water keeps on increasing. This behaviour could be consistent with a competing complexation equilibrium promoted by concentration effects. The trend is confirmed 72 hours later, since the methyl shift is reduced to 0.3 ppm. Upon five days at room temperature the water

resonance still increases but gradually moves back to its usual chemical shift (1.56 ppm). Methyl singlet reverts back close to the value of starting material as well. ^{31}P NMR spectrum shows a similar trend of shifts, in this case a 0.5 ppm upfield shift that gradually moves back to the starting value *(Fig. 31)*.

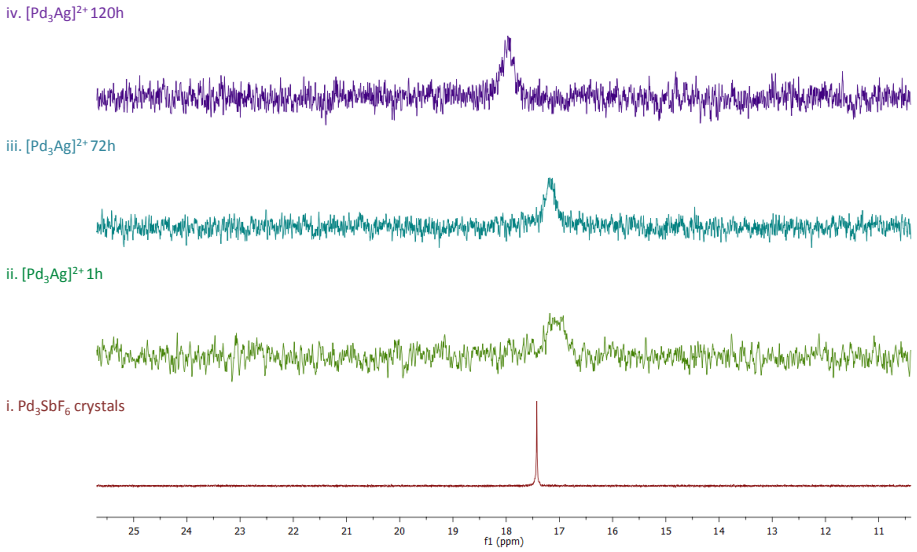

Fig. 31: ^{31}P NMR spectra of reaction 20

Taken together these results are in agreement with a coordination-like bonding mode.

We did not manage to obtain crystals suitable for X-Ray diffraction, thus we performed modelling studies to further support these experimental observations. The solid state structure of **59** was optimized without any constraints using various DFT functional and basis sets. The best correlation was obtained at the M11/Def2-SVP level, with a 0.01 Å difference between DFT data and X-Ray structure.

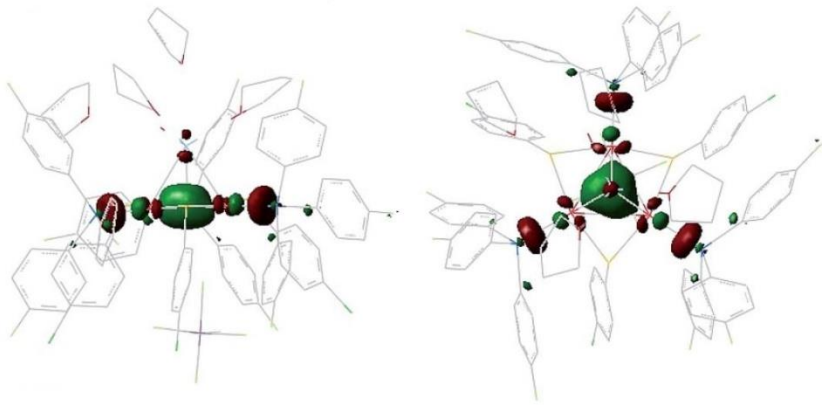

*Fig. 32: Calculated HOMO of **59** upon optimization of X-Ray geometry at the M11/Def2-SVP level*

Calculated Pd-Pd distances were 2.921, 2.905 and 2.901 Å. Values were slightly higher using other combinations of functional (B3LYP, BP86, PBE0 and M06) and basis sets (lacvp(d)), which nonetheless gave comparable results regarding orbitals, population analysis and charges. The same trend is observed using Def2-TZVP on a simpler system with PMe_3, SMe and H_2O fragments. The latter cluster was freely optimized at the MP2 and double hybrid B2PLYP level with Def2-TZVP triple-ζ set for metals only. In all cases no meaningful differences appeared on delocalized orbitals. Calculated natural and Mulliken charges showed only small differences with the starting Pd_3^+ cluster. Those of palladium nuclei increased as expected by 2-8% upon the coordination of a cation. Metal d_{x2-y2} atomic orbitals of the three palladium atoms in **59** combines to form the bonding HOMO *(Fig. 32)* and two empty molecular orbitals which are almost degenerate, LUMO and $LUMO^{+1}$ (Δ=0.8 kcal/mol). Resulting HOMO-LUMO gap is large, 36.5 kcal/mol, as expected for an aromatic molecule.[80] The HOMO has a sigmoid symmetry and gives Pd_3^+ d-orbital aromatic properties.[28-30-40-42-49] It is fully delocalized among the metal

[80] P. V. Schleyer, H. J. Jiao, *Pure and Appl. Chem*., **1996**, *68*, 209.

core in the starting cluster and it is slightly expanded towards the silver atom in the tetranuclear metal complex. Upon coordination of Ag^+ the energetic level of the HOMO increases by +2.1 kcal/mol, while the two degenerate LUMOs of **13** moved inversely and resulted lower in **59** by -1.7 and 3.8 kcal/mol. This outcome is similar to that displayed by regular arenes upon metal coordination.

We then performed NCI (Non-Covalent Interactions) analysis on the X-Ray structure of **59**.[81] NCI is a useful tool which helps to visualize weak interactions with colour encoding, ranging from blue, which represents the strongest, to green, highlighting dispersion forces, and eventually red for repulsive interactions.

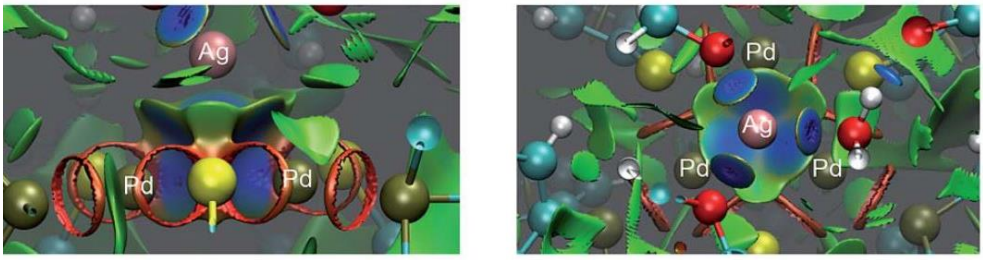

*Fig. 33: NCI topological analysis on **59***

The blue area visible among the four metal nuclei in *Figure 33* indicates the bonding interaction. However, the volume described by this surface is closer to the Pd_3 face than to the center of the pyramid.

The complementary ELF (Electron Localization Function) confirms that there are only two electrons inside the metal cage. As proven by NCI, they settle closer to the Pd_3 face than to the center of the tetrahedron *(Fig. 34)*.

[81] J. Contreras-Garcia, E. R. Jhonson, S. Keinan, R: Chaudret, J.-P. Piquemal, D. N. Beratan, W. Yang, *J. Chem. Theory Comput.*, **2011**, *7*, 625.

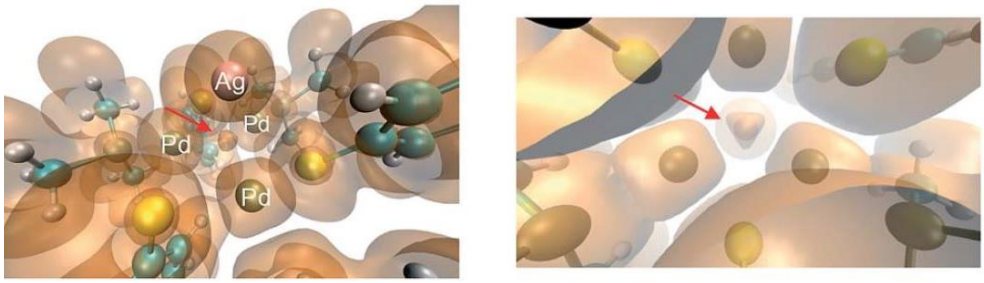

*Fig. 34: ELF topological analysis on **59***

HOMO of **59** tethers together Pd_3^+ and $[AgL_3]^+$ fragments. Since palladium and silver have a similar atomic radius, the four metal nuclei in $[Pd_3Ag]^{++}$ describe the vertex of an almost equilateral ideal pyramid, in analogy to those observed for the adamantyl dication and $[Au_4]^{++}$. All other modelled structures of $[Pd_3M]^{++}$ show on the contrary a shorter height if the nucleus is smaller (Li^+ and Cu^+), or a longer one if it is bigger (LAu^+). To have a further confirmation of our hypothesis of a coordination-like bonding mode, we performed NICS measurements comparing $[Pd_3M]^{++}$ (with M = Li, Ag, Au) and $[Au_4]^{++}$ *(Fig. 35)*. The latter provided as expected negative values up to 5 Å away from the center of its cage. We modelled a series of points on the axis perpendicular to each one of the pyramid faces and in all cases we obtained identical values and comparable curves. This outcome is perfectly in agreement with both its high symmetry and the sigmoid shape of its four-centre, two electron metal-metal bond, that make this complex a rare example of three dimensional aromaticity. The same approach on $[Pd_3Li]^{++}$ gave a strikingly different results, since calculated values were significantly different for the Pd_3 face (pink line) compared to each Pd_2Li face (pink dots).

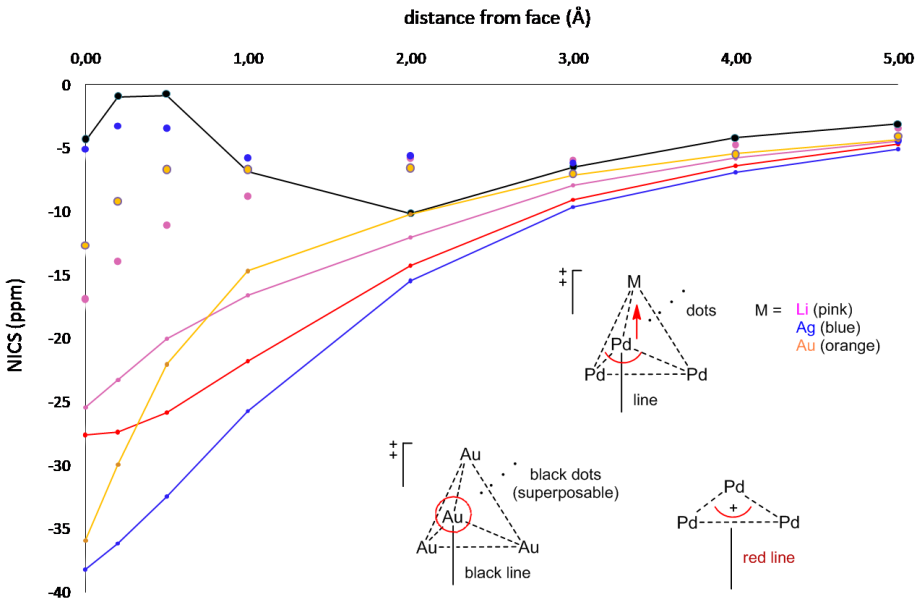

Fig. 35: NICS$_{zz}$ analysis for [Pd$_3$]$^+$, [Au$_4$]$^{++}$, [Pd$_3$Li]$^{++}$, [Pd$_3$Ag]$^{++}$ and [Pd$_3$Au]$^{++}$, comparing the differences from their M$_3$ (lines) and M$_2$M' (dots) faces

[Pd$_3$Ag]$^{++}$ and [Pd$_3$Au]$^{++}$ showed the same behaviour (blue and orange respectively). This suggested that delocalized electrons remain localized on the Pd$_3$ face in agreement with a coordination-like bonding mode. The analysis provided very different values, since two flex points were calculated for [Au$_4$]$^{++}$ and none for [Pd$_3$]$^+$ and [Pd$_3$M]$^{++}$, further highlighting the difference among these species. In all modelled [Pd$_3$M]$^{++}$ complexes we did not find any other bonding orbital among the four metal nuclei beside the bonding HOMO. Other molecular orbitals, including LUMO and LUMO^{+1}, were unaffected too, compared to [Pd$_3$]$^+$. This could be consistent with a minimal structural reorganization of **13** in [Pd$_3$Ag]$^{++}$. Both NBO and AdNDP supported these results, showing that each palladium atom retains four doubly occupied d-type lone pairs while silver has expectedly five (always above 1.93 occupation each).

Taken together all these features parallel those of traditional cation-aromatic bonding interactions, in which valence p_z electrons are engaged in delocalized molecular orbitals of π symmetry that can interact with Lewis acids.

4.3 Conclusions

We tried to further develop the potential of all-metal aromatic molecules finding new applications in coordination chemistry. Thanks to their negative quadrupolar moment, Pd_3^+ complexes can interact with other cations. We successfully obtained tetranuclear dicationic clusters with Li^+ and cations of group XI, namely Cu^+, Ag^+ and Au^+.

They can thus mimic regular aromatics playing the role of donor ligands and consequently coordinate Lewis acidic cations.

4.4 Experimental section

4.4.1 General remarks

$Pd(dba)_2$, phosphines, disulfides and Ag salts were purchased from commercial sources and used as received. Solvents were degassed by bubbling N_2 for at least 30 minutes prior to use. Reactions and filtrations were carried out under N_2 using standard Schlenk technique.

^1H NMR and ^{13}C NMR spectra were recorded in acetone-d_6 at 300 K on Bruker 500 AVANCE spectrometer fitted with a BBFO probe-head at 500 and 125 MHz respectively, using the solvent as internal standard (2.05 ppm for ^1H NMR and 29.84 ppm for ^{13}C NMR).

^{31}P NMR spectra were recorded in acetone-d_6 at 300 K on Bruker 500 AVANCE spectrometer fitted with a BBFO probe-head at 202 MHz, using 85% H_3PO_4 as external standard (0 ppm).

^{19}F NMR spectra were recorded in acetone-d_6 at 300 K on Bruker 300 AVANCE spectrometer fitted with a BBFO probe-head at 282 MHz, using hexafluorobenzene as external standard (-164.9 ppm).

Exact masses were recorded on a Agilent Q-TOF 6540 spectrometer (electrospray source).

UV-Vis spectra were recorded on a Shimadzu UV-2101 spectrophotometer.

IR spectra were collected with a Bruker Tensor 27 ATR diamante PIKE spectrometer.

4.4.2 Synthesis of complex 60

$AgBF_4$ (4 eq., 0.044 mmol, 8.6 mg) was added to a solution of compound **55** (1 eq., 0.011 mmol, 19.6 mg) in $CHCl_3$ (5 ml) under Ar. The deep red solution was put in the dark. Stirring was maintained for 1 hour and the mixture was then filtered through a short pad of celite under Ar. The solvent was removed under vacuum to afford a deep red solid. The compound was then purified by

recrystallization. Crystals of **60** suitable for X-Ray diffraction were obtained by vapour diffusion using $CHCl_3$/hexane. Crystals of **60** were characterized by ^{1}H, ^{31}P, ^{19}F, ^{13}C NMR spectroscopy, ESI^{+}-Tof HRMS, UV-Vis spectroscopy and IR spectrometry.

4.4.3 Spectroscopic data of complex 60

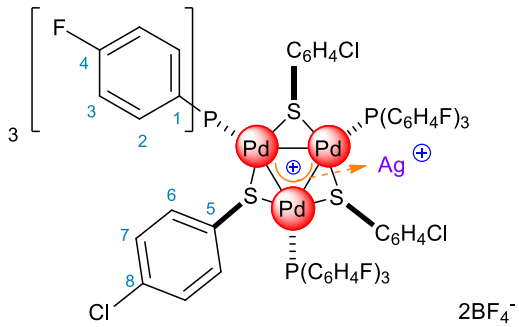

Isolated as deep red crystalline solid.

Mass recover = 73%. Recrystallization yield = 51%.

HRMS calculated for $C_{72}H_{48}Cl_3F_9P_3Pd_3S_3AgBF_4$ $[M]^{+}$: 1891.7261, found: 1891.7207.

^{1}H NMR (500 MHz, acetone-d_6) δ (ppm): 7.28 (bs, 18H, H_2), 7.10 (t, J = 8.0 Hz, 18H, H_3), 6.94 (d, J = 7.4 Hz, 6H, H_7), 6.61 (d, J = 7.3 Hz, 6H, H_6).

^{13}C NMR (125 MHz, acetone-d_6) δ (ppm): 165.3 (d, J = 252.1 Hz, C_4), 137.2 (bs, C_2), 137.0 (s, C_6), 135.2 (C_8), 134.4 (C_5), 129.9 (C_7), 127.5 (bs, C_1), 116.9 (d, J = 20.7 Hz, C_3).

^{31}P NMR (202 MHz, acetone-d_6) δ (ppm): 15.35 (s, $P(C_6H_4F)_3$).

^{19}F NMR (282 MHz, acetone-d_6) δ (ppm): -109.15 (s, $P(C_6H_4F)_3$), -151.93 (s, BF_4^-).

IR (ATR) ν (cm^{-1}): ν 2955, 2926, 2857, 1657, 1587, 1498, 1468, 1392, 1232, 1160, 1092, 1011, 826.

UV-Vis (c = 5·10^{-6} M, $CHCl_3$): λ_{max} = 245 nm, ε_{max} = 9.4·10^4 $M^{-1}cm^{-1}$.

4.4.4 Summary of X-Ray diffraction analysis on complex 60

X-Ray crystallographic data were collected on a Rigaku Rapid II (IP area detector system) diffractometer equipped with a rotating anode mm007 HF generator and Osmic mirrors (Cu Kα radiation, λ = 1.54187 Å) using ω-scans. Data were indexed, integrated and scaled using FS_Process from the *CrystalClear* software suite. They were also corrected for polarization, Lorentz and absorption effects, *ABSCOR*. The structure was solved with the ShelXT structure solution program using Direct Methods and refined with the ShelXL refinement package using Least Squares minimization. All non-hydrogen atoms were refined with anisotropic displacement parameters and H atoms have been added geometrically and treated as riding on their parent atoms. Rigid body restrains were applied along the entire connectivity set of complex **60** leading to more reasonable anisotropic displacement parameters, using standard deviation values: sigma for 1-2 distances of 0.004 and sigma for 1-3 distances of 0.004. Some large electron peaks due to solvent $CHCl_3$ molecules were found during refinement of complex. The rest of the molecule was refined without the effect of the solvent molecule(s) by the PLATON SQUEEZE technique.

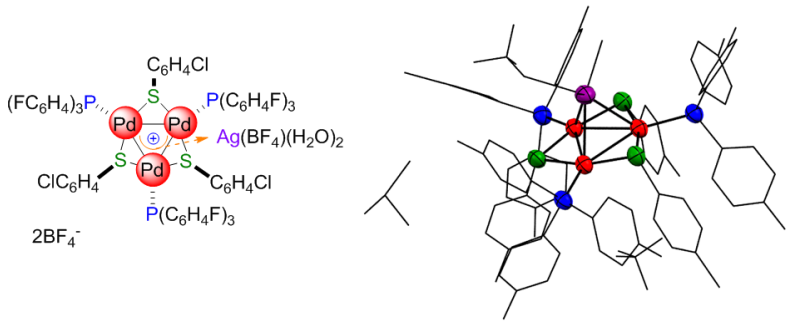

*Fig. 36: X-Ray structure of $[Pd_3Ag]^{++}$ complex **60***

Crystal data and structure refinement

CCDC number	1410440	
Empirical formula	C72 H52 Ag Cl3 F9 O2 P3 Pd3 S3, 2(B F4), 0.75(C H Cl3)	
Formula weight	2105.79	
Temperature	200 K	
Wavelength	1.54187 Å	
Crystal system	Orthorhombic	
Space group	Pccn	
Unit cell dimensions	a = 19.9665(4) Å	α= 90°.
	b = 30.9093(6) Å	β= 90°.
	c = 32.546(2) Å	γ = 90°.
Volume	20085.5(15) $Å^3$	
Z	8	
Density (calculated)	1.393 Mg/m^3	
Absorption coefficient	8.716 mm^{-1}	
F(000)	8284	
Crystal size	0.20 x 0.17 x 0.13 mm^3	
Theta range for data collection	2 to 69.9°.	
Index ranges	-18<=h<=22, -23<=k<=34, -30<=l<=36	
Reflections collected	70255	
Independent reflections	14426 [R(int) = 0.0685]	
Max. and min. transmission	1.000 and 0.483	
Data / restraints / parameters	14426 / 942 / 983	
Goodness-of-fit on F2	1.202	
Final R indices [I>2sigma(I)]	R1 = 0.0802, wR2 = 0.2131	
R indices (all data)	R1 = 0.1117, wR2 = 0.2819	
Extinction coefficient	n/a	
Largest diff. peak and hole	1.71 and -1.58 $e.Å^{-3}$	

Atomic coordinates (x 10^4) and equivalent isotropic displacement parameters ($Å^2$ x 10^3). U(eq) is defined as one third of the trace of the orthogonalized U^{ij} tensor

	x	y	z	U(eq)
C1	7646(6)	4504(4)	4864(4)	68(3)
C2	8056(7)	4505(5)	4501(4)	84(4)
C3	8016(8)	4165(5)	4213(4)	100(5)
C4	7558(8)	3840(5)	4292(4)	93(4)
C5	7131(7)	3849(4)	4622(4)	87(4)
C6	7166(6)	4185(4)	4902(4)	75(3)
C7	7651(6)	5421(4)	4905(4)	65(3)
C8	6997(7)	5586(4)	4805(4)	76(3)
C9	6909(8)	5922(4)	4552(4)	89(4)
C10	7494(8)	6117(4)	4368(4)	86(4)
C11	8108(8)	5985(5)	4448(4)	92(4)
C12	8200(7)	5632(4)	4708(4)	74(3)
C13	8621(5)	4956(4)	5382(4)	69(3)
C14	8829(6)	5313(5)	5595(4)	78(3)
C15	9492(7)	5318(5)	5751(5)	92(4)
C16	9904(7)	4990(5)	5641(5)	88(4)
C17	9699(6)	4628(5)	5429(4)	79(3)
C18	9049(6)	4615(4)	5293(4)	76(3)
C19	5998(5)	6444(3)	6320(3)	53(2)
C20	5757(6)	6465(4)	5916(4)	71(3)
C21	5908(7)	6808(4)	5653(5)	87(4)
C22	6312(8)	7115(5)	5800(5)	92(4)
C23	6574(7)	7114(4)	6181(5)	86(4)
C24	6422(6)	6781(3)	6447(4)	66(3)
C25	4884(6)	5984(4)	6673(4)	66(3)
C26	4563(6)	5649(4)	6858(4)	78(4)

C27	3882(6)	5640(5)	6884(5)	97(5)
C28	3525(6)	5977(5)	6734(4)	77(3)
C29	3818(6)	6319(5)	6572(4)	93(4)
C30	4502(6)	6333(5)	6529(4)	90(4)
C31	6087(6)	6145(4)	7140(4)	66(3)
C32	6724(6)	6026(4)	7261(4)	73(3)
C33	6985(7)	6150(4)	7649(4)	81(3)
C34	6577(8)	6382(5)	7891(5)	92(4)
C35	5947(7)	6504(4)	7797(4)	90(4)
C36	5707(7)	6379(4)	7412(4)	76(3)
C37	6182(6)	3842(3)	7397(4)	66(3)
C38	6559(7)	3792(4)	7735(4)	80(3)
C39	6301(8)	3813(5)	8133(5)	107(5)
C40	5627(8)	3915(5)	8171(5)	94(4)
C41	5217(8)	3962(4)	7830(5)	95(4)
C42	5502(7)	3927(4)	7442(5)	86(4)
C43	6076(6)	3375(3)	6635(4)	65(3)
C44	5995(7)	3374(4)	6213(5)	86(4)
C45	5656(8)	3035(4)	6033(6)	110(5)
C46	5430(8)	2714(5)	6267(6)	108(4)
C47	5471(8)	2708(4)	6681(6)	109(5)
C48	5793(6)	3053(4)	6866(5)	81(3)
C49	7371(6)	3610(3)	6963(3)	62(3)
C50	7877(6)	3885(4)	7096(4)	64(3)
C51	8515(6)	3758(4)	7176(4)	67(3)
C52	8658(6)	3333(4)	7104(5)	91(4)
C53	8199(7)	3043(4)	6981(6)	124(7)
C54	7556(7)	3179(4)	6893(5)	96(5)
C55	7367(5)	5942(3)	5932(4)	58(2)
C56	7751(6)	5859(3)	6282(4)	66(3)
C57	8307(7)	6125(4)	6372(4)	80(3)
C58	8458(6)	6467(4)	6098(4)	78(3)

C59	8090(6)	6527(4)	5747(4)	80(3)
C60	7537(6)	6273(3)	5664(4)	68(3)
C61	8073(5)	4126(4)	6088(4)	63(3)
C62	8442(6)	4434(4)	6300(3)	64(3)
C63	9103(6)	4371(5)	6372(4)	74(3)
C64	9406(7)	4001(5)	6241(4)	83(3)
C65	9034(7)	3686(5)	6046(5)	95(4)
C66	8354(7)	3752(4)	5964(4)	80(4)
C67	6238(5)	4959(3)	7386(4)	56(2)
C68	6934(5)	4976(3)	7441(3)	57(3)
C69	7190(7)	5052(4)	7824(4)	72(3)
C70	6785(8)	5109(4)	8151(4)	80(3)
C71	6093(8)	5101(5)	8108(4)	94(4)
C72	5818(6)	5021(4)	7717(4)	67(3)
Ag1	5673.9(4)	4720.7(3)	5892.5(3)	691(3)
B1	8789(10)	5251(7)	7194(6)	92(4)
Cl1	9142.2(19)	6783.7(12)	6203.7(15)	1130(13)
Cl2	10255.8(19)	3919.6(16)	6307.3(15)	127.6(16)
Cl3	7103(3)	5222.7(18)	8626.2(13)	130.3(16)
F1	7530(5)	3511(3)	4032(2)	121(3)
F2	7386(5)	6451(3)	4111(3)	138(3)
F3	10541(4)	4997(3)	5796(3)	114(3)
F4	6499(6)	7447(3)	5537(3)	144(4)
F5	2839(3)	5958(3)	6760(3)	109(3)
F6	6818(5)	6500(3)	8275(3)	130(3)
F7	5356(5)	3948(3)	8548(3)	136(3)
F8	5113(6)	2363(3)	6082(3)	159(4)
F9	9294(4)	3189(3)	7189(4)	146(4)
F10	8360(5)	5580(3)	7231(3)	134(3)
F11	8462(4)	4861(3)	7207(3)	119(3)
F12	9170(5)	5263(3)	7560(3)	128(3)
F13	9209(4)	5294(3)	6879(3)	113(3)

P1	7729.1(15)	4949.7(10)	5220.5(10)	62.3(8)
P2	5799.3(14)	5991.2(9)	6640.1(10)	58.8(8)
P3	6543.0(14)	3814.7(9)	6883.8(10)	59.0(8)
Pd1	7045.4(4)	4909.1(3)	5792.3(3)	57.3(3)
Pd2	6234.5(4)	5344.6(3)	6409.1(3)	55.6(3)
Pd3	6569.1(4)	4445.6(3)	6502.9(3)	57.3(3)
S1	6670.8(14)	5608.6(9)	5812.4(9)	61.2(8)
S2	7200.6(15)	4197.4(9)	5963.8(9)	61.9(8)
S3	5868.4(14)	4862.2(9)	6895.6(9)	60.2(7)
F14	5660(4)	4111(3)	5350(3)	110(3)
F15	4764(5)	3701(4)	5465(4)	152(4)
F16	5466(6)	3510(4)	4979(4)	186(4)
F17	4788(6)	4077(4)	4914(4)	178(4)
B2	5212(13)	3868(8)	5162(8)	126(5)
O1	4851(6)	4242(4)	6136(4)	133(4)
O2	5016(7)	5160(4)	5478(4)	155(5)
Cl6	9709(8)	2650(4)	4946(7)	462(14)
Cl5	9132(7)	3471(5)	4670(5)	370(11)
Cl4	1046.5(6)	3456(6)	5046(5)	384(10)
C73	9880(6)	3169(4)	4738(3)	293(14)

Chapter 5

SYNTHESIS OF PERFLUORO-IMIDAZOLIUM SALTS AS PRECURSORS FOR *N*-HETEROCYCLIC CARBENE (NHC) LIGANDS*

*This work has been carried out in the group of Prof. István T. Horváth at City University of Hong Kong, Hong Kong (SAR).

5.1 Introduction

5.1.1 Birth and development of fluorous chemistry

Fluorous chemistry probably entered the scene when the first liquid perfluoroalkane was synthesized in 1937.[82] However, just in late 1980s scientists of Exxon Corporate Research Laboratories recognized its huge potential while looking for a new approach for the selective oxidation of methane to methanol using supported[83] liquid phase catalysis. They chose perfluorotributyl amine as supported liquid, intrigued by its ability to dissolve methane and oxygen and its low miscibility with methanol at room conditions. A two-phase system was thus designed and perfluoroalkyl chains were attached to the catalyst to avoid its oxidation and to ensure high solubility in the perfluorotributyl amine phase. Although this approach did not lead to methane oxidation, it represented a fundamental step towards the development of the fluorous biphase concept.[84] At the same time, Horváth and Rabai introduced the adjective *fluorous*, which can be defined as follows: "*of, relating to, or having the characteristics of highly fluorinated saturated organic materials, molecules or molecular fragments*".[85]

Fluorous biphase chemistry is based on the limited miscibility of perfluoroalkanes, perfluorodialkyl ethers and perfluorotrialkyl amines with common organic solvents, such as toluene, THF and acetone. A fluorous biphase system *(Fig. 37)* thus consists of a fluorous phase that should preferentially solubilize a fluorous substrate or catalyst, and a second phase generated by an organic or a nonorganic solvent that should contain the reaction products.

---

[82] J. H. Simons, L. P. Block, *J. Am. Chem. Soc.*, **1937**, *59*, 1407.
[83] a) J. P. Arhencet, M. E. Davis, J. S. Merola, B. E. Hanson, *Nature (London)*, **1989**, *339*, 454; b) I. T. Horváth, *Cat. Lett.*, **1990**, *6*, 43.
[84] I. T. Horváth, J. Rábai, *Science,***1994**, *266*, 72; US Patent 5,463, 08 2 (1995).
[85] J. A. Gladysz, D. P. Curran, I. T. Horváth, *Handbook of fluorous chemistry*, **2004**, WILEY-WCH, Weinheim.

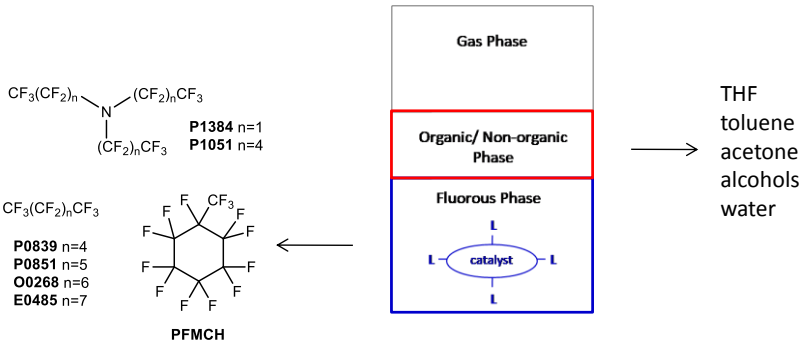

Fig. 37: Fluorous biphase system

Chemical transformations can occur both in the fluorous phase or at the interface, but the most interesting feature of this system is represented by the fact that the two-phase could become a one-phase system simply increasing the temperature. The advantage of a fluorous catalyst is thus represented by the possibility of combining the efficiency of the one-phase homogeneous catalysis with a biphase product separation, since the reaction can be performed at high temperature and products can be then separated from the catalyst at lower temperature *(Fig. 38)*.

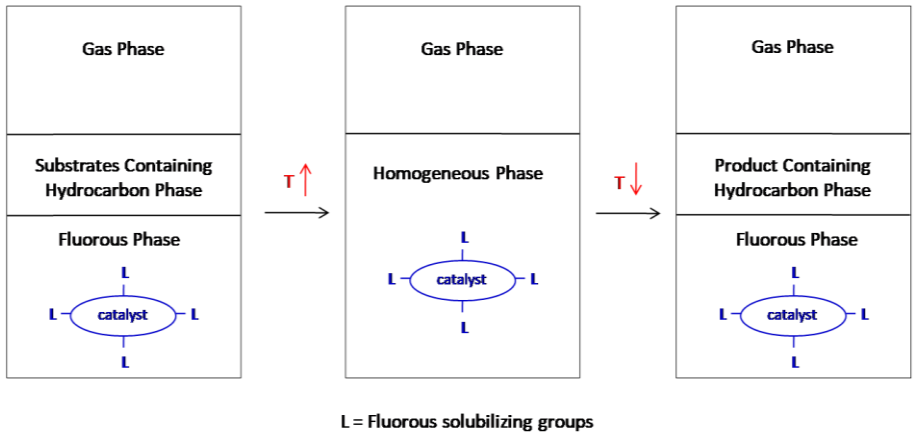

Fig. 38: The temperature-dependent fluorous-liquid/liquid biphase concept

The concept was exploited for the first time in the hydroformylation of olefins.[84] Separation of higher C_n-aldehydes (n > 8) from the catalyst is one of the major issues associated to the use of phosphine-modified rhodium catalysts such as $HRh(CO)(PPh_3)_3$. Complexes soluble in hydrocarbons usually decompose during distillation of the aldehyde from the reaction mixture, while the employment of an aqueous medium and a water-soluble catalyst could limit the solubility of higher olefins and the efficiency of the transformation. Horváth and Rabai modified the classic rhodium catalyst replacing triphenylphosphine with $P(CH_2CH_2(CF_2)_5CF_3)_3$ to make it soluble in a fluorous medium *(Fig. 39)*. They successfully performed the semicontinuous hydroformylation of 1-decene in a biphasic system $C_6F_{11}CF_3$/toluene, reaching a total turnover of more than 35000 in nine consecutive reaction/separation cycles, with a loss of 1.18 ppm of Rh/mol of aldehyde.

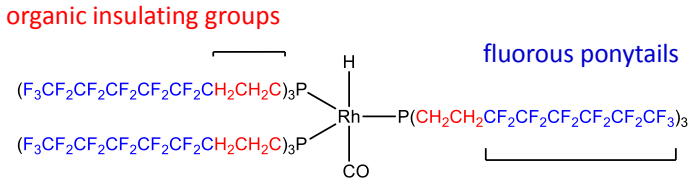

Fig. 39: Fluorous-rhodium catalyst for the hydroformylation of olefins

As shown in this example, substrates and catalysts can be suitably modified introducing fluorous moieties in appropriate size and number, in order to make them soluble in the fluorous phase. Best results can be obtained with linear or branched perfluoroalkyl chains of high carbon number, the *fluorous ponytails*, which may also contain heteroatoms. Nevertheless, when designing a similar catalytic system, it is worth considering that the electron-withdrawing effect exerted by fluorine atoms could significantly modify the electronic properties of the molecule and in turn the reactivity of fluorous substrates and

catalysts. The introduction of an organic spacer before the fluorous ponytail may be necessary to decrease this effect.

Despite their commercial attractiveness, processes that employ fluorous compounds bearing long perfluoroalkyl chains should be designed in order to keep the fluorous compounds inside the production plant. Their accidental release and emission to the environment could lead to their oxidative and homolytic fragmentation with the consequent formation of long-chain perfluoroalkyl carboxylates (LCPFACs), among which perfluoro-octanoic acid (PFOA) is the best known. LCPFACs and some of their precursors are persistent in humans and environment, have half-lives of years in humans, can cause adverse effects in laboratory animals and are associated with developmental and reproductive problems, liver toxicity and cancer.[86] Under the Toxic Substances Control Act, US Environmental Protection Agency (EPA) has recently proposed a new set of rules to regulate the use of LCPFACs.[87] On the contrary, analogues of perfluoroalkyl carboxylates with shorter perfluoroalkyl chains have significantly lower toxicity. The new challenge of fluorous chemistry is now to replace long linear with short or highly branched non-toxic fluorous chains (C_1-C_4), while keeping the high performances of C_6 and C_8 chains *(Fig. 40)*.

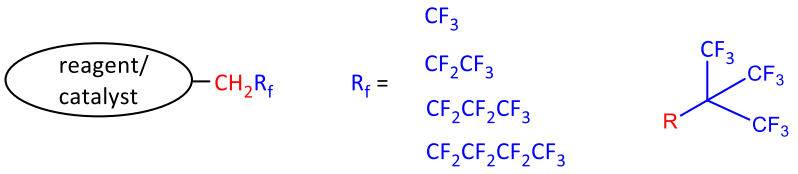

Fig. 40: Short fluorous chains

[86] a) N. Kudo, N. Bandi, E. Suzuki, M. Katakura, Y. Kawashima, *Chem.-Biol. Interact.*, **2000**, *124*, 119; b) K. P. Das, B. E. Grey, R. D. Zehr, C: R. Wood, J. L. Butenhoff, S.-C-Chang, D. J. Ehresman, Y.-M. Tan, C. Lau, *Toxicol. Sci.*, **2008**, *105*, 173.

[87] US EPA Perfluorooctanoic acid (PFOA) and Fluorinated telomers: www.epa.gov/oppt/pfoa/index.htlm (accessed on November 2, 2016).

5.2 Results and discussion

5.2.1 Synthesis of perfluoro-imidazolium salts as precursors for fluorous *N*-Heterocyclic Carbene (NHC) ligands

N-Heterocyclic Carbenes (NHCs) are excellent ligands for transition metals. They were originally employed as alternative ligands to phosphines, but in several examples, they can lead to better results in activity and scope.[88] In addition, they show excellent air and moisture stability. However, recovery and recycling of an NHC metal catalyst is still an important issue in homogeneous catalytic systems. Our purpose was to overcome this limit exploiting the concept of fluorous chemistry. We thus thought to synthesize fluorous NHC ligands that could be easily recovered from the reaction mixture by a liquid-liquid biphasic separation.

Imidazole reacts with fluorous iodides or triflates to form perfluoro imidazolium salts.[89] Literature examples are exclusively related to NHC ligands bearing long linear perfluoroalkyl chains, usually with C_6 or C_8 fluorous ponytails. On the contrary, we chose perfluoropropylethyl- and perfluorobutylethyl- iodides as alkylating agents, since we were interested in fluorous moieties with short perfluoroalkyl chains to ensure low toxicity.

The reaction of imidazole with 2 equivalents of the desired iodide led to the formation of the corresponding dialkylated imidazolium salts *(Scheme 21)*.

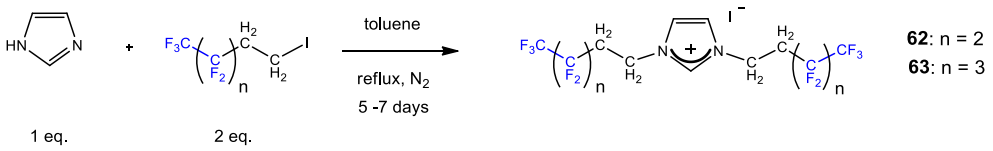

*Scheme 21: Synthesis of dialkylated imidazolium salts **62** and **63***

[88] V. César, S. Bellemin-Laponnaz, L. H. Gade, *Chem. Soc. Rev.*, **2004**, *33*, 619.

[89] a) L. Xu, W. Chen, J. F. Bickley, A. Steiner, J. Xiao, *J. Organometal. Chem.*, **2000**, *598*, 409; b) M. Skalicky, M. Rybáčková, O. Kysilka, M. Kvíčalová, J. Cvačka, J. Čejka, J. Kvíčala, *J. Fluorine Chem.*, **2009**, *130*, 966; c) H. Yu, L. Wan, C. Cai, *J. Fluorine Chem.*, **2012**, *140*, 107.

We obtained two symmetric fluorous imidazolium salts, diperfluoropropylethyl imidazolium iodide (**62**) and diperfluorobutyl imidazolium iodide (**63**), with a C_2 organic insulating spacer and a C_3 or C_4 fluorous chain respectively. Compounds **62** and **63** were isolated in 29 and 15% yield respectively. Such low values likely result from the strong electron-withdrawing effect exerted by the fluorous chain, which makes the iodide much less reactive compared to its organic analogue. Crystals suitable for X-Ray diffraction were obtained through vapour diffusion using ethyl acetate/hexane. *Figure 41* highlights that at the solid state fluorous chains of neighbouring molecules are stacked in a parallel fashion and aligned in a head to head pattern.

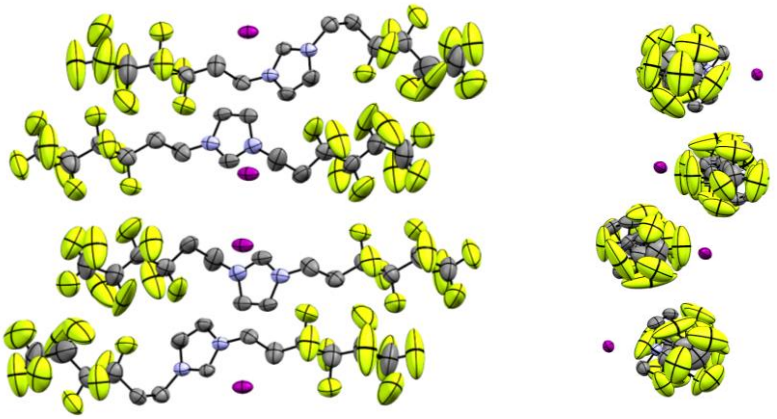

*Fig. 41: Arrangement of **63** in the solid state*

Following the same protocol employed for the synthesis of dialkylated imidazolium salts, monoalkylated imidazole could be obtained mixing imidazole with 1 equivalent of fluorous iodide. Further treatment with 1 equivalent of a fluorous iodide with a perfluoroalkyl chain of different length led to the formation of a non-symmetric imidazolium salt *(Scheme 22)*.

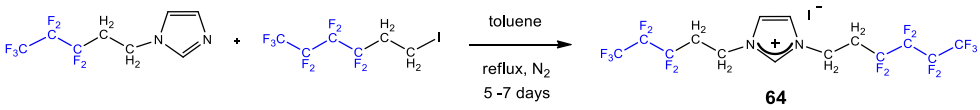

*Scheme 22: Synthesis of imidazolium salt **64***

Perfluororopylethyl-perfluorobutylethyl imidazolium iodide **64** was obtained in 10% yield mixing the monoalkylated imidazole with a C_3 fluorous chain and perfluorobutylethyl iodide.

5.2.2 Synthesis of fluorous palladium-NHC complexes

Perfluoro imidazolium salts **62-64** were consequently tested as precursors of NHC ligands for transition metals. They easily reacted with palladium acetate in refluxing THF to form mononuclear palladium (II) complexes with two perfluoro carbenes and two iodides as ligands *(Scheme 23)*.

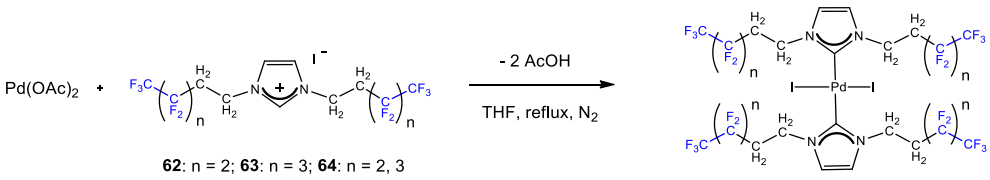

Scheme 23: Synthesis of fluorous palladium NHC complexes

Complex **65** bearing **62** as ligand was structurally characterized by multinuclear NMR analysis and X-Ray diffraction, since it easily crystallized by vapour diffusion using CH_2Cl_2/hexane *(Fig. 42)*.

The complex has a square-planar core geometry and carbene ligands are in trans position. Pd-C and Pd-I distances are comparable to those of analogue complexes with C_6 perfluoroalkyl chains[89] (2.037(1) and 2.598(1) Å respectively).

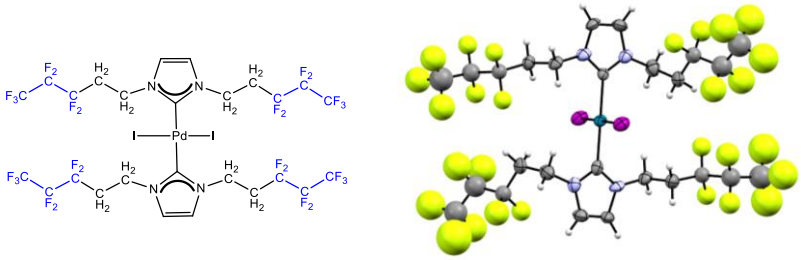

*Fig. 42: Structure of **65***

The plane of the imidazolium rings is tilted by 84.24(2)° in respect to the square planar environment of the metal, minimizing steric interactions between iodides and alkyl chains. Large ellipsoids corresponding to fluorine atoms result from conformational disorder due to the high mobility of fluorous chains.

5.2.3 Catalytic application of fluorous palladium-NHC complexes

The catalytic activity of palladium complexes was tested in the Suzuki cross-coupling reaction *(Scheme 24)*. Literature examples of similar complexes in catalysis only refer to mononuclear complexes of palladium with NHC-carbenes with long perfluoroalkyl chains. In 2009 Kvíčala and co-workers synthesized a mononuclear palladium complex with a fluorous NHC ligand bearing a C_2 oganic spacer and a C_6 perfluoroalkyl chain, coordinated in trans position to a 3-chloro pyridine. Chloride and iodide anions in a molar ratio of 3:1 completed the coordination sphere of the palladium. 2 mol% of the present catalyst provided the coupling product of 4-iodotoluene and phenylboronic acid in modest yield (54%). Moreover, the recycling of the complex proved unsuccessful.[90] Few years later, the analogue of our palladium complexes with a C_8 perfluoroalkyl chain was supported on fluorous silica gel by Cai and his

[90] M. Skalicky, M. Rybáčková, O. Kysilka, M. Kvíčalová, J. Cvačka, J. Čejka, J. Kvíčala, *J. Fluorine Chem*, **2009**, *130*, 966.

research group.[91] They obtained Suzuki-coupling products of several aryl halides and arylboronic acids in good yields (18-98%). However, both these methods violate new sustainability standard because of the use of long linear fluorous chains.

We thus started from an initial screening of available palladium complexes. We chose as model reaction the coupling between 4-bromoanisole and phenylboronic acid in the presence of cesium carbonate as base and 1 mol% of catalyst. According to the fluorous biphase concept, the reaction was performed in a two-phase system with DMF/H_2O and perfluoromethylcyclohexane in a 1:1.2:1 ratio.

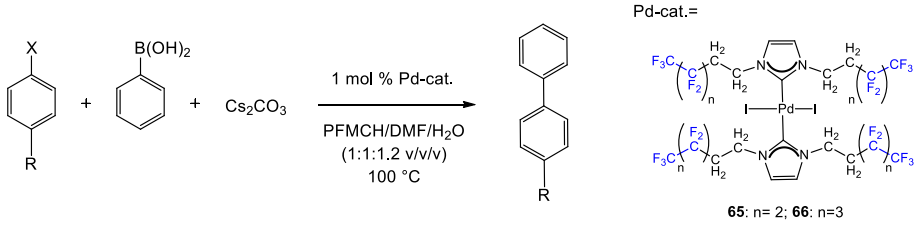

Scheme 24: Suzuki coupling reaction

Complex **65** gave slightly better results compared to complex **66**, since they provided a maximum conversion of the aryl halide of 95 and 85% upon 48 hours respectively. Coupling was much faster switching to 4-iodotoluene, since the reaction with **65** was complete in 3 hours. Analysing the composition of the two phases, we could however notice that the palladium complex settled at the interface, showing a low solubility in both DMF/H_2O and fluorous solvent. After the complete conversion of the substrate, traces of free ligand were found in the DMF/H_2O phase, showing that our catalyst had poor stability in the reaction medium and was not suitable to be recovered in the fluorous phase.

[91] H. Yu, L. Wan, C. Cai, *J. Fluorine Chem*, **2012**, *140*, 107.

5.3 Conclusions

During my activity in Prof. Horváth research group I synthesized several fluorous imidazolium salts with short perfluoroalkyl chains. Unlike long linear perfluoroalkyl chains, C_3 and C_4 moieties ensure low toxicity. They served as precursors of fluorous N-Heterocyclic Carbene ligands for palladium. I exploited this possibility preparing palladium complexes with two iodides and two NHC ligands, which were tested in the Suzuki coupling reaction. The complex showed poor stability in the reaction conditions and was fairly soluble in a fluorous medium. These results suggest that the ligand should be reshaped in order to increase the fluorous content with other strategies, always trying to avoid long alkyl chains with a view of sustainability.

5.4 Experimental section

5.4.1 General remarks

Perfluoro iodides were purchased from commercial sources and stored over molecular sieves in a glovebox (MBraun UNIlab). $Pd(OAc)_2$ was purchased from commercial sources and used as received. Dry solvents were distilled prior to use and stored over molecular sieves in a glovebox. Reactions were performed using standard Schlenk technique or in a glovebox.

^{1}H NMR spectra were recorded in $CDCl_3$ or acetone-d_6 at 298 K on Bruker 600 AVANCE and Bruker 300 AVANCE spectrometers fitted with a BBFO probe-head at 600 and 300 MHz respectively, using the solvent as internal standard (7.26 ppm for $CDCl_3$ and 2.05 ppm for acetone-d_6).

^{13}C NMR spectrum of complex **65** was recorded in $CDCl_3$ on Bruker 600 AVANCE spectrometer fitted with a BBFO probe-head at 151 MHz, using the solvent as internal standard (77.16 ppm).

^{19}F NMR spectra were recorded in $CDCl_3$ or acetone-d_6 at 298 K on a Bruker 300 AVANCE spectrometer fitted with a BBFO probe-head at 282 MHz, using hexafluorobenzene as internal standard (-164.9 ppm).

The terms m, s, d, t, q represent multiplet, singlet, doublet, triplet, quadruplet respectively, and the term br means a broad signal.

5.4.2 Synthesis of imidazolium iodides 62 and 63

The desired fluorous iodide (2.1 eq., 5.68 mmol), imidazole (1 eq., 2.70 mmol, 0.184 g) and dry toluene (8 ml) were added to a pressure tube in a glovebox. The reaction mixture was kept under magnetic stirring at 110°C for 6 days, until a white solid precipitated out from the solution. The solid was then filtered, washed with cold toluene, redissolved in ethyl acetate (10 ml) and extracted three times with ethyl acetate and cold water. The organic layer was

dried over anhydrous Na_2SO_4 and purified by flash column chromatography (eluent: dichloromethane/methanol = 10/1) to afford a solid.

5.4.3 Synthesis of imidazolium iodide 64

1,1,1,2,2,3,3,4,4-nonafluoro-6-iodohexane (1.1 eq., 0.49 mmol, 0.182 g), (1,1,1,2,2,3,3-heptafluoro-5-pentyl)imidazole (1 eq., 0.44 mmol, 0.117 g) and dry toluene (10 ml) were added to a pressure tube in a glovebox. The reaction mixture was kept under magnetic stirring at 110°C for 72 hours. The yellow solid suspended in the solution was filtered off and washed with 10 ml of cold toluene. Volatiles were removed under vacuum to afford a yellow solid.

5.4.4 Synthesis of complex 65

1,3-Bis(1,1,1,2,2,3,3-heptafluoropentyl)imidazolium iodide (2 eq., 0.16 mmol, 97 mg) and $Pd(OAc)_2$ (1 eq., 0.08 mmol, 18.1 mg) were introduced in a 25 ml schlenk and the vessel underwent three vacuum/N_2 cycles. Freshly degassed THF (0.8 ml) was immediately added and the mixture was kept under magnetic stirring at reflux for 2 hours. Volatiles were then removed under vacuum to afford a brown solid.
Crystals suitable for X-Ray diffraction were obtained upon crystallization by vapour diffusion using CH_2Cl_2/hexane.

5.4.5 Suzuki coupling reaction

The desired aryl halide (1 eq., 0.47 mmol), phenylboronic acid (1.5 eq., 0.70 mmol, 85 mg), cesium carbonate (2 eq., 0.94 mmol, 305 mg) and the palladium complex (0.01 eq., 0.0047 mmol) were added to a test tube. DMF (0.6 ml), water (0.7 ml) and perfluoromethylcyclohexane (0.6 ml) were then syringed to afford a biphasic system. The mixture was stirred at 100°C and monitored by NMR.

5.4.6 Spectroscopic data of compounds 62-65

- **Imidazolium iodide 62**

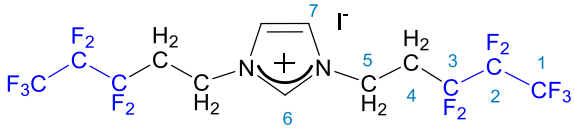

The product was obtained from 1,1,1,2,2,3,3-heptafluoro-5-iodopentane and imidazole according to the general procedure described above.

Isolated as a light yellow solid. Yield = 29%

^{1}H NMR (300 MHz, acetone-d$_6$) δ (ppm): 10 (s, 1H, H_6), 8.13 (s, 1H, H_7), 8.12 (s, 1H, H_7), 4.94 (t, $^{3}J_{HH}$= 7.1 Hz, 4H, H_5), 3.21 (tt, $^{3}J_{HH}$= 7.1 Hz, $^{3}J_{HF}$= 18.9 Hz, 4H, H_4).

^{19}F NMR (282 MHz, acetone-d$_6$) δ (ppm): -81.66 (t, $^{3}J_{FF}$= 9.8 Hz, 6F, F_1), -115.61 (m, 4F, F_2), -128.73 (m, 4F, F_3).

- **Imidazolium iodide 63**

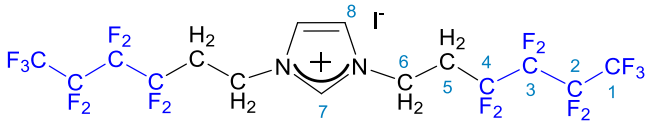

The product was obtained from 1,1,1,2,2,3,3,4,4-nonafluoro-6-iodohexane and imidazole according to the general procedure described above.

Isolated as a light yellow solid. Yield = 15%

^{1}H NMR (300 MHz, acetone-d$_6$) δ (ppm): 9.81 (s, 1H, H_7), 8.09 (s, 1H, H_8), 8.01 (s, 1H, H_8), 4.94 (t, $^{3}J_{HH}$= 7.1 Hz, 4H, H_6), 3.21 (tt, $^{3}J_{HH}$= 7.1 Hz, $^{3}J_{HF}$= 19.0 Hz, 4H, H_5).

^{19}F NMR (282 MHz, acetone-d$_6$) δ (ppm): -81.98 (tt, J_1= 9.8 Hz, J_2= 3.1 Hz, 6F, F_1), -114.67 (m, 4F, F_2), -125.01 (m, 4F, F_3), -126.74 (m, 4F, F_4).

- **Imidazolium iodide 64**

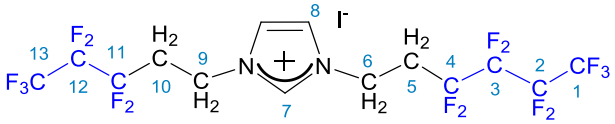

Isolated as a light yellow solid. Yield = 10%

^{1}H NMR (300 MHz, acetone-d$_6$) δ (ppm): 9.98 (s, 1H, H_7), 8.11 (bs, 2H, H_8), 4.92 (t, $^{3}J_{HH}$= 7.1 Hz, 4H, H_6), 3.21 (m, 4H, H_5).

^{19}F NMR (282 MHz, acetone-d$_6$) δ (ppm): -81.66 (t, $^{3}J_{FF}$= 9.8 Hz, 3F, F_{13}), -82.23 (tt, J_1= 9.7 Hz, J_2= 3.1 Hz, 3F, F_1), -114.85 (m, 2F, F_{12}), -115.6 (m, 2F, F_2), -125.21 (m, 2F, F_3), -126.98 (m, 2F, F_4), -128.74 (m, 2F, F_{11}).

- **Complex 65**

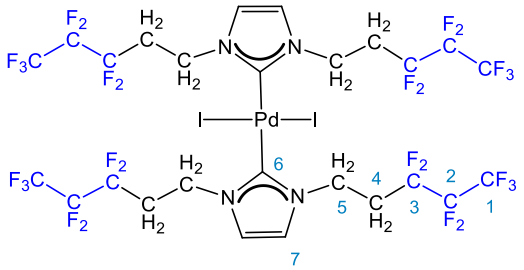

Isolated as yellow crystals. Yield = 29%

MS calculated for $C_{26}H_{22}F_{28}I_2N_4Pd$ $[M+Na]^+$: 1302.8, found: 1302.0.

^{1}H NMR (600 MHz, CDCl$_3$) δ (ppm): 7.02 (s, 4H, H_7), 4.72 (t, $^{3}J_{HH}$= 7.5 Hz, 8H, H_5), 2.93 (m, 8H, H_4).

^{19}F NMR (282 MHz, $CDCl_3$) δ (ppm): -83.69 (t, $^3J_{FF}$= 8.8 Hz, 12F, F_1), -118.12 (m, 8F, F_2), -131.03 (m, 8F, F_3).

^{13}C NMR (151 MHz, $CDCl_3$) δ (ppm): 169.33 (C_6), 122.33 (C_7), 118.80 (t, $^2J_{CF}$= 33.5 Hz, C_3), 117.00 (q, $^2J_{CF}$= 31.6 Hz, C_2), 115.42 (t, $^2J_{CF}$= 32.1 Hz, C_1), 43.27 (C_5), 31.47 (t, $^2J_{CF}$= 21.5 Hz, C_4).

5.4.7 Summary of X-Ray diffraction analysis on complex 65

X-Ray crystallographic data were collected at 193(2) K on a Oxford Diffraction Gemini S Ultra X-Ray single crystal diffractometer, using a graphite monochromator and a Cu Kα fine-focus sealed tube (λ = 1.54178 Å). The structure was solved using SHELXS-97 and refined on F^2 with full-matrix least squares (SHELXS-97).

Crystal data and structure refinement

Identification code	1	
Empirical formula	C26 H20 F28 I2 N4 Pd	
Formula weight	1280.66	
Temperature	193(2) K	
Wavelength	1.54178 Å	
Crystal system	Monoclinic	
Space group	P 2_1/n	
Unit cell dimensions	a = 16.8485(2) Å	α= 90.00°.
	b = 30.6534(4) Å	β= 110.878(2)°.
	c = 16.9892(2) Å	γ = 90.00°.
Volume	8198.20(17) $Å^3$	
Z	8	
Density (calculated)	2.075 Mg/m^3	
Absorption coefficient	16.939 mm^{-1}	
F(000)	4864	
Index ranges	-20<=h<=19, -36<=k<=36, -20<=l<=15	
Reflections collected	60862	
Independent reflections	15018 [R(int) = 0.0920]	
Refinement method	Full-matrix least-squares on F2	
Data / restraints / parameters	15018 / 34 / 699	
Goodness-of-fit on F2	1.066	

Final R indices [I>2sigma(I)]	R1 = 0.1070, wR2 = 0.2982
R indices (all data)	R1 = 0.1307, wR2 = 0.3270
Extinction coefficient	n/a

Atomic coordinates (x 10^4) and equivalent isotropic displacement parameters (Å^2 x 10^3). U(eq) is defined as one third of the trace of the orthogonalized U^{ij} tensor

The asymmetric unit corresponds to two molecules of **65** with a different spatial arrangement *(Fig. 43)*.

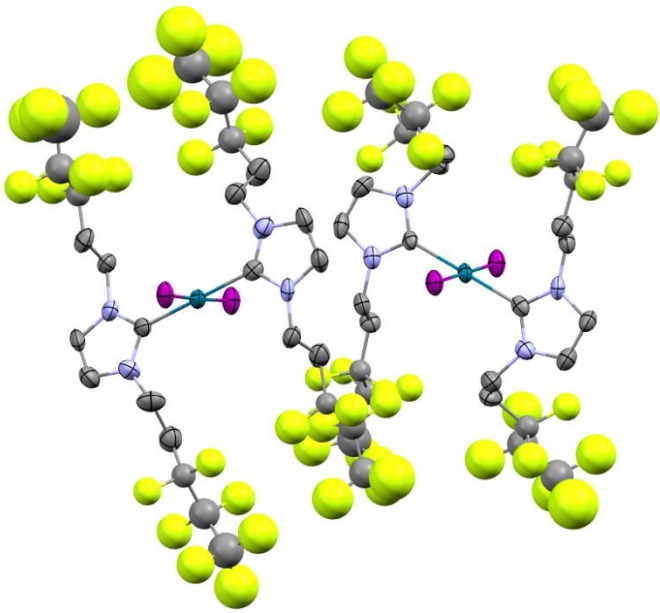

*Fig. 43: Asymmetric unit in **65***

	x	y	z	U(eq)
Pd1	7469.8(6)	2488.0(3)	5258(5)	35(2)
Pd2	7382.1(5)	2525.6(3)	179.4(5)	31(1)
I1	8709.7(6)	2706.0(3)	6631.1(5)	48(2)
I2	6233.2(6)	2294.7(3)	3863.8(5)	50(1)
I3	8692.2(5)	2608.3(3)	1566.2(5)	44(1)
I4	6090.8(6)	2443.6(3)	-1215.7(5)	47(1)
N1	7106(8)	1775(4)	6337(7)	50(3)
N2	6204(8)	2289(4)	6119(7)	43(2)
N3	8664(7)	2651(4)	4309(6)	41(2)
N4	7921(7)	3218(4)	4279(7)	48(3)
N5	6272(7)	2626(4)	1233(6)	40(2)
N6	6349(7)	3230(3)	650(6)	39(2)
N7	8401(7)	1812(3)	-297(6)	40(2)
N8	8490(7)	2428(4)	-869(6)	38(2)
C1	8942(17)	69(9)	5719(15)	127(10)
C2	8201(13)	374(8)	5654(12)	95(7)
C3	8338(10)	799(5)	6115(10)	59(4)
C4	7604(10)	1093(5)	5893(10)	59(4)
C5	7839(10)	1522(5)	6393(11)	60(4)
C6	6877(8)	2172(4)	5933(7)	36(2)
C7	6544(10)	1665(5)	6739(9)	52(3)
C8	5997(11)	1988(5)	6613(9)	52(3)
C9	5812(8)	2728(4)	5929(8)	40(3)
C10	6297(10)	3042(5)	6642(9)	51(3)
C11	5921(11)	3476(6)	6507(11)	61(4)
C12	6454(14)	3814(8)	7158(12)	93(6)
C13	629(2)0	4308(9)	713(2)0	24(3)0
C14	8718(17)	724(9)	2956(17)	95(7)
C15	8422(13)	1178(7)	2987(13)	75(5)
C16	8869(9)	1481(5)	3736(9)	48(3)

C17	8535(10)	1939(5)	3650(9)	54(3)
C18	8988(9)	2205(5)	4442(9)	47(3)
C19	8061(7)	2808(4)	4573(7)	34(2)
C20	8879(9)	2955(5)	3828(9)	49(3)
C21	8442(10)	3319(6)	3829(9)	56(4)
C22	7318(10)	3519(5)	4415(9)	53(3)
C23	6650(11)	3641(7)	3571(10)	69(5)
C24	5927(13)	3908(6)	3612(13)	76(5)
C25	6161(16)	4377(7)	3924(19)	116(9)
C26	5444(16)	4649(9)	4033(17)	139(11)
C27	5158(14)	641(6)	936(13)	117(9)
C28	5085(12)	1113(5)	617(12)	68(4)
C29	5763(9)	1417(5)	1180(9)	48(3)
C30	5665(8)	1893(4)	914(8)	39(3)
C31	6390(8)	2170(4)	1510(8)	40(3)
C32	6613(7)	2810(3)	724(6)	29(2)
C33	5780(8)	2919(5)	1492(8)	44(3)
C34	5828(8)	3305(5)	1113(9)	47(3)
C35	6585(10)	3565(4)	158(9)	51(3)
C36	7440(9)	3768(4)	575(9)	48(3)
C37	7557(9)	4033(5)	1364(9)	52(3)
C38	8367(15)	4291(8)	1670(15)	90(6)
C39	8531(16)	4575(9)	2391(16)	112(8)
C40	6668(16)	283(8)	-1925(14)	109(8)
C41	6650(16)	638(8)	-1300(15)	96(7)
C42	7423(10)	905(5)	912(10)	55(3)
C43	7342(11)	1238(5)	-290(11)	59(4)
C44	8143(10)	1485(5)	194(9)	52(3)
C45	8162(8)	2235(4)	-364(7)	35(2)
C46	8934(9)	1746(5)	-741(9)	48(3)
C47	9000(8)	2127(4)	-1110(8)	42(3)
C48	8413(8)	2881(4)	-1103(8)	41(3)

C49	9177(9)	3142(4)	-551(9)	46(3)
C50	9131(9)	3609(5)	-834(9)	50(3)
C51	9890(13)	3902(6)	-291(12)	74(5)
C52	9905(16)	4347(7)	-707(15)	113(8)
F1	9378(12)	0(6)	6563(12)	143(6)
F2	8727(16)	-334(9)	5400(15)	199(10)
F3	9500(13)	281(7)	5456(13)	161(7)
F4	7862(9)	464(5)	4803(9)	115(4)
F5	7594(10)	144(6)	5844(10)	125(5)
F6	9023(7)	990(4)	6027(7)	86(3)
F7	8587(7)	696(4)	6954(7)	78(3)
F8	5803(10)	3630(6)	5740(10)	125(5)
F9	5131(10)	3476(5)	6497(10)	117(5)
F10	7304(13)	3828(8)	7134(14)	179(8)
F11	6544(9)	3668(5)	7962(9)	110(4)
F12	6332(16)	4416(9)	6362(17)	197(9)
F13	5495(19)	4232(10)	7083(17)	222(11)
F14	6969(19)	4466(11)	7782(19)	241(13)
F15	8827(14)	498(8)	3627(14)	172(8)
F16	8249(14)	521(8)	2290(14)	165(7)
F17	9491(18)	745(10)	2919(17)	213(10)
F18	8302(8)	1378(5)	2277(8)	99(4)
F19	7625(11)	1125(6)	3051(11)	133(5)
F20	9686(10)	1494(5)	3777(9)	113(4)
F21	8986(10)	1282(5)	4464(10)	119(5)
F22	5315(12)	3952(7)	2808(11)	142(6)
F23	5553(11)	3710(6)	4063(11)	131(5)
F24	6635(17)	4575(10)	3623(17)	207(10)
F25	6630(12)	4336(6)	4797(12)	143(6)
F26	4912(19)	4712(11)	3242(14)	269(15)
F27	5732(19)	5035(9)	4401(17)	256(14)
F28	502(2)	4448(10)	4482(19)	299(17)

F29	4529(11)	402(6)	380(11)	134(5)
F30	5899(11)	458(6)	960(11)	141(6)
F31	5078(11)	585(6)	1682(11)	135(6)
F32	5109(7)	1124(4)	-144(7)	77(3)
F33	4323(7)	1257(3)	598(6)	73(3)
F34	6541(6)	1268(3)	1198(6)	69(2)
F35	5803(6)	1381(3)	1995(6)	68(2)
F36	6904(8)	4318(4)	1199(8)	90(3)
F37	7494(7)	3785(4)	1994(7)	75(3)
F38	9020(11)	4000(6)	1891(11)	139(6)
F39	8501(12)	4526(7)	1068(12)	148(6)
F40	9318(15)	4768(8)	2655(14)	181(8)
F41	8412(14)	4402(7)	3056(14)	170(8)
F42	7939(15)	4882(8)	2319(15)	185(9)
F43	6741(13)	485(7)	-2618(13)	163(7)
F44	7401(18)	74(11)	-1766(19)	257(14)
F45	5946(14)	51(8)	-2289(14)	176(8)
F46	6317(13)	473(7)	-795(13)	162(7)
F47	5980(13)	895(7)	-1716(13)	161(7)
F48	8121(11)	643(6)	-528(10)	128(5)
F49	7595(7)	1100(4)	-1552(7)	78(3)
F50	8399(6)	3795(3)	-844(6)	73(3)
F51	9111(6)	3629(3)	-1648(6)	73(3)
F52	1059.3(8)	3704(4)	-216(8)	91(3)
F53	9823(9)	3920(5)	470(9)	112(4)
F54	1006.2(16)	4351(9)	-1421(15)	203(10)
F55	1052.3(14)	4575(8)	-99(14)	180(8)
F56	9205(15)	4575(9)	-730(15)	193(9)